The preparation and characterisation of highly selective adsorbents for fission product removal from acid solutions

by

Parthiv Chetan Kavi

A thesis submitted in partial fulfilment for the requirements for the degree of Doctor of Philosophy at the University of Central Lancashire

July 2016

STUDENT DECLARATION FORM

Concurrent registration for two or more academic awards

Either *I declare that while registered as a candidate for the research degree, I have not been a registered candidate or enrolled student for another award of the University or other academic or professional institution

~~or *I declare that while registered for the research degree, I was with the University's specific permission, a *registered candidate/*enrolled student for the following award:~~

Material submitted for another award

Either *****I declare that no material contained in the thesis has been used in any other submission for an academic award and is solely my own work

~~or *I declare that the following material contained in the thesis formed part of a submission for the award of~~

_____

(state award and awarding body and list the material below):

* *delete as appropriate*

Collaboration

Where a candidate's research programme is part of a collaborative project, the thesis must indicate in addition clearly the candidate's individual contribution and the extent of the collaboration. Please state below:

Signature of Candidate 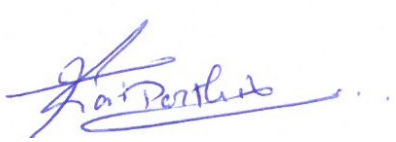

Type of Award **Doctor of Philosophy**

School **Forensics and Applied Sciences**

Abstract

Nuclear fuel reprocessing of fissile materials is carried out in order to provide recycled fuel for existing and future nuclear power plants. One aim of reprocessing is to recover unused uranium (U-238 and U-235) and plutonium isotopes thereby preventing them from being wasted. This can save up to 30% of the natural uranium that is required each year for the fabrication of new nuclear fuel. A second aim is to reduce the volume of high-level radioactive waste. Along with the separation of uranium and plutonium there has been a significant interest in the extraction of short-lived fission products such as caesium and strontium, which play critical role during high-level waste handling and disposal.

The PUREX process for reprocessing of irradiated fuel has been unchallenged for more than half a century even though it has several deficiencies such as flexibility, non-specificity of Tri-Butyl Phosphate (TBP), degradation of the extractant, TBP, and diluent. This project addresses the development of an alternative separation process to either replace and/or complement the PUREX process. Our process is based on the chromatographic separation of fission products from U and Pu. This research focuses on the synthesis of highly stable and selective materials which could be used as a stationary phase in a continuous chromatographic separation for short lived fission products (Cs, Sr); a technique patented by UCLan.

The objectives of this project were to synthesis highly selective adsorbents for fission products (primarily Cs and Sr) capable of extracting these cations from acidic liquor (up to 3 M HNO_3). In addition to selectivity (specificity) and acid stability, the materials under investigation would require fast cation uptake and high capacity.

The research explored three key approaches for ion sorption:

(1) Creating charge imbalance into ordered mesoporous MCM-41 structure (chapter 4),

(2) Examination of molecular sieves based on their size exclusive property (chapter 5), and,

(3) Preparation of ammonium phosphomolybdate (AMP) encapsulated polymeric composites (chapter 6).

Various physical and chemical properties of the materials were characterised by XRD, SAXS, surface area, pore volume, pore size distribution, SEM, TEM, ATR-IR, ^{29}Si NMR and TGA techniques. The cation uptake performance of the materials were evaluated for single ion and mixed ions against various nitric acid conditions. The study was further extended to rate of uptake in the best performing AMPPAN composites and identified area of improvement.

Insertion of heteroatom e.g. boron into silicate structures, did not produce the desired effect; selectivity and capacity for the target fission products (Cs and Sr) were negligible compared with the required criteria. The incorporation of a mesoporous shell around zeolite structure was effective but the uptake of fission products from nitric acid solutions was again disappointing. The uptake of fission products from slightly acid solutions (pH value ~5) was more encouraging but not specific to any single ion (e.g. Cs or Sr) and this approach could form the basis of further studies.

The preparation of AMP composites addressed both inorganic and organic substrates; AMP alumina composites in a suitable form i.e. spheres/beads was challenging and produced materials that were unsuitable and incorporated low AMP concentrations. This produced composites with low Cs uptake. The use of an organic substrate such as polyacrylonitrile (PAN) produced a composite that had a high selectivity for Cs, near specific, from nitric acid solutions but with comparatively low capacity and rate of uptake compared to pure AMP. These properties could be improved by manipulation of the composite structure; future work in this area is recommended.

Table of Contents

Declaration 2

Abstract 3

Table of contents 5

List of Figures 11

List of Tables 14

Acknowledgements 16

Abbreviations 17

Chapter 1 Introduction 19

1.1 Nuclear fuel cycle 19

1.1.1 Uranium Mining 20

1.1.2 Conversion 21

1.1.3 Uranium Enrichment 22

1.1.4 Fuel fabrication 22

1.1.5 Power generation 23

1.1.6 Reprocessing 24

1.1.7 Waste management 26

1.1.8 Advanced reprocessing 28

1.2 UCLan's concept of advanced reprocessing 30

1.2.1 Mobile phase 31

1.2.2 Stationary phase 32

1.3 Continuous chromatography 34

1.4 Potential Stationary Phases 37

1.4.1 Natural Ion exchangers 37

1.4.1.1 Natural inorganic Ion exchangers 37

1.4.1.2 Natural organic Ion exchangers 38

1.4.2 Synthetic Ion exchangers 39

1.4.2.1 Synthetic inorganic Ion exchangers 39

1.4.2.1.1 Molecular sieves and zeolites 39

(i) Preparative routes for synthesis of zeolites and molecular sieves 40

(ii) Important factors during synthesis 40

1.4.2.1.2 Advanced synthetic zeolites 41

(i) Crystalline SilicoTitanates (CST) 41

(ii) Zirconium phosphates (ZrP) 42

(iii) Ammonium phosphomolybdates (AMP) 42

(iv) Transitional metal cyanoferrates 42

1.4.2.1.3 Mesoporous inorganic materials 42

1.4.2.2 Synthetic organic Ion exchangers 44

(i) Polystyrene divinylbenzene 45

(ii) Phenolic 45

(iii) Acrylic 46

1.4.2.3 Organic-Inorganic ion exchangers 46

1.5 Aims and Objectives 47

1.6 References 48

Chapter 2 Literature Review **54**

2.1 Literature review for Cs and Sr removal 54

2.2 References 58

Chapter 3 Characterisation and experimental methods **61**

3.1 Instruments 61

3.2 Analytical Techniques 62

3.2.1 Powder X-ray Diffraction Spectroscopy (PXRD) 62

3.2.2 Small Angle X-ray scattering (SAXS) 63

3.2.3 Surface area and pore analysis 65

3.2.3.1 Brunauer-Emmett-Teller (BET) Method 67

3.2.3.2 Barrett-Joyner-Halenda (BJH) Method 67

3.2.3.3 Horvath-Kawazoe (HK) Method 68

3.2.4 Attenuated Total Reflectance Infrared spectroscopy (ATR-IR) 68

3.2.5 Scanning electron Microscopy (SEM) and Transmission Electron Microscopy (TEM) 69

3.2.6 Thermogravimetric analysis (TGA) and Differential Thermal Analysis (DTA) 70

3.2.7 Solid State Nuclear Magnetic Resonance Spectroscopy (NMR) 71

3.2.8 Laser diffraction 72

3.2.9 Inductively Coupled Plasma Mass Spectrometer (ICP-MS) 72

3.2.10 Uptake Measurements 74

3.2.11 Rate of Uptake Measurements 76

3.3 References 77

Chapter 4 Preparation of modified mesoporous MCM-41 79

4.1 Introduction 79

4.1.1 Role of surfactant during MCM-41 synthesis 80

4.1.2 Silicate chemistry during MCM-41 synthesis 82

4.1.3 Role of catalyst 83

4.1.4 Boron substituted MCM-41 83

4.2 Materials and Method 84

4.2.1 Materials 84

4.2.2 Synthesis method 85

4.2.2.1 Synthesis of Si-MCM-41 85

4.2.2.2 Synthesis of boron substituted MCM-41 85

4.2.3 Characterisation 86

4.3 Results and Discussion 86

4.3.1 PXRD 87

4.3.2 Surface area and Pore analysis 91

4.3.3 ATR-IR 95

4.3.4 ^{29}Si NMR 97

4.3.5 SEM 101

4.3.6 TEM 102

4.3.7 TGA analysis 103

4.3.8 Cation Uptake measurements 104

4.4 Conclusions 110

4.5 References 111

Chapter 5 Molecular sieves and mesoporous zeolite molecular sieves 113

5.1 Introduction 113

5.1.1 Molecular sieves 113

5.1.2 Mesoporous zeolite molecular sieves 115

5.1.2.1 Post treatment synthesis 115

5.1.2.2 Template assisted synthesis 116

5.1.2.2.1 Hard/Solid templating 116

5.1.2.2.2 Soft templating 117

5.2 Material and Methods 119

5.2.1 Materials 119

5.2.2 Zeolite molecular sieves 3A, 4A and 5A 120

5.2.3 Synthesis of mesoporous zeolite molecular sieve 5A 120

5.2.4 Characterisation 121

5.3 Results and Discussion 122

5.3.1 PXRD 122

5.3.2 SAXS 123

5.3.3 Surface area and pore analysis 124

5.3.4 SEM 127

5.3.5 Cation Uptake measurements 128

5.3.6 Uptake measurements of mesoporous zeolite in 0.5 M HNO_3 133

5.3.7 Rate of uptake in molecular sieves 5A 135

5.4 Conclusions 137

5.5 References 138

Chapter 6 AMP composites **140**

6.1 Introduction 140

6.1.1 Ammonium phosphomolybdate (AMP) 140

6.1.2 AMP-Al_2O_3 composite 142

6.1.3 AMPPAN composite 144

6.2 Material and Methods 146

6.2.1 Materials 146

6.2.2 Synthesis Method 147

6.2.2.1 AMP- Al_2O_3 composite 147

6.2.2.2 AMPPAN composite 149

6.2.3 Characterisation 152

6.3 Results and Discussions 153

6.3.1 SEM 157

6.3.2 Surface area and Pore analysis 162

6.3.3 ATR-IR 165

6.3.4 TGA and DTA analysis 167

6.3.5 Acid Stability 171

6.3.6 Cation uptake measurements 173

6.3.7 Rate of uptake of AMPPAN composites 180

6.4 Conclusion 183

6.5 References 184

Chapter 7 Summary and Future work **187**

7.1 Summary 187

7.2 Future work 190

List of Figures

1.1	Schematic representation of various processes in Closed Fuel cycle	19
1.2	Schematic representation of various processes in Open Fuel cycle	19
1.3	Processes involved in Uranium purification	22
1.4	Schematic representation of processes involved in UO_2 production	23
1.5	Multistage extraction process during reprocessing	25
1.6	Structure of CyMe4-BTBP	28
1.7	Structure of TBP	29
1.8	GANEX process	29
1.9	DIAMEX/SANEX process	30
1.10	Proposed separation stages in UCLan's concept	34
1.11	Schematic representation of moving bed separation technique	36
1.12	Continuous annular chromatography	37
1.13	Schematic representation of M41S family, MCM-50 (Layered), MCM-41 (hexagonal) and MCM-48 (Cubic)	43
1.14	Schematic representation of liquid crystal templating mechanism of MCM-41	44
3.1	Bragg's Law	62
3.2	Basic construction of typical XRD instrument	63
3.3	Difference between SAXS and WAXS (XRD) techniques	64
3.4	N_2 gas sorption, (a) six types of adsorption isotherm, and (b) hysteresis loop of type IV isotherm	66
3.5	Principle of ATR-IR	69
3.6	A schematic representation of Everhart-Thornley secondary detector in SEM	70
3.7	A schematic representation of ICP-MS	73
4.1	Schematic representation of liquid crystal templating mechanism in two possible pathways	79
4.2	Mechanism of formation of MCM-41	80
4.3	(1) Schematic representation of micelles formation and sub-sequentially transformation into different mesoporous phases, (2) Schematic representation of C_{16}TAB in water and its transformation into different phases	81

4.4	Schematic representation of possible interaction between types of silicate species to surfactant molecules	82
4.5	Low angle PXRD comparison of different amount of NaOH synthesised Si-MCM-41	87
4.6	Low angle PXRD pattern of boron substituted MCM-41	89
4.7	Isotherm comparison of different amount of Na synthesised Si-MCM-41	92
4.8	Isotherms comparison with 0.43 Si-MCM-41 and boron substituted MCM-41	93
4.9	Comparison of pore size distribution of different amount of Na synthesised Si-MCM-41	93
4.10	Comparison of pore size distribution in boron substituted MCM-41	94
4.11	ATR-IR Study of 0.43 Si-MCM-41	95
4.12	ATR-IR Study of boron substituted MCM-41	96
4.13	^{29}Si NMR peaks analysis on (a) Si-MCM-41 and (b-e) boron substituted MCM-41	98-100
4.14	SEM Image of Si-MCM-41 with 4000X magnification	101
4.15	SEM Image of boron substituted MCM-41 with 4000X magnification	101
4.16	TEM images of (a and b) Si-MCM-41, (c, d, e and f) boron substituted MCM-41	102
4.17	TGA evaluation of MCM-41	103
4.18	Cs ion Kd value for various aqueous systems	105
4.19	Sr ion Kd value for various aqueous systems	106
4.20	Mixed ions Kd values for various aqueous systems	108
5.1	Schematic representation of type A zeolite molecular sieve	114
5.2	Synthesis of mesoporous zeolite by post treatment	116
5.3	Synthesis of mesoporous zeolite by hard/solid templating method	116
5.4	Synthesis of mesoporous zeolite Y by soft templating method	117
5.5	Zeolite Molecular sieves 3A, 4A, and 5A	120
5.6	PXRD profile comparison of molecular sieves 5A and mesoporous molecular sieves 5A	122
5.7	SAXS profile comparison of synthesised mesoporous 5A zeolites	123
5.8	Isotherm comparison of 5A and mesoporous 5A	125
5.9	SEM image of zeolite 5A	127

5.10	SEM image of mesoporous zeolite 5A@Si	127
5. 11	Mixed ions Kd values for various aqueous solutions	131
5. 12	Proposed mechanism of multivalent ion sorption on Si surface	133
5. 13	Rate of uptake of various ions on molecular sieve 5A in 0.5 M HNO_3	136
6.1	Schematic representation of AMP in (a) Ball stick structure, (b) crystal structure, and (c) chemical structure	140
6.2	Molecular structure of polyacrylonitrile	144
6.3	Synthesis of Al_2O_3 and AMP-Al_2O_3, (a) Column setup, and (b) Bowl setup	149
6.4	Continuous pumping setup for AMPPAN composite production	151
6.5	Softer gel formation	155
6.6	Synthesised Al_2O_3 granules	155
6.7	Synthesised AMP- Al_2O_3 composite granules	155
6.8	Image of synthesised AMPPAN composites	156
6.9	SEM image of (a) AMP- Al_2O_3 granules and (b) Al_2O_3 granules	157
6.10	SEM images of AMPPAN 12.5 composite	158
6.11	SEM images of AMPPAN 25 composite	159
6.12	SEM images of AMPPAN 50 composite	160
6.13	SEM images of AMPPAN 70 composite	161
6.14	Isotherm comparison of AMP- Al_2O_3 and Al_2O_3 materials	162
6.15	Isotherm comparison of AMPPAN composites	162
6.16	IR spectra comparison for Al_2O_3 and AMP- Al_2O_3 composite	165
6.17	ATR-IR Study of various AMPPAN composites	166
6.18	TGA comparison profile of AMP- Al_2O_3 composite	167
6.19	DTA comparison profile of AMP- Al_2O_3 composite	168
6.20	TGA comparison profile of AMPPAN composite	170
6.21	DTA comparison profile of AMPPAN composite	171
6.22	Cs ions uptake in AMPPAN composites in different HNO_3 system	175
6.23	Cs ions rate of uptake at different temperature in 1 M HNO_3	180
6.24	Cs ions rate of uptake at 25 °C in different acidity	181

List of tables

1.1	Dissolver liquor concentrations	32
1.2	Summary of general properties present in various ion exchangers	47
3.1	List of instruments, manufacturer, models, and software	61
3.2	SAXS experiment set up parameters	64
3.3	Composition of various cationic solutions	75
4.1	Reagents, their purity and source of purchase	84
4.2	Amount of reagents used for Si-MCM-41 synthesis	85
4.3	Amount of reagents used for B-MCM-41 synthesis	86
4.4	Lattice parameters in Si-MCM-41	88
4.5	Lattice parameters of boron incorporated MCM-41	90
4.6	Amount of boron in MCM-41 structure measured by ICP-MS	90
4.7	Surface area and Pore analysis of Si-MCM-41	94
4.8	Surface area and Pore volume analysis of boron substituted MCM-41	95
4.9	Observed IR band position in MCM-41	96
4.10	Observed chemical shifts in solid state NMR	97
4.11	Caesium ion concentrations in various aqueous systems	104
4.12	Strontium ion concentrations in various aqueous systems	105
4.13	Mixed ions concentrations in various aqueous systems	107
5.1	Reagents, their purity and source of purchase	119
5.2	Reagent quantities used to synthesis mesoporous zeolites	121
5.3	Surface area and pore analysis of various molecular sieves	126
5.4	Caesium ion concentrations in various aqueous systems	128
5.5	Strontium ion concentrations in various aqueous systems	129
5.6	Mixed ions concentrations in various aqueous systems	130
5.7	Hydrated ionic diameter	132
5.8	Mixed ions concentrations in 0.5 M HNO_3	134
5.9	Rate of uptake on molecular sieve 5A in 0.5 M HNO_3	136
6.1	Reagents, their purity and source of purchase	146
6.2	Amount of reagents used for preparation of stock solution	147
6.3	Amount of AMP used during AMP- Al_2O_3 composite preparation	148
6.4	Amount of reagents used AMPPAN composite preparation	150
6.5	Stock solution for Al_2O_3 and AMP- Al_2O_3 preparation	153

6.6	Feed composition for Al_2O_3 and AMP-Al_2O_3 preparation	154
6.7	Conductivity monitoring during washing	154
6.8	Surface area and Pore analysis of various AMP based composites	163
6.9	Observed IR band position in Al_2O_3 and AMP- Al_2O_3 composites	165
6.10	Observed IR band position in pure AMP and AMPPAN composites	166
6.11	Weight loss comparison in AMP- Al_2O_3 composites	168
6.12	Weight loss in AMPPAN composites	170
6.13	Acid Stability of various composites in HNO_3	172
6.14	Uptake measurements of AMP- Al_2O_3 composites in various conditions	173
6.15	Cs ions uptake measurements in AMPPAN composites	175
6.16	Sr ions uptake measurements in AMPPAN composites	176
6.17	Ce ions uptake measurements in AMPPAN composites	176
6.18	Mixed ions uptake measurements in AMPPAN composites	177
6.19	Capacity comparison of Cs ions in AMP- Al_2O_3 composite	178
6.20	Capacity comparison of Cs ions in AMPPAN composites	178
6.21	Rate of uptake at different temperature in 1 M HNO_3	180
6.22	Cs ions rate of uptake at 25 °C in different acidity	181

Acknowledgements

There are many people who have helped and supported me during this work and to whom I owe a great deal of thanks.

Firstly, I would like to thank my supervisor Gary Bond, Professor of Materials Chemistry, and Associate Head School of Forensics and Applied Sciences for providing me the opportunity to work on this project. I appreciate his help providing extremely valuable discussions, encouragement, and input throughout this research.

I would like to thank Harry Eccles, Professor of Nuclear Materials, School of Physical Sciences, and Computing, for sharing his valuable experience, knowledge, time, and enthusiasm. His patience and generosity have had a big impact on this work and I am truly grateful to him. I truly admire his always willing to help attitude and lots of coffee over our discussion.

I am grateful to University of Central Lancashire and Centre of Material Science for providing international scholarship.

Thanks must be extended to Dr Runjie Mao for his help and support during my overall lab work, TGA, and porosimetry analysis. Dr Jennifer Readman for XRD analysis, Dr Tapas Sen for TEM analysis and Dr Chandrashekhar Kulkarni for SAXS analysis. Many thanks are also expressed to James Donnelly, Pat Cookson, Sal Tracey, and Tamar Garcia Sorribes for their help with handling instrumentation and reagents.

I am also grateful to Prof Michel Rapport and Dr Amin Dilmaghani, University of Leeds for providing SAXS facility free of cost and same gestures to Dr Xander Warren at University of Bristol for providing SEM facilities.

I have met many memorable people during my time at UClan. Thanks to everyone in Department of Chemistry, and Materials Science for keeping things fun and reminding me of the breadth and importance of the work we are all doing. I would like to extend thanks to all the administrative staff and research colleagues in School of Forensics and Applied Science.

On a more personal note, I would like to thank my family and especially my parents for their love, encouragement, and financial support throughout my PhD to whom I dedicate this work. Without that, perhaps I am incapable to finish this work.

Abbreviations

3A, 4A, and 5A	Zeolite 3A, 4A, and 5A
Å	Angstrom
AGR	Advanced Gas cooled Reactor
AMP	AMmonium Phosphomolybdate
AMP-Al_2O_3	AMmonium Phosphomolybdate - aluminium oxide
AMPPAN	AMmonium Phosphomolybdate PolyAcryloNitrile
AMP-Silica gel	AMmonium Phosphomolybdate-Silica gel
AR-1	Mordenite
ATR-IR	Attenuated Transmission InfraRed
BET	Brunauer-Emmett-Teller
BJH	Barrett-Joyner-Halenda
B-MCM-41	Boron Mobile Composition of Matter No 41
BNFL	British Nuclear Fuel Limited
Bq	Becquerel
BSE	Back-Scattered Electrons
BTBP	Bis-Terpyridine Bis-Pyridine
BTP	2, 6 –Bis-(5, 6-dialkyl-1, 2, 4-Triazin-3-yl) Pyridine
BWR	Boiling Water Reactor
C_{16}TAB	HexadecylTrimethylAmmonium Bromide
CAC	Continuous Annular Chromatograph
Calix [4] arene-R14	1,3-[(2,4-diethylheptylethoxy)oxy]-2,4-crown-6-Calix[4]arene
$Ce(NH_4)_2(NO_3)_6$	Ammonium Cerium Nitrate
cis-DCH18C6	cis-DiCycloHexano-18-Crown-6
CMC	Critical Micelle Concentration
$CsNO_3$	Caesium Nitrate
CST	Crystalline SilicoTitanates
d.w.	deionised water
DIAMEX/SANEX	DIAMide EXtraction- Selective ActiNide EXtraction
DMDOHEMA	DiMethyl-DiOctyl-HexylEthoxy MalonAmide
DMSO	DiMethyl SulfOxide
DTA	Differential Thermal Analysis
FPs	Fission Products
GANEX	Group ActiNide EXtraction
Gy	Gray (a unit of ionising radiation dose; defined as the adsorption of 1 joule of radiation energy per kilogram of matter)
HF	Hydrogen Fluoride
HK	Horvath-Kawazoe
HLW	High Level Waste
HMTA	HexaMethyleneTetrAmine
ICP – MS	Inductive Coupled Plasma-Mass Spectrometry
ILW	Intermediate Level Waste
INEEL	Idaho National Engineering and Environmental Laboratory
IUPAC	International Union of Pure and Applied Chemistry
Kd	Distribution Coefficient
kHz	kiloHertz
kV	kiloVolts
LCDs	Liquid Crystal Displays
LCT	Liquid Crystal Templating
LLW	Low Level Waste
LTA	Linde Type A

mA	milliAmps
MAs	Minor Actinides
mbar	millibar
mS	milliSiemens
MCM-41	Mobile Composition of Matter No 41
mM	milliMolar
MODB	MethylOctyl-2-Di-methyl Butanemide
MOX	Mixed OXide
Nb-CST	Niobium-Crystalline SilicoTitanates
NFC	Nuclear Fuel Cycle
nm	nanometre
NMR	Nuclear Magnetic Resonance
ORNL	Oak Ridge National Laboratory
PAN	PolyAcryloNitrile
ppb	parts per billion
ppm	parts per million
PUREX	Plutonium Uranium Redox EXtraction
PWR	Pressurised Water Reactors
PXRD	Powder X-ray Diffraction
R.T.	Room Temperature
SAXS	Small Angle X-ray Scattering
SDA	Structure Directing Agents
SE	Secondary Electrons
SEM	Scanning electron microscopy
Si-MCM-41	Silica Mobile Composition of Matter No 41
SIXEP	Sellafield Ion exchange Effluent Plant
SMB	Simulated Moving Bed
$Sr(NO_3)_2$	Strontium Nitrate
TBP	Tri-Butyl Phosphate
TBP/OK	Tri-Butyl Phosphate in Odourless Kerosene
TEM	Transmission Electron Microscopy
TEOS	TetraEthOxySilane or TetraEthylOrthoSilicate
TGA	ThermoGravimetric Analysis
TMOS	TetraMethoxySilane
U.V	Ultra Violet
UCLan	University of Central Lancashire
UF_6	Uranium hexafluoride
UOC	Uranium Ore Concentrate
UO_2	Uranium dioxide
UOP	Universal Oil Products
vLLW	very Low Level Waste
ZrHP-AMP	Zirconium HydrogenPhosphate- AMmonium Phosphomolybdate
β	Beta
γ	Gamma

Chapter 1

Introduction

1.1 Nuclear Fuel Cycle

The nuclear fuel cycle (NFC) comprises of a number of discrete process stages that encompass the mining of uranium to its conversion and enrichment and subsequent use in a nuclear reactor to reprocessing of irradiated fuel and waste management with the subsequent disposal of radioactive wastes.

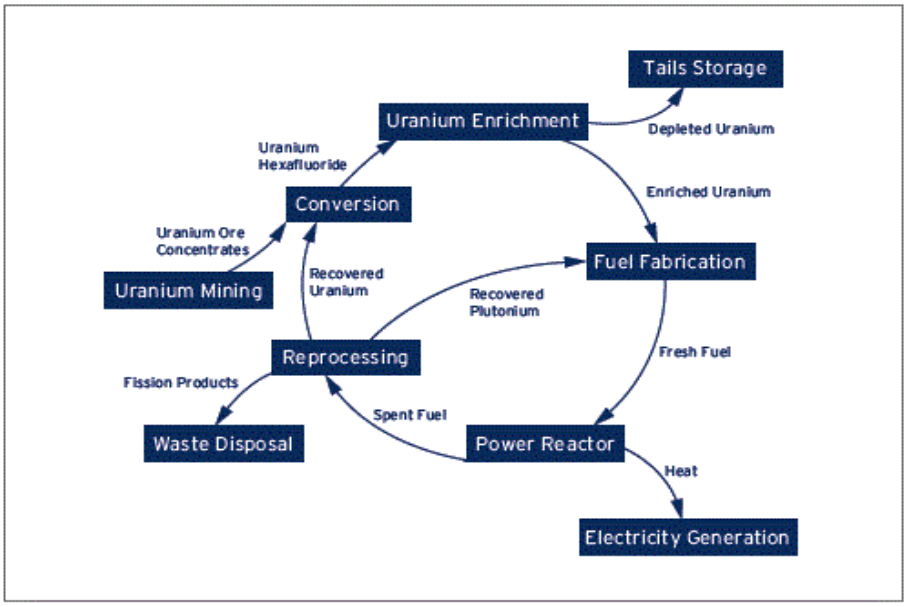

Figure 1.1 Schematic representation of various processes in Closed Fuel cycle [1]

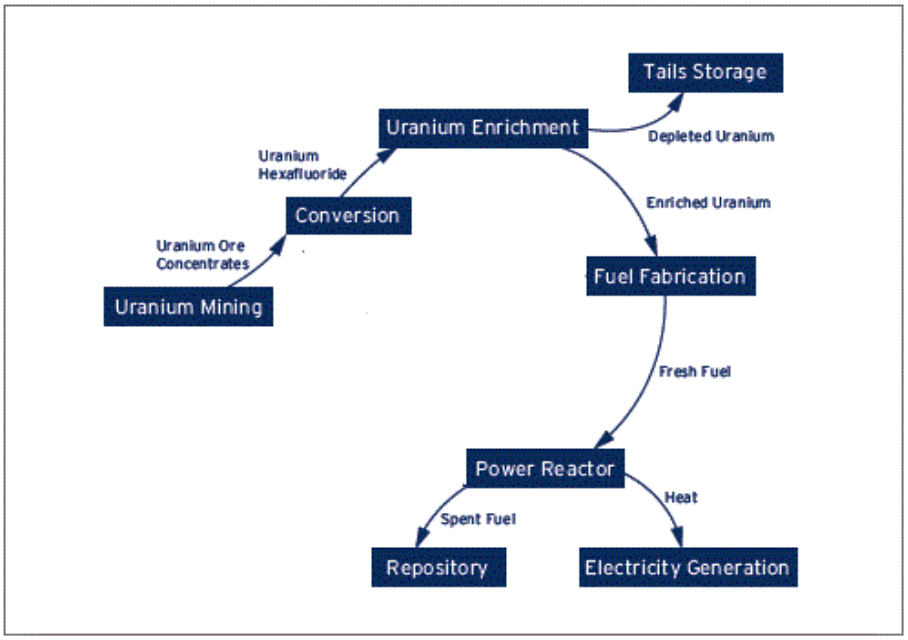

Figure 1.2 Schematic representation of various processes in Open Fuel cycle [1]

When the irradiated fuel is reprocessed to allow the uranium and plutonium to be subsequently converted into new fuel and recycle to a new reactor, this scheme is called the closed nuclear fuel cycle (figure 1.1) [1, 2].

When reprocessing is not carried out but the irradiated fuel is stored for an interim period in engineered, usually concrete structures and then finally treated to ensure minimal environmental impact prior to disposal in a purpose constructed repository this scheme is called the open fuel cycle (figure 1.2) [1, 2].

1.1.1 Uranium mining

Uranium is a relatively abundant element in the earth's crust some 500 times more abundant than precious metals such as gold and as common as tin [1]. Uranium exists in several geological forms such as pitchblende, carnotite, tyuyamunite, torbernite and autunite and locations Australia, Canada, S Africa, Kazakistan etc. [1]. It is present in rocks, sediments, sand/soil, and in seawater (3 ppb). It is extracted from the earth's crust by:

1 Underground mining

2 Open cast mining

3 In situ leaching

Both underground and open cast mining have several similarities with the UK's coal mining industry of the 1990s. In underground mining, the ore body will normally contain 500 to 1000 ppm uranium and is extracted by mechanical means but process operatives are present and therefore they have to be protected from radioactive dust and gases such as radon and hence adequate ventilation is necessary [1]. Ventilation is not a significant factor in open cast mining as the uranium ore is extracted using massive diggers and excavators, which gouge huge basins into the earth. In both cases, the excavated ore body is transported from the mine to the mill where it is crushed producing particles of about 200 microns to assist the sulfuric acid leaching of uranium from the ore body [1]. The leaching process uses hot sulfuric acid of pH around 1.0, which produces uranyl sulphate solution containing many other elements and a leached ore body that are separated. The ore body now depleted of uranium is sent to the tailings dam. The uranyl sulphate liquor is processed to recover and purify the uranium using either ion exchange and/or solvent extraction technology. The purified uranium is precipitated from solution as a diuranate of sodium, ammonium, calcium (depending on

which alkali has been used). The diuranate is filtered and the solid calcined to produce uranium ore concentrate or yellow cake before being shipped to the refinery [1].

In-situ leaching is used when the geology of the ore body is appropriate, generally a sandy type, with the area devoid of natural water courses; no mechanical extraction is used simply pumping the sulfuric acid through the sandy soil to liberate the uranium as uranyl sulphate, which is purified and treated as per mined uranium. Currently the majority of uranium is recovered by in-situ leaching [1].

1.1.2 Conversion

The uranium from the mining site is shipped to the refinery in 300 kg quantities (in 200 l mild steel drums) where it undergoes further purification. The uranium from the mine is still not sufficiently pure to be converted into reactor fuel i.e. it is not of reactor grade [3]. The uranium ore concentrate will contain uranium that is about 95% pure but still contains thorium, radium, several various transition metals such as V, Mo Cr and neutron poisons such as Hg, Cd, and B ions [3]. All these named elements have to be removed as they will either follow the uranium through the process conversion stages and arrive in the uranium hexafluoride (UF_6) or will impinge on the nuclear chain reaction in the reactor.

The purification of the uranium in the UOC (Uranium Ore Concentrate) is accomplished by first dissolving in hot 60% nitric acid to produce a uranyl nitrate /nitric acid solution (~350 g U/l) which is contacted with 20% v/v TBP/OK (Tri-Butyl Phosphate in Odourless Kerosene, BNFL system). The solvent extraction circuit produces a uranium of greater than 99% purity [3]. The purified uranyl nitrate (~110g U/l) from the solvent extraction circuit is first evaporated to produce 1100g U/l solution, which is then thermally denitrated to produce UO_3, reduced to UO_2 with hydrogen, then reacted with anhydrous HF to produce UF_4, and finally reacted with fluorine gas to produce uranium hexafluoride (figure 1.3) [3].

The UF_6 is of natural U isotopic composition i.e. 99.3% U-238 and 0.71% U-235 [3]. Reactors these days require enriched uranium i.e. uranium with a U-235 content greater than 0.71%, usually 2.5 - 4.5 % of U-235. To achieve this higher U-235 content the UF_6 is shipped in specially designed cylinders to the enrichment plant [3].

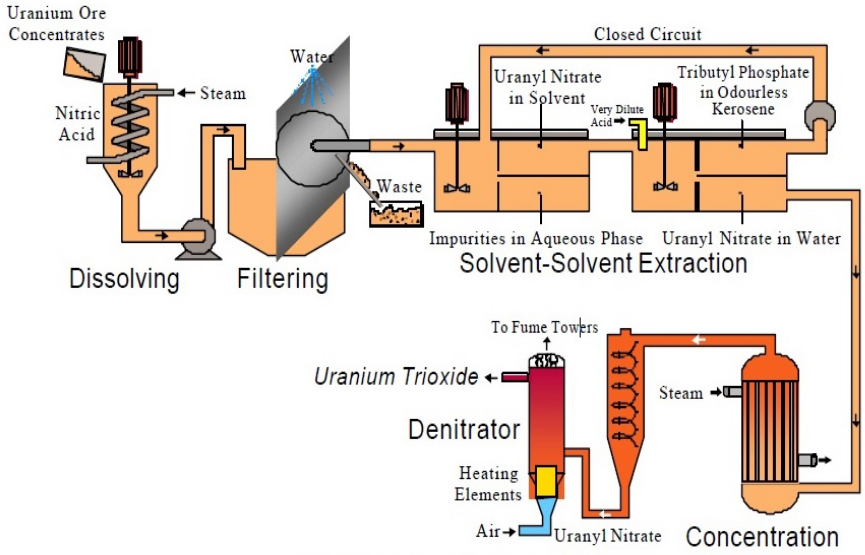

Figure 1.3 Processes involved in Uranium purification [3]

1.1.3 Uranium enrichment

UF_6 can exist as a liquid, solid and gas simultaneously (triple point 64 ˚C). It is the latter that is important for the enrichment process. The UF_6 is vaporised from the cylinders and passed into the enrichment process, which these days is based on centrifugation. Although the mass difference between U-238 and U-235 is small ($^{235}UF_6$ is only 0.852% lighter than $^{238}UF_6$) by subjecting the uranium hexafluoride to numerous separation stages the two isotopes can be separated and U-235 subsequently enriched to the required value for the particular reactor system e.g. AGR, PWR, BWR. As U-235 is being enriched in some UF_6 then some UF_6 is being depleted of U-235 i.e. depleted uranium [4].

The enriched UF_6 is now contained in smaller diameter cylinders awaiting shipment to the fuel fabrication facility. The depleted UF_6 is returned to the same size cylinders that contained the natural UF_6 and is stored as currently there are few uses for depleted uranium [4].

1.1.4 Fuel fabrication

After enrichment, the uranium hexafluoride (UF_6) with a U-235 enrichment greater than 0.71% is sent to the fabrication facility to convert UF_6 to ceramic UO_2 pellets (figure 1.4) [5]. First, the enriched UF_6 is vaporised to exit from the cylinder and reacted with steam and hydrogen to produced powder UO_2, which is granulated to helping pressing and pressed into pellets before sintering at 1800 ˚C to produce the fuel pellet [5]. Depending on the type of reactor, e.g., gas cooled AGR or water-cooled PWR the pellets are contained in either stainless steel or zircaloy tubes (pins) respectively [5].

The pins now containing many pellets are sealed and then subjected to an external pressure to squeeze them onto the pellets to ensure good heat transfer and prevent pellet rattling whilst in the reactor. Further, they are assembled into a cylindrical formation inside a graphite sleeve for AGR reactors and into a square assembly for PWRs. The assemblies are transported to the reactor site.

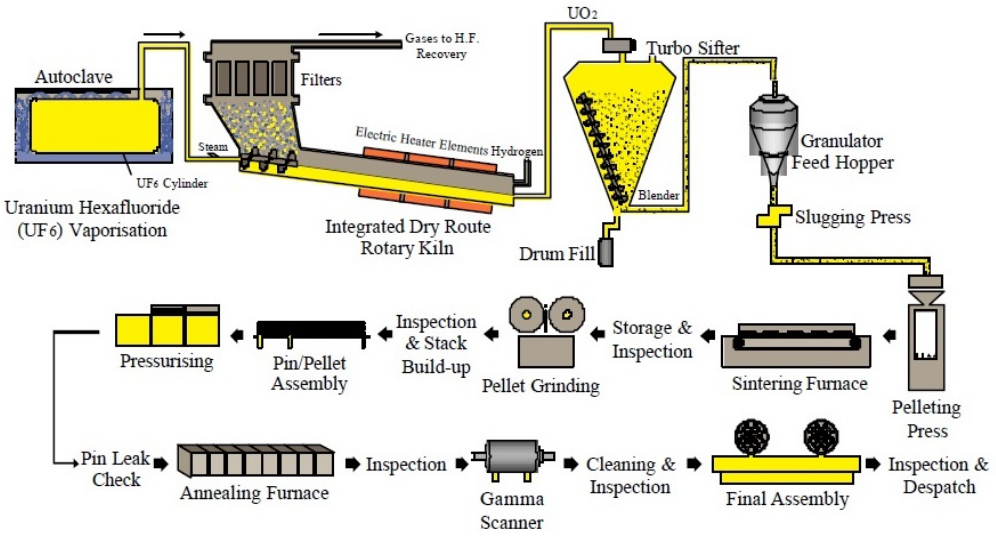

Figure 1.4 Schematic representation of processes involved in UO_2 production [5]

1.1.5 Power generation

A few hundred-fuel assemblies are needed for the initial load (~250 te of U depending on the size and type of reactor). In the reactor, the fuel undergoes several changes.

During its time in the reactor, the fuel (rods, pins) is subject to important physical and composition modifications due to the neutron irradiation:

- The fissile material content (U-235 or Pu-239, Pu-241) decreases progressively by fission.
- Accumulation of new elements in the fuel, resulting from the chain reaction progress
  – Transuranic elements (Np, Am, Cm),
  – Fission Products (Sr, Cs, Tc etc.) some of them are neutrons poison such as Gd.
- The fuel composition changes due to the strong heat released by fission, provoking important changes in the physical state of the fuel.
- Crystals structure modifications (holes or concentrations of atoms)
- Variation of the volume:

– The volume occupied by the atoms created by fission is greater than the one of the disappeared matter.
– Moreover, some fission products are gaseous and their solubility in uranium is practically non-existent

All of these changes will alter the physical properties and the structure of the fuel with modifications of the thermal, mechanical, dimensional characteristics. Consequently, the cladding can deteriorate which can result in the formation of cracks or even break [6].

This implies that, after a certain period of irradiation time, it is necessary to take the fuel out of the reactor due to decrease in the content of fissile material, progressive poisoning of the fuel, and risk of cladding break [6].

In the reactor, the U-235 isotopes undergo fission due to neutron bombardment to produce fission products, energy, and more neutrons (chain reaction) whilst the major U isotope U-238 adsorbs one neutron to transmute to U-239, which by two sequential β decays produces Np-239 and then Pu-239, which is a fissile isotope that produces fission products, heat and more neutrons [6].

When the fissile energy has decreased and it is no longer cost effective to leave the fuel in the reactor it is removed, stored under water at the reactor site to allow the very short-lived fission products to decay before transport to a reprocessing plant or remains on the reactor site for subsequent storage either wet i.e. in ponds or in concrete casks/silos.

This initial storage period could be about one year to three years depending on the type of fuel, burn-up etc. Depending on the country's spent fuel management strategy the fuel can be either:

1 Reprocessed,
2 Direct disposal,
3 Interim storage awaiting a decision if to reprocess or dispose.

For this research, we are considering option 1 only.

1.1.6 Reprocessing

Reprocessing is currently practised for commercial irradiated fuel by France, UK, Russia and Japan, the latter is awaiting the commissioning of its Rokkasho reprocessing plant in 2016 [7]. The UK government has declared that reprocessing at Sellafield will

cease after 2018, which will result in about half of the current reprocessing capacity being removed from the market, leaving only about 2,500 te capacity available worldwide [7]. The US has reprocessing capacity but adopted years ago not to reprocess irradiated fuel from civil reactors and its strategy is one of delayed storage and/or direct disposal.

Reprocessing is undertaken to:

- Conserve natural resources, e.g. uranium,
- Optimise waste management and disposal conditions,
- Minimise environmental impact,
- Improve fuel cycle economics,
- Improve proliferation resistance

The reprocessing of irradiated fuel uses a tested and well-documented process, PUREX (**P**lutonium **U**ranium **R**edox **Ex**traction). The objective of the reprocessing operation is to separate U and Pu from fission products (FPs) and minor actinides (MAs) such as Np, Am and Cm so that the U and Pu can be converted to new fuel and recycled (figure 1.5) [7]. This reprocessing results in other benefits such as better waste management, particular for the final disposal repository.

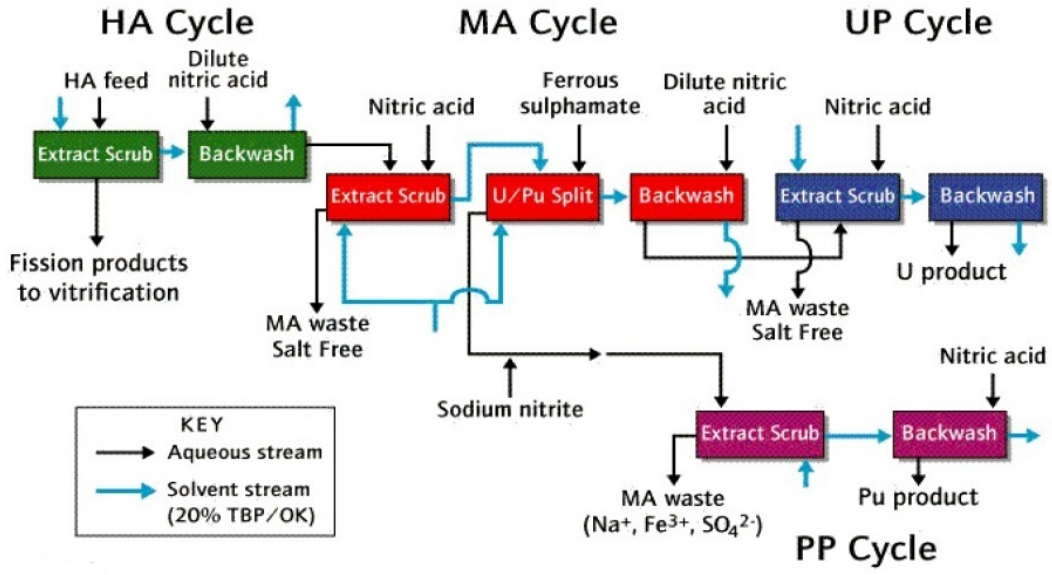

Figure 1.5 Multistage extraction process during reprocessing [7]

The separation of U, Pu, FPs, and MAs is achieved by first dissolving the ceramic pellets in hot nitric acid to produce a ~350 g U/l and ~3 g Pu/l and ~3 M nitric acid solution. This solution is subsequently contacted with 30% TBP/OK in pulsed columns to separate the U and Pu from the other radionuclides; the two actinides are extracted into the solvent phase leaving the remaining radionuclides in the aqueous phase [7]. This latter phase is the high active waste discussed latter. The recovery of the Pu from the solvent phase is achieved by manipulating its oxidation state; TBP's affinity for Pu depends on its oxidation state, TBP has no affinity for the Pu (III) oxidation state but a moderate affinity for Pu (IV and VI). The reducing agents do not affect the uranyl ion (VI) and this is recovered from the solvent phase by adjusting the nitric acid conditions (~0.01 M) and at a slightly elevated temperature (~60 $^{\circ}$C) [7]. Both U and Pu undergo further purification separately again using a solvent extraction process based on TBP/OK to produce very pure U and Pu nitrate solutions that are subsequently converted to UO_2 and PuO_2 by thermal denitration and precipitation as oxalate followed by calcinations respectively. The final oxides can be blended to produce MOX fuel.

1.1.7 Waste management

Solid, liquid, or gaseous wastes arise at all stages of the NFC in varying and significant amounts, which require treatment before being discharged under strict control and authorisations into the environment. Specific to the nuclear industry is further categorisation particular for solid and liquid wastes such as: high-level waste (HLW), intermediate-level waste (ILW), low-level waste (LLW), and now very low level waste (vLLW) [7]. The latter was introduced to accommodate the large quantities of wastes that will arise from the decommissioning of nuclear facilities, plant, and equipment in the next several decades worldwide. The distinguishing features of these other categories (HLW, ILW, and LLW) are:

- **High Level Waste (HLW)**

High Level Waste is heat-generating waste that has been generated primarily from the reprocessing of spent nuclear fuel [8]. The temperature of HLW may rise significantly and as a result, this factor has to be taken into account when designing storage or disposal facilities.

Less than 1% of all radioactive wastes (by volume) are in the HLW category. HLW only arises in a liquid form but is converted into a solid product through a process called 'vitrification' [8]. It is generated as a by-product during the reprocessing of spent fuel from nuclear reactors.

- **Intermediate Level Waste (ILW)**

ILW is waste with radioactivity levels exceeding the upper boundaries for Low Level Waste (LLW), but which does not need heating to be taken into account in the design of storage or disposal facilities [8].

About 6% of all radioactive wastes (by volume) are in the ILW category [8].

ILW can be any material that has been activated or contaminated by radioactivity. ILW may be solid wastes, or in the form of sludges and effluents. ILW arises mainly from the reprocessing of spent fuel, and from general operations, maintenance, and decommissioning of radioactive plant.

- **Low Level Waste (LLW)**

LLW includes radioactive wastes which are not suitable for disposal as ordinary wastes, but only have low levels of radioactivity i.e. < 4 GBq/m^3 of alpha activity and < 12 GBq/m^3 of beta/gamma activity [8]. About 94% of all radioactive wastes (by volume) are in the LLW category [8].

LLW can be any material that has been activated or contaminated by radioactivity. LLW may be solid wastes, or in the form of sludges and effluents.

The front end of the nuclear fuel cycle generates largely LLW during the day to day operations; ILW is largely associated with post uranium conversion stage and HLW is exclusive to the reprocessing operations but also to reactors if interim storage and/or direct disposal is practised for irradiated fuel. HLW represents ~1% of the total waste generated by NFC operations but accounts for >99% of the radioactivity [8]. It therefore requires special and unique attention when considering treatments and disposal options.

1.1.8 Advanced reprocessing

The next fleet of nuclear reactors to be constructed worldwide will be the third generation (GEN III) thermal reactors i.e. moderated neutrons, and will be largely pressurised water reactors [7]. The fuel in these reactors will operate at slightly higher enrichments (~3.5%) and at significant higher burn-ups and for longer time periods (at least 60 years) [7]. Some of the irradiated fuel from these reactors will be reprocessed, particularly for France, but the majority (>90%) will be either stored or sent for direct disposal when a suitable repository is constructed.

Advanced reprocessing is targeting the next generation of reactors (GEN IV), fast neutron reactors such as the fast reactors [7]. For this generation of reactors even more attention will have to be paid to waste management in particular reducing the impact of HLW. To achieve this a new advanced reprocessing concept (partitioning) is under development that will not only separate the U and Pu for recycle but also FPs and the lanthanide elements and MAs so that these can be fabricated into fuels and placed in a reactor (likely to be a fast breeder) to allow transmutation of the radionuclides into others which have much shorter half-lives i.e. reduced to a few years from $>10^4$ years [7].

Two well-known extractants with different properties are combined in one diluent system:

1. *bi*-Terpyridine *bis*-Pyridine or BTBP**,** known to extract trivalent actinides and separate them from the trivalent lanthanides. This is used to extract pentavalent actinides (figure 1.6) [7].

Due to strong acid and irradiation, a stable BTBP is needed: CyMe4-BTBP

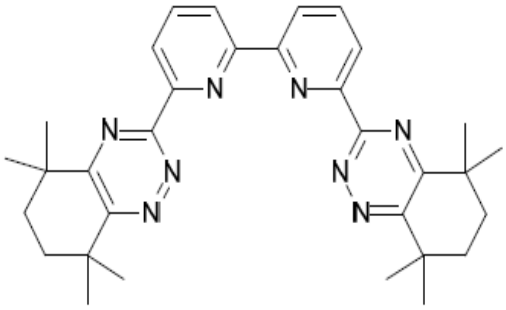

Figure 1.6 Structure of CyMe4-BTBP [7]

2. Tri-Butyl Phosphate or TBP; known to extract tetra- and hexavalent actinides (PUREX process) (figure 1.7) [7].

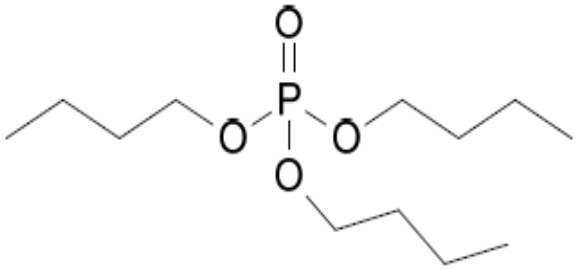

Figure 1.7 Structure of TBP [7]

Combining processes 1+2, there is no need to adjust actinide oxidation states

This will be achieved by extending the current PUREX process by adding on downstream other solvent extraction technology such as:

- **G**roup **A**cti**N**idE **EX**traction (GANEX) is a two extractant system aimed at replacing PUREX, without the separation of uranium and plutonium, i.e. more proliferation safe – no pure plutonium stream (Homogenous) (figure 1.8) [8]. The aim is to extract all the actinides as a group directly from dissolved used fuel.

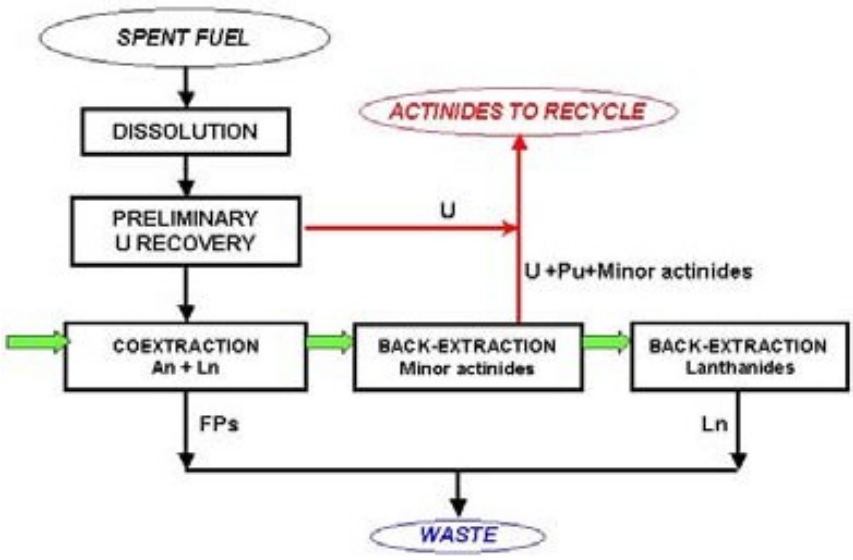

Figure 1.8 GANEX process [7]

- DIAMEX/SANEX; this uses a Modified PUREX process upstream of the DIAMEX/SANEX solvent extraction circuit (figure 1.9). The main differences in the modified PUREX compared with the standard are:

- A specific Tc scrubbing cycle is incorporated
- Co-extraction of Np with Pu and U

Co-extraction of actinides and lanthanides using DMDOHEMA;

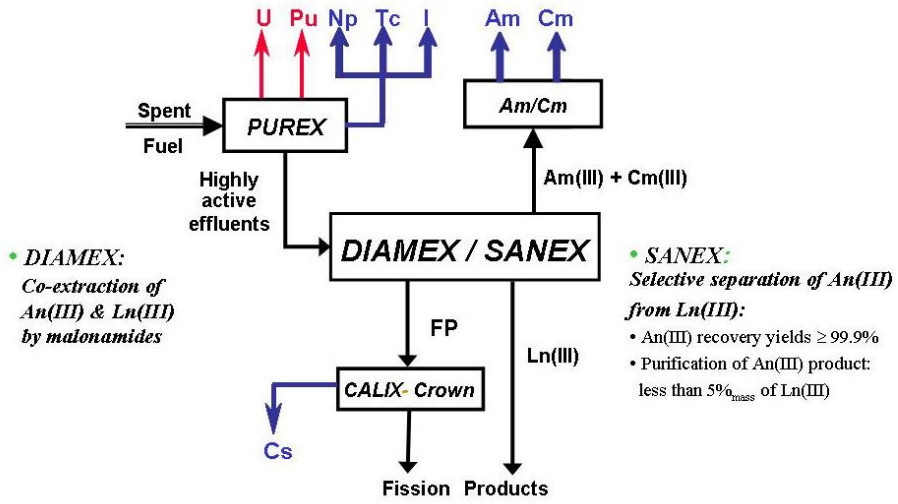

Figure 1.9 DIAMEX/SANEX process [7]

It is the development/introduction of GEN IV reactors systems, which offers an opportunity to reconsider the sustainability of the PUREX process.

1.2 UCLan's concept of advanced reprocessing

Although well proven and predictable, the PUREX process is not without its challenges. The generation of significant quantities of highly active aqueous liquid, containing Fission products (FPs) and Minor actinides (MAs), the degradation of the solvent phase reagents and non-specific nature of the extractant Tri-Butyl Phosphate (TBP) may have contributed to only a fraction of the total annual output of irradiated fuel being reprocessed. The PUREX process or really the lack of specificity of TBP requires strict control of process conditions (flow sheet parameters) to ensure the decontamination of uranium and plutonium are achieved. In addition as the bulk of the heavy metals (U and Pu isotopes) are extracted from the aqueous phase into the organic phase requires appropriately sized, large, contactors.

It is the future nuclear waste management considerations coupled with a renaissance of reactor build that will promote greater reprocessing of irradiated fuel. To date (2016) about 90,000 te of fuel have been reprocessed of 290,000 te discharged from commercial power reactors; based on current reactors and projected reactor installations between now and 2030 some 400,000 te of used fuel will be generated worldwide [7]. By this date (2016), the PUREX process will be entering its ninth decade, certainly mature technology but could it be passed its 'sell by date'? Any new process must overcome the PUREX challenges as well as offering some distinct advantages as both regulators and operators have become acclimatised to sixty-year-old technology.
The concept developed at the University of Central Lancashire [9] is a radical departure from PUREX and will offer many advantages as described later. It is based on the separation of FPs and MAs from uranium and plutonium isotopes using Continuous Chromatographic (CC) separation.

Chromatography comprises of two distinct components:

1. The mobile phase, and
2. The stationary phase

In developing an alternative to the PUREX process, both components will require significant effort.

1.2.1 Mobile phase

The composition of the mobile phase will be dependent on the upstream operations, i.e. dissolution and downstream, post separation circuit requirements such as waste management. At this stage of the development of this alternative PUREX process, a nitrate base system is under consideration, but this does not exclude other aqueous systems. Nitrate based systems have several advantages, for example:

- UCLan's technology could fit upstream to a PUREX process, having removed a significant radiation source (Cs and Sr) thus reducing solvent degradation
- Recovery of uranium as an oxide is relatively easy by thermal denitration.

As discussed later the concentration of U and Pu of the separation process feed liquor will not dominate the continuous chromatography process conditions unlike the PUREX process.

The head-end operations of the PUREX process involve the de-cladding of the irradiated nuclear fuel which is then dissolved in hot acid (nitric acid preferred but

sulfuric acid could be considered in the UCLan process) to produce a uranium solution of 100 – 300 g/l concentration with a free acidity of about 3 M (UCLan process will consider 0.5 - 3 M acidity). At this uranium concentration, some of the more important Fission products (FPs) and Minor actinide (MA) concentrations are reported in table 1.1; these concentrations are based on a typical irradiated PWR 3.5 % U-235 fuel with a burn up of 33 GWd/t HM, cooled for 3 years.

Table 1.1 Dissolver liquor concentrations [10]

Radionuclide	**Approximate Concentration (g/l)**
U	300
Y and lanthanides	3.5
Pu	3.2
Ru, Rh, Pd	1.3
Zr	1.2
Mo	1.1
alkali metals (Cs, Rb)	1
alkaline earth metals (Sr and Ba)	0.9
Tc	0.260
Am	0.200
Np	0.150
Se and Te	0.150
Ag, Cd, Sn. Sb	0.030
Cm	0.007

1.2.2 Stationary phase

A vast number of stationary phases have been developed for chromatographic separations but few, if any for nuclear reprocessing applications [11]. Both organic and inorganic ion exchangers have been used in chromatographic separations largely for nuclear waste management applications [12]. These exchangers have included

conventional polystyrene-divinely benzene copolymers with sulphonic acid groups, but the greater number has involved inorganic materials such as zeolites, hydrous oxides, titanates, phosphates, and silicates. Some have demonstrated very good separation factors for Cs and Sr from other radionuclides in highly active liquors [13, 14]; however, such liquors are depleted of uranium and plutonium isotopes, i.e. the major heavy metals.

The separation of FPs and MAs will rely heavily on the selection/development of appropriate stationary phases; it is highly unlikely that a single stationary phase will be appropriate for all FPs and MAs. The three major characteristics that the stationary phases should exhibit are:

- Stability to radiation
- Acid stability, and
- High selectivity for the FP and/or family of FPs and for a specific MA or family of MAs.

The other, secondary, properties of the stationary phases are:

- Availability
- Cost
- Durability i.e. low attrition
- Appropriate physical properties such as size, density, porosity, surface area etc.
- Appropriate chemical characteristics such as fast kinetics, reversible extraction, medium/high capacity for the appropriate radionuclide/s, etc.

As the stationary phase will be subjected to high radiation fields whilst in contact with the dissolver liquor, and will increase as the radionuclide concentration of the stationary phase increases (i.e. the radionuclide/s will be concentrated when extracted by the stationary phase), it is unlikely that organic materials will be suitable due to radiolytic damage. This radiolytic damage will be true for certain FPs (high-energy gamma emitters), but not all (low-energy gamma emitters). This damage could be reduced/removed by first separating the offending radionuclides onto an appropriate stationary phase (stages 1 and 2 of figure 1.10) [9]. It is extremely unlikely that the stationary phases will be sufficiently effective to accomplish isotopic separation of a particular radionuclide and therefore in stage 1 short, medium and long-lived isotopes of a specific radionuclide will be removed. Thereafter for stage 3 and 4 organic polymeric

materials could be employed that have been functionalised with the appropriate ligand. Each stage is likely to involve more than one stationary phase for specific radionuclides.

Each stage will consist of a series of columns or other contactor devices connected in series as illustrated in stage 1 (figure 1.10) [9]. For stage 1 and likely for stage 2, the first choice stationary phase could be based on modified silica, metal oxides, titanates etc. as these could satisfy most of the above conditions.

In subsequent sections some of these stationary phases under consideration, particularly their preparative routes, are described in more detail.

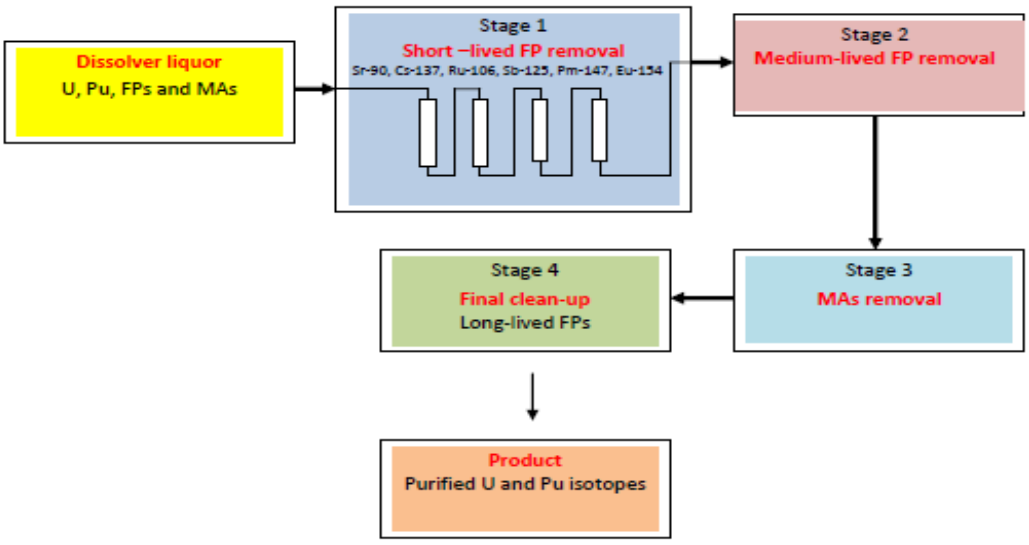

Figure 1.10 Proposed separation stages in UCLan's concept [9]

1.3 Continuous Chromatography

Chromatography is one of the most relied upon technologies available to engineers and scientists in a variety of fields that include pharmaceuticals, forensics, environment, and energy. It has found uses in a wide range of applications where the separation of compounds would be incredibly difficult, prohibitively costly or due to the chemistry involved, impossible by other means. Continuous Chromatography is based on the principle of multiplication of single-stage separation factors by arranging the separation medium such that the products of one separation stage directly feed additional stages, thus significantly enhancing the degree of separation obtained (figure 1.11) [17]. The physical arrangement usually employed is to put the separation medium (typically an ion exchange resin) in a vertical column [15]. The feed solution enters from the top or bottom of the column where it attaches to the exchange sites of the resin. The

chromatographic process occurs as the ions to be separated are eluted preferentially through the column with a carefully chosen eluent.

The single biggest challenge associated with chromatography has always been the inability of the technique to scale up from the laboratory scale to an industrial process; the major limiting factor being the continuous throughput ability of the technology [16].

To counter this issue, a number of attempts have been made towards developing a continuous chromatographic system. These have included; moving and approximated moving beds, counter flow, annular beds, radial flow, and disk chromatographic systems [15]. However, wide spread industrial use of these techniques is rare even within biological and organic applications and virtually non-existent in inorganic separations, in particular nuclear reprocessing.

The first mention of continuous chromatography in the literature is attributed to Martin [16], who envisaged methods to move chromatography into the large scale, i.e. an industrial separation technique. The author described two methods in which this may be achieved which generally persist today; the first is a moving bed configuration in which the stationary phase is forced against the flow of mobile phase within a thin tube. If the mobile and stationary phase flow rate were balanced correctly, components with higher affinity for the mobile phase would be carried further with this than the stationary phase. Movement of the mobile phase is inherently plagued with hydrodynamic challenges; to overcome them a certain number of fixed beds are connected in series to form a closed loop, and the counter-current movement of the solid and liquid phase is simulated by periodically shifting the fluid inlets and outlets in the direction of the fluid flow i.e. Simulated Moving Bed (SMB) [17]. An example of a laboratory SMB reactor is shown in Figure 1.11.

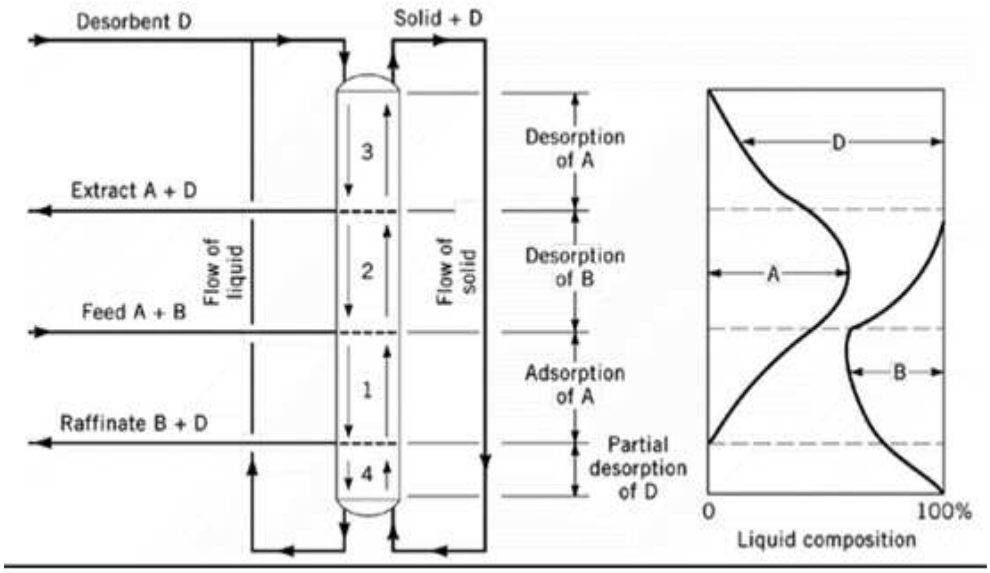

Figure 1.11 Schematic representation of moving bed separation technique [17]

The other idea was continuous annular chromatograph (CAC); it employs continuous feed and separation of several species simultaneously. The innovation is embodied in equipment that permits continuous feed and separation of chemical species on an apparatus consisting of an annular bed of adsorbent particles. The apparatus is rotated slowly about its axis while eluent and feed solution are fed into one end of the bed. Eluent is fed to the entire bed circumference while the feed mixture is introduced into a narrow sector of the circumference at a single point. Helical component bands develop with the passage of time extending from the feed point, with slopes dependent on eluent velocity, rotational speed, and the distribution coefficient of the component between the fluid and sorbent phases. The separated components are continuously recovered once steady state is attained as they emerge from the annular column, each at its unique position on the circumference of the annular bed opposite the feed end (figure 1.12) [19]. Separations can be carried out with simple or gradient elution, wherein the eluent concentration is changed [18].

Figure 1.12 Continuous annular chromatography [19]

Current developments have largely concerned biological separations based on simulated moving bed (SMB), although there have been attempts to further promote CAC for both organic molecules (biotechnology and protein separations) and on a limited scale inorganic ions (metal) [19]. The practical applications, which have been reported generally, give very encouraging results with good separation and efficiencies equivalent to that of conventional batch chromatography [20].

1.4 Potential Stationary Phases

1.4.1 Natural Ion Exchangers

There are wide range of materials thoroughly researched but only few of them are commercially available. Only some inorganic, organometallic, organic type of materials have been described in this thesis as they have some of the required stationary phase properties; Materials that are not suitable are pharmaceutical ion exchange gels and liquid ion exchangers. There are different solid materials, which could be considered as a stationary phase as they function as ion exchangers and/or adsorbent.

1.4.1.1 Natural Inorganic Ion Exchangers

Many natural compounds such as clays (e.g. bentonite, kaolinite, and illite), vermiculite, and natural zeolite (e.g. analcite, chabazite, sodalite, and clinoptilolite) have shown some ion exchange properties.

A short review was studied on application of natural zeolites for environmental remediation, which focused on use of clinoptilolite type of natural materials for

immobilization of radioactive caesium isotopes [21]. British Nuclear Fuels Limited. (BNFL) was the first organisation in the UK to make use of clinoptilolite to remove caesium and strontium from cooling pond water in the Sellafield Ion Exchange Effluent Plant (SIXEP) [22]. The removal of radioactive Cs-137 and Sr-90 isotopes using clinoptilolite from the environment post Three Mile Island and Chernobyl nuclear accidents and for the decontamination of waters was evaluated. The review also stressed their potential importance for the removal of heavy metals (e.g. Fe, Pb, Cd, Zn) from acid mine drainage [23].

A different comparative study on natural zeolites such as clinoptilolite, chabazite, and mordenite was performed for their caesium uptake in low-level radioactive liquid waste with consideration of key parameters such as solution pH, contacting time, potassium ion concentration, waste solution volume/sorbent weight ratio and Cs ion concentration. The study concluded that natural chabazite had the highest distribution coefficient and capacity for Cs ion compared to others [23].

Another very interesting batch sorption study was conducted in Turkey for the treatment of radioactive liquid waste using natural zeolite, which focused on use of clinoptilolite for removal of Cs, Co, Sr, and Ag ions from radioactive low-level waste [24]. The study revealed that clinoptilolite had high selectivity for Cs and Ag ions. It also concluded that in the absence of potassium ions, it could potentially remove Co^{2+} and Sr^{2+} efficiently from the waste at pH value 6 to 10 [24]. General properties of this type of material are summarised in Table 1.2 (page 47).

1.4.1.2 Natural Organic Ion Exchangers

There are number of organic materials available with varied ion exchange properties such as polysaccharides (cellulose, algic acid, straw, and peat), proteins (casein, keratin, and collagen) and carbonaceous materials (charcoals, lignites, and coals) [25 - 32]. Although these materials have low ion exchange properties, they were nonetheless still evaluated as potential sorbents. General properties of these types of material are summarised in Table 1.2 (page 47).

1.4.2 Synthetic Ion Exchangers

Synthetic ion exchangers can be inorganic or organic polymer based materials, which are produced by varying process parameters such as nature of the chemicals species, altering pH, temperature, pressure, and use of catalysis etc.

1.4.2.1 Synthetic inorganic Ion Exchangers

1.4.2.1.1 Molecular Sieves and Zeolites

Molecular sieves are generally porous solids with pore size of 0.3 - 2 nm in diameter, which are commercially mass produced for various applications. Zeolites, carbons, glasses, and oxides are a few examples of such materials. Zeolites represents the majority of molecular sieves in general.

Zeolites are crystalline aluminosilicate based materials that can be classified based on Si/Al composition. There are four categories in general: (i) Low silica, (ii), Intermediate, (iii) High silica, and (iv) Silica molecular sieves.

They are represented by empirical formula:

$$M_{2/n}O.Al_2O_3.{}_ySiO_2.{}_wH_2O$$

Where $_y$ is 2-200,

M is the cation

$_n$ is the cation valence,

$_w$ is the water contained in the voids of the zeolite

Zeolites are structurally complex crystalline inorganic polymers extended in three-dimensional, four connected frameworks of AlO_4 and SiO_4 tetrahedra bridged to each other by sharing oxygen ions. Each AlO_4 tetrahedron in the framework bears a negative charge, which is balanced by the extra framework cations. The whole zeolite framework contains crystalline channels that are occupied by cations (e.g. Na, K, Ca etc.) and water molecules. The cations in the voids can undergo ion exchange and water may be removed by heat. The crystalline channels can be one, two, or three-dimensional.

There are more than 70 known and distinct framework structures of zeolites [33, 34]. Zeolite structures are made up of Aluminium oxide or Silicon oxide tetrahedra, assembled into secondary building units, which may be polyhedral such as cubes, hexagonal or octahedral.

The pore size of zeolites varies from 0.3 - 1 nm and pore volumes from about 0.10 - 0.35 cm^3/g [33, 34]. Typical pore size includes:

(i) Small pore with eight ring pores; diameters of 0.3 - 0.5 nm (Zeolite A),
(ii) Medium pore with 10 ring; pores size of 0.6 - 0.8 nm (ZSM-5),
(iii) Large pore zeolite with 12 ring; pore size of 0.6 - 0.8 nm (zeolite X, Y)
(iv) Extra-large pore with 14 ring pores (UTD-1)

(i) Preparative routes for synthesis of zeolites and molecular sieves

There are numerous publications available from International Zeolite Association for the different strategies and preparation routes for Zeolites. They are far too extensive to summarise all of them in the thesis and hence, this chapter focuses on general and commonly used commercially available zeolite synthesis and factors that are important during synthesis.

Typical aluminosilicate zeolite synthesis includes silica as feed material in the form of sodium or other alkali silicate solutions, precipitated, colloidal, or fumed silica or tetraalkylorthosilicate (alkyl = methyl or ethyl) and certain mineral silicates such as clay and kaolin. Alumina is in the form of sodium aluminate, aluminium sulphate solution, hydrous aluminium oxide, aluminium nitrate, or aluminium alkoxides. High purity reagents are frequently used. In general, water is used as solvent to solubilise all the primary oxide components. The two solutions (Si and Al) are mixed together with controlled agitation that results in the zeolite gel. Depending on the desired zeolite, sometimes the gel is aged at mild temperature to allow initial nucleation of the system. The mixture is then digested in a stainless steel autoclave at higher temperature (between 50 - 200 °C for a specific period (usually 3 - 7 days) until the desired level of product crystallinity is obtained. The digested zeolite gel is washed with sufficient amount of distilled water and then air dried subsequently.

(ii) Important factors during synthesis

The order of mixing various reagents into the gel stage can be critical. One order of mixing may give a coarse slurry while a reversed order of mixing the same reagent may give a thick gel.

The agitation speed of the reaction mixture may result in undesired phase due to non-uniform nucleation conditions, which can promote potentially an amorphous structure,

or particulate material, or unexpected morphology. The method of heating a reaction mixture can also be a critical factor.

Water stoichiometry in a resulting gel can be critical to produce desired phase and crystal size and product morphology. Water solubilizes the reagent mixture to a different degree, develops the concentration and pH, which influence the nature of the framework, and aids in ultimate stabilisation of the crystalline microporosity by coordinating with charge balancing cations in the final product and by void filling part of the resulting microporosity.

The final pH is also very critical factor during synthesis, since hydroxide ions are involved into fulfilling mineralizing and complexing role in crystallization.

Filtration and washing of zeolites can also be very important step during zeolite synthesis. The aim of this step is to separate crystalline products from mother liquor and washing of the material for further use. It is important to note that over washing results into decationisation, which involves replacement of cations with H_3O^+. This may affect the product efficiency in various applications. General properties of inorganic resins are summarised in Table 1.2 (page 47)

1.4.2.1.2 Advanced Synthetic zeolites

Numerous synthetic zeolites have been studied and many review articles have been written. This section of the chapter has focused on materials with potential application to nuclear reprocessing.

(i) Crystalline SilicoTitanates (CST)

Silicotitanates are engineered to adsorb strontium ions from high alkaline nuclear wastes. The preparation method is similar to other zeolite preparation as mentioned previously where reaction mixture contains titanium source and a silicon source followed by hydrothermal treatment to allow these reaction mixtures to form silicotitanates composition. The titanium source is from titanium alkoxides, titanium halides, and titanium oxides. The silicon source could be silicon alkoxides, colloidal silica, silicon oxides, sodium silicates etc. [35, 36].

The advancement in silicotitanates affinity for important fission products such as caesium and strontium was achieved by preparing crystalline silicotitanates [36]. Further advancement includes incorporation of transition metals such as niobium to improve uptake of radioactive caesium and strontium in high acidic media [36].

(ii) Zirconium phosphates (ZrP)

Zirconium phosphates are another important type of zeolite for nuclear waste treatment due to their acidic nature, high thermal and chemical stability, resistance to ionizing radiation, and capacity to incorporate different type of metal ions with different sizes in their structure [37, 38]. The first characterisation of this kind of zeolite was performed by Clearfield and co-workers and subsequently their structure, ion exchange capacity etc. were studied [37]. Most of research focused on two type of zirconium phosphates; alpha (α) and gamma (γ) with formulas α-$Zr(HPO_4)_2.H_2O$, and γ-$ZrPO_4(H_2PO_4).2H_2O$ respectively [37]. Advancement of synthesis techniques and modifications were undertaken on this type of materials, which resulted in various applications in catalysis, nanocomposites, nuclear waste management, and drug delivery etc.

(iii) Ammonium phosphomolybdates (AMP)

This inorganic ion exchanger can be synthesised by heating ammonium molybdate in phosphoric acid and nitric acid. There are numerous examples of their application as a very strong caesium adsorbent in acidic media, a key feature for caesium separation in nuclear waste [39, 40]. The main benefit of this inorganic material is that it is soluble in solution pH value >4 and consequently it is most suitable for separation in acidic media. Captured caesium can be easily removed from the zeolite matrix by concentrated ammonium salt solutions (NH_4NO_3, NH_4Cl etc.) [41].

(iv) Transitional metal cyanoferrates

Cyanoferrates have been widely demonstrated by various research groups for their strong affinity for caesium in low pH from 1 - 5 [39, 42, 43]. Numerous attempts have been made to improve their ion exchange capacity by incorporating transitional metal ions such as nickel, cobalt, zinc etc. [42 - 45]

1.4.2.1.3 Mesoporous Inorganic Materials

The development of porous materials with large surface area and slightly larger pore size (larger then zeolites) is currently an area of extensive research, particularly with regard to potential applications in adsorption, separation, catalysis etc. An upsurge began in 1992 with the development of the class of periodic Mesoporous silica known as the M41S phase. This class of materials are characterized by very large specific surface areas, ordered pore channels, and well-defined pore size distributions [46 - 48]. Mesoporous materials have pore diameters from approximately 2 - 50 nm and exhibit

amorphous pore walls. The most well-known representatives of this class include the silica solids MCM-41 (Mobile Composition of Matter) which exhibits hexagonal structure; MCM-48, which is cubic, and MCM-50, which is a layered structure [46 - 48].

Figure 1.13 Schematic representation of M41S family, MCM-50 (Layered), MCM-41 (hexagonal) and MCM-48 (Cubic) [46]

The liquid crystal templating (LCT) mechanism was first proposed in 1991 by Mobile Corporation, in which use of surface directing agents such as surfactant micelles were used to form the mesoporous particles (figure 1.13) [47]. Since the evolution of these novel materials, there have been numerous studies to understand the templating mechanism. Templating is defined as a reaction in which organic species act as a mould on which oxide moieties organize into a crystalline lattice [46, 47]. Here, organic species are the templates and oxide moieties are the inorganic materials. Further, the templates in the structures can be removed which results into hollow inorganic crystalline structure [46, 47]. The typical mesoporous synthesis is generally carried out under high pH (9 - 11) where, cationic or neutral surfactant molecules, and anionic silicate species form hexagonal, lamellar, or cubic structures.

Figure 1.14 illustrates the mechanism where micelle forms a rod shaped micelle and self assembles into hexagonal liquid crystals (multiple rods) when they reach critical micelle concentration (CMC). Further addition of inorganic species (e.g. silicate etc.) form two or three monolayers of silica, which spontaneously pack on the outer surface of hexagonal liquid crystal [47]. Further calcination (burning) of these templates results into highly ordered hexagonal structure with cylindrical pores.

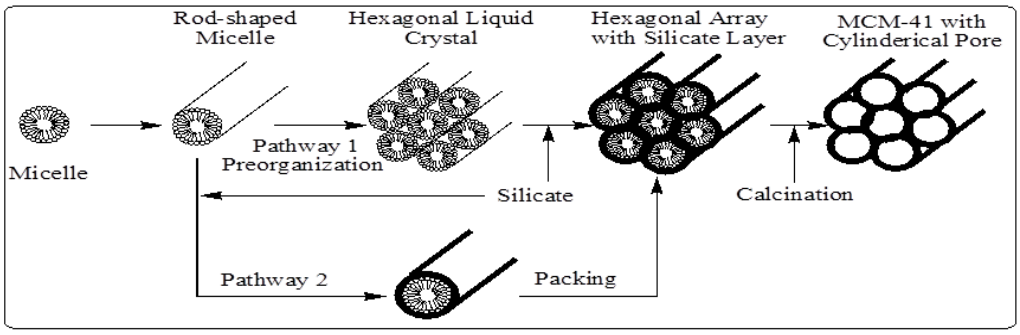

Figure 1.14 Schematic representation of liquid crystal templating mechanism of MCM-41[47]

Advancement in mesoporous materials

Due to their periodic ordered porous structure and high surface area, there are numerous ways to manipulate their structure for more suitable applications. Mesoporous materials are largely used in catalysis, separation, and adsorption purposes.

There are various ways these materials can be functionalised but here, the three most acceptable techniques are described suitable for nuclear applications.

(i) One pot-functionalisation; the functional entity such as organic or organometallic molecule, nanoparticles, or ions are mixed with the precursors of the matrix which is then directly incorporated into the framework during synthesis.

(ii) Grafting, where functional entities are anchored onto the surface of the voids via covalent or ionic interactions. Functional entities were mixed with matrix precursors

(iii) Last approach is the one incorporation of ions into a porous matrix with the hope that enough ions will be present at the surface of the pore.

Post synthesis grafting technique have been used very regularly in catalytic applications however, due to leaching effects of this method in harsh conditions, such as nitric acid its potential application is limited for nuclear waste separations [48].

1.4.2.2 Synthetic Organic Ion exchangers

These are the largest group of ion exchangers commercially available today for a variety of application. Their structure of is made of hydrocarbon chains, which are randomly networked. This flexible network carries ionic charge at various locations. Extensive researches resulted in an insoluble resin by cross-linking hydrocarbon chains.

The degree of cross-linking plays a very crucial role since it determines the mesh width of the matrix, swelling ability, ion movement, hardness, and mechanical durability [49 - 54].

The properties that influence ion exchange are:

- The solvent polarity,
- The degree of cross linking,
- The exchange capacity,
- The size and extent of the solvation of counter ions,
- The concentration of the external solution,
- The extent of the ionic dissociation of functional group

General properties of organic resins are summarised in Table 1.2 and the main groups of synthetic organic ion exchangers are mentioned below.

(i) Polystyrene divinylbenzene

This is the most common form of ion exchange resin available with a range of applications. This is based on co-polymer of styrene and divinylbenzene [51]. The degree of cross-linking is the most critical factor for their synthesis and it can be adjusted by varying the divinylbenzene content and expressed as the percentage of divinylbenzene in the matrix. Lowering the amount of cross-linking results in softer resins, which swell strongly in solvents [51].

The main advantage of this type of resin is that fixed ionic groups can be introduced in the matrices to create a cation and/or anion ion exchanger. A variety of cation and anion functional groups such as $–SO_3H$, $-NH_3^+$ or $–N_2^+$ where, H^+ and OH^- become mobile or counter ion respectively [51].

(ii) Phenolic

Phenolic resin is formed from carbon based alcohol and aldehyde [52]. Formaldehyde is the most common raw material for this type but other related chemicals can be used. The phenolic structure allows molecules to link to other molecules at selected sites around the ring. A functional group aldehyde allows bridging other molecules and creates regular pattern or phenol groups. The phenolic –OH groups are very weak acid exchangers. Sulphonation of the phenol prior to polymerisation usually used to increase the acid strength. The degree of cross-linking is achieved by the amount of formaldehyde used in synthesis [52].

This resin is hard, heat resistant, and can be mixed with a wide range of materials for variety of uses [52].

(iii) Acrylic

This type of resin is prepared by co-polymerisation of acrylic or methacrylic acid with divinylbenzene [53]. This resin has excellent transparency, durability, and resistance to heat, weather, chemical, water and hence; it has broad range of applications including moulding materials, coatings for automotive, architectural, plastic etc., binders for paper/fibre, display windows for cellular phones and backlight for liquid crystal displays (LCDs) etc. [53].

1.4.2.3 Organic- Inorganic ion exchangers

The combination of the properties of organic and inorganic building blocks within a single material is particularly attractive because of the possibility to combine the enormous functional variation of organic chemistry with the advantages of a thermally stable and robust inorganic substrate. The symbiosis of organic and inorganic components can lead to materials whose properties differ considerably from those of their individual, isolated components. Adjustment of the polarity of the pore surfaces of an inorganic matrix by the addition of organic building blocks extends considerably the range of materials that can be used for example in chromatography and ion sensing devices [54].

These techniques will be considered simultaneously with selection of the functional group and the appropriate combinations tested. There have been many cases where large organic molecules such as calixarenes and crownether complex have been incorporated by either Post-synthetic functionalization of silica (“Grafting”) or Co-Condensation (Direct Synthesis) into/onto a silica substrate [49, 55].

These hybrid resins are in fine powder form or bead shaped structures made with interconnected porosity, similar to sponge. All the pores are uniformly functionalised with ion specific organic ligands such as calix-crown complex, Tri-Butyl Phosphate (TBP) and 2, 6 –bis-(5, 6-dialkyl-1, 2, 4-triazin-3-yl) pyridine (BTP) which contains hydrophobic cavity suitable to capture different ions in aqueous solutions [56 - 59].

Table 1.2 Summary of general properties present in various ion exchangers

Property	Adsorptive material				
	Natural		Synthetic		
	Inorganic	Organic	Inorganic	Organic	Organic-inorganic
Acid stability	✔	✘	✘	✔	✘
Radiation Stability	✔	✘	✔	✘	✔
Selectivity	✘	✘	✘	✔	✔
Capacity	✘	✘	✘	✔	✔
Mechanical Stability	✘	✘	✘	✘	✔
High Temperature stability	✔	✘	✔	✘	✔
Rate of uptake	✘	✘	✘	✔	✔
Ease of preparation	✔	✔	✔	✘	✘
cost	✔	✔	✔	✘	✘
Availability	✔	✔	✔	✘	✘

1.5 Aims and Objectives

The research will encompass the preparation and characterisation of solid materials with selective cation exchange properties for the removal of fission products from nitric acid solutions.

To achieve these objectives the research programme will address:

1. Simple and low cost preparative routes that produced materials that have engineered pore size and surface area,
2. The potential of modified silica templates and/or composite materials,
3. Materials that have ion exclusion, affinity or ion selectivity properties or a combination,
4. Preparation of granular solid materials and/or spheres that have high cation selectivity and capacities and are nitric acid resistant,
5. Selective removal of Cs and Sr ions from stimulated PUREX spent fuel dissolver liquor,
6. The use of Ce (IV) ions as surrogate for Pu and U.

1.6 References

1 World Nuclear Association, http://www.world-nuclear.org/info/Nuclear-Fuel-Cycle/Mining-of-Uranium/Uranium-Mining-Overview/, Accessed May 2015

2 Evans N., The Nuclear fuel cycle, Radiochemistry group, Royal Society of Chemistry, issue no 7, Accessed May 2015

3 World Nuclear Association, http://www.world-nuclear.org/info/Nuclear-Fuel-Cycle/Conversion-Enrichment-and-Fabrication/Conversion-and-Deconversion/, Accessed May 2015

4 World Nuclear Association, http://www.world-nuclear.org/info/Nuclear-Fuel-Cycle/Conversion-Enrichment-and-Fabrication/Uranium-Enrichment/, Accessed June 2015

5 World Nuclear Association, http://www.world-nuclear.org/info/Nuclear-Fuel-Cycle/Conversion-Enrichment-and-Fabrication/Fuel-Fabrication/,Accessed June 2015

6 World Nuclear Association, http://www.world-nuclear.org/info/Nuclear-Fuel-Cycle/Power-Reactors/Nuclear-Power-Reactors/, Accessed July 2015

7 World Nuclear Association, http://www.world-nuclear.org/info/Nuclear-Fuel-Cycle/Fuel-Recycling/Processing-of-Used-Nuclear-Fuel/, Accessed July 2015

8 World Nuclear Association, http://www.world-nuclear.org/info/Nuclear-Fuel-Cycle/Nuclear-Wastes/Radioactive-Waste-Management/, Accessed July 2015

9 Bond G., and Eccles H., Continuous Chromatographic Separation of fission Products and Minor Actinides from Irradiated Fuel, UK patent Application No. 1317553.4, Nov 2013.

10 IAEA Spent Fuel Reprocessing Options, TECDOC 1587, August 2008.

11 Zwir-Ferenc A., and Biziuk M., Solid Phase Extraction Technique – Trends, Opportunities and Applications, Polish Journal of Environmental Studies, 2006. (15), p 677-690.

12 Abdel Rahman R.O., Ibrahium H.A., and Yung-Tse H., Liquid Radioactive Wastes Treatment, A Review, Water, 2011. 3, p. 551 - 565.

13 Harjula R., Development of selective caesium and strontium Removal System for the JAERI Tokai-Mura Site, Laboratory tests, Proceedings of Waste Management, March 2000, Accessed July 2015

14 Naushad M., Inorganic and Composite Ion Exchange Materials, and their Applications. A Review, Ion Exchange Letters, 2009. (2), p. 1 - 14.

15 Sensson H., Agrell C.E., Dehlen S.O., and Hagdahl L., An apparatus for Continuous Chromatographic Separation, Science Tools, 1955. 2, p. 17 - 21.

16 Martin A.J.P, Discussions of the Faraday Society, Royal Society of Chemistry, 1949. 7, p. 332 - 338.

17 Seidel-Morgenstern A., Kessler L.C., and Kasperel M., New Developments in Simulated Moving Bed Chromatography, Chem. Eng. Tech., 2008. 6, p. 826 - 837.

18 Canon R. M, and Sisson W. G., Operation of an Improved Continuous Annular Chromatograph, Journal of Liquid Chromatography and related technologies, 1978. 4, p. 427 - 441.

19 Sisson J.M., and Begovich W.G., Continuous Ion Exchange Separation of Zirconium and Hafnium using Annular Chromatography, Hydrometallurgy, 1983. 10, p. 11 - 20.

20 Hilbrig F., and Freitag R., Continuous Annular Chromatography, Journal of Chromatography B, 2003. 790, p. 1 - 15.

21 Panagiotis M., Application of natural zeolites in environmental remediation: A short review. Microporous and Mesoporous Materials, 2011. 144,(1-3), p. 15 - 18.

22 Hutson G.V., Waste Treatment in The Nuclear Fuel Cycle from Ore to Waste ed. P.D.Wilson, Oxford University Press, Oxford, 1996, 162.

23 Borai E.H., Efficient removal of caesium from low-level radioactive liquid waste using natural and impregnated zeolite minerals. Journal of Hazardous Materials, 2009. 172(1), p. 416 - 422.

24 Ahmet Erdal O., Treatment of radioactive liquid waste by sorption on natural zeolite in Turkey. Journal of Hazardous Materials, 2006. 137,(1), p. 332 - 335.

25 Zhang L., Adsorption of cadmium and strontium on cellulose/alginic acid ion-exchange membrane. Journal of Membrane Science, 1999. 162, (1-2), p. 103 - 109.

26 Zhou D., Cellulose/chitin beads for adsorption of heavy metals in aqueous solution. Water Research, 2004. 38(11), p. 2643 - 2650.

27 Pehlivan E. and Arslan G., Removal of metal ions using lignite in aqueous solution—Low cost biosorbents. Fuel Processing Technology, 2007. 88(1), p. 99 - 106.

28 Kumar A., Rao N.N., and Kaul S.N., Alkali-treated straw and insoluble straw xanthate as low cost adsorbents for heavy metal removal – preparation, characterization and application. Bioresource Technology, 2000. 71(2), p. 133 -142.

29 Sassi M., Removal of heavy metal ions from aqueous solutions by a local dairy sludge as a biosorbant. Desalination, 2010. 262(1–3), p. 243 - 250.

30 Khosa M.A., and Ullah A., In-situ modification, regeneration and application of keratin biopolymer for arsenic removal. Journal of Hazardous Materials, 2014. 278, p. 360 - 371.

31 Wang J., Collagen/cellulose hydrogel beads reconstituted from ionic liquid solution for Cu(II) adsorption. Carbohydrate Polymers, 2013. 98(1), p. 736 - 743.

32 Wang F.Y., Wang H., and Ma J.W., Adsorption of cadmium (II) ions from aqueous solution by a new low-cost adsorbent—Bamboo charcoal. Journal of Hazardous Materials, 2010. 177 (1–3), p. 300 - 306.

33 Baerlocher C.H, McCusker L.B, and Olson D.H, Atlas of Zeolite Framework Types, 6th edition, Amsterdam: Elsevier , 2007

34 Baerlocher C.H., McCusker L.B., and Olson D.H., Atlas of Zeolite Framework Types, 5th edition, Amsterdam: Elsevier , 2001

35 Anthony R.G., and Dosch R.G., Silico-titanates and their methods of making and using, US patent application No. US6479427 B1, Nov 2002.

36 Chitra S., Optimization of Nb-substitution and $Cs^{+/}Sr^{2+}$ ion exchange in crystalline silicotitanates (CST). Journal of Radioanalytical and Nuclear Chemistry, 2013. 295(1), p. 607 - 613.

37 Clearfield A., and Smith G.D., Crystallography and structure of α-zirconium bis(monohydrogen orthophosphate) monohydrate. Inorganic Chemistry, 1969. 8, p. 431 - 436.

38 Vivani R., New advances in zirconium phosphate and phosphonate chemistry: Structural archetypes. Microporous and Mesoporous Materials, 2008. 107(1–2), p. 58 - 70.

39 Todd T.A., Law J.D., and Herbst R.S., Caesium and Strontium Separation Technologies Literature Review, INEEL/EXT-04-01895, INEEL, 2004.

40 Ingale S.V., Synthesis, and characterization of ammonium molybdophosphate–silica nano-composite (AMP–SiO_2) as a prospective sorbent for the separation of Cs-137 from nuclear waste. Journal of Radioanalytical and Nuclear Chemistry, 2014. 301(2), p. 409 - 415

41 Sebesta F., Composite Sorbents of Inorganic Ion-Exchangers and Polyacrylonitrile Binding Matrix. I. Methods of Modification of Properties of Inorganic Ion-Exchangers for Application in Column Packed Beds, Journal of Radioanalytical and Nuclear Chemistry, 1997. 220(1), p. 77 - 88.

42 Mimura H., Lehto J., Harjula R., Selective Removal of Caesium from Simulated High-Level Liquid Wastes by Insoluble Ferrocyanides, Journal of Nuclear Science and Technology, 1993. 28(17-18), p. 2479 - 2506.

43 Kazemian, H., Zakeri H., and Rabbani S.M., Cs and Sr removal from solution using potassium nickel hexacyanoferrateimpregnated zeolites, Journal of Radioanalytical and Nuclear Chemistry, 2006. 268(2), p. 231 - 236.

44 Bondar Y., Kuzenko S., Han D.H., and Cho H.K., Development of novel nanocomposite adsorbent based on potassium nickel hexacyanoferrate-loaded polypropylene fabric. Nanoscale Research Letters, 2014. 9(1), p. 180 - 180.

45 Kourim V., Rais J., Million B., Exchange properties of Complex Cyanides-I: Ion Exchange of Cesium on Ferrocyanides, Journal of Inorganic Nuclear Chemistry, 1964. 26, p. 1111 - 1115.

46 Meynen V., Cool P., and Vansant E.F., Verified syntheses of mesoporous materials. Microporous and Mesoporous Materials, 2009. 125(3), p. 170 - 223.

47 Alothman Z., A Review: Fundamental Aspects of Silicate Mesoporous Materials. Materials, 2012. 5(12), p. 2874.

48 Makowski P., Mesoporous materials in the field of nuclear industry: Applications and perspectives. New Journal of Chemistry, 2012. 36(3), p. 531 - 541.

49 Kumar S. and Jain S., History, Introduction, and Kinetics of Ion Exchange Materials. Journal of Chemistry, 2013. p. 13 - 19.

50 Luca C., Organic Ion Exchangers in Encyclopedia of Separation Science, Ion Exchange, Wilson I.D., Editor 2000, Academic Press: Oxford. p. 1617 - 1632.

51 Fréchet J.M.J., and Farrall M.J., Functionalization of crosslinked polystyrene resins by chemical: A Review, in Chemistry & Properties of Crosslinked Polymers, 1977, William Andrew Publishing: Norwich, NY. p. 59 - 83.

52 Pilato L., Phenolic resins: 100 Years and still going strong. Reactive and Functional Polymers, 2013. 73(2), p. 270 - 277.

53 Fink J. K., Acrylic Resins, in Reactive Polymers Fundamentals and Applications, Chapter 9, Fink J. K., Editor 2005, William Andrew Publishing: Norwich, NY. p. 349 - 372.

54 Arora V., and Chawla H.M., Calixarenes as sensor materials for recognition and separation of metal ions, Arkivoc, 2007. 2, p. 172 - 200.

55 Naik P.W., and Dhami P.S., Use of organophosphorus extractants impregnated on silica gel for the extraction chromatographic separation of minor actinides from high level waste solutions. Journal of Radioanalytical and Nuclear Chemistry, 2003. 257(2), p. 327 - 332.

56 Zhang A., and Xiao C., Molecular modification of a novel macroporous silica-based impregnated polymeric composite by tri-n-butyl phosphate and its application in the adsorption for some metals contained in a typical simulated HLLW. Journal of Hazardous Materials, 2007. 147(1–2), p. 601 - 609.

57 Usuda S., and Wei Y., Development of a simplified separation process of trivalent minor actinides from fission products using novel R-BTP/SiO2-P adsorbents, Journal of Nuclear Science and Technology, 2012. 49(3), p. 334 - 342.

58 Pedersen C.J., Cyclic polyethers and their complexes with metal salts, Journal of the American Chemical Society, 1967. 89(26), p. 7017 - 7036.

59 Hamid S.A, and Tarmizi A.A, Application of a Newly Synthesized Calixarene in Metal Ions Extraction, CLEAN – Soil, Air, Water, 2008. 36(5-6), p. 498 - 503.

Chapter 2
Literature review for Cs and Sr removal

2.1 Literature review for Cs and Sr removal

This chapter is focused on different examples and discussion of both inorganic and hybrid (organic-inorganic) materials used for removal of Cs and Sr in nuclear waste.

A comparative study was performed on commercially available zeolites such as 13X, AR-1 (mordenite), 4A and ZSM-5 to study their caesium removal performance in acidic waste. The study was performed in batch and column to measure their uptake performance [1]. The study concluded that zeolites 13X and 4A had shown good Cs uptake in pure solutions, however, they were not effective for the treatment of actual waste and were not suitable in acidic solutions with pH 2 or lower. AR-1 (mordenite) had shown good selectivity for Cs in actual waste consisting of low dissolved solids content but not effective in high dissolved solids contents. ZSM-5 was found very low ion exchange capacity for Cs in this study [1].

Natural zeolite, clinoptilolite has been used post various nuclear disasters such as Three Mile Island and Chernobyl where Cs and Sr were removed from the environment [2, 3]. Sellafield's ion exchange effluent plant (SIXEP) used clinoptilolite to reduce Cs and Sr in the final discharge of nuclear waste to the Irish Sea previously [4].

A very comprehensive study of various titanosilicate materials (ETS-4, ETS-10, CST, AM-2, AM-3, AM-4, etc.) was undertaken to influence physical parameters, chemical composition, and modification, structure, and uptake properties [5]. The detailed study concluded that various titanosilicate materials display very high ion exchange capacity, resistance to high irradiation doses (up to 200 kGy), have remarkable uptake capacity for various radioactive cations, which does not depend on their ionic radius, hydration energy, electropositivity etc., and has shown fast sorption kinetics. The investigations also pointed out possible limitations such as high operation and manufacturing costs compared to the cost of other natural inorganic ion exchangers, titanosilicates limited their potential application [5].

Crystalline silicotitanates (CST) have shown remarkable uptake and capacity for Cs and Sr ions from radioactive wastes [6, 7]. The study investigates the synthesis, characterisation, and ion exchange properties of crystalline silicotitanates (CST) and niobium substituted crystalline silicotitanates (Nb-CST). The study pointed out that the morphology of these materials were crystalline with bright cubic and rod shaped crystals with varying amounts of Ti, Si, Nb, and O. The result of the study concluded that rate of uptake for Sr for both materials was similar however; Nb-CST had slightly slower kinetics for Cs compared to Sr kinetics. Hence, promising ion exchanger for removal of Cs and Sr from radioactive nuclear waste [6, 7].

IONSIV IE-911 molecular sieves are a similar type of crystalline silicotitanates, which are currently commercially mass-produced by UOP and originally developed by Sandia National Laboratories, USA. This type of material was synthesised by partially replacing titanium (Ti) with niobium (Nb), typically called Nb-sitinakite which has very strong affinity for both Cs and Sr ions [8, 9]. The research was undertaken to show the effect of Na, K, Ca, Mg, and Ba ions on rates of uptake and uptake measurement of trace concentration of Cs and Sr onto this type of ion exchanger [8]. The first part of the study concluded that the rates of uptake for both Cs and Sr ions were very similar but rates of exchange were little affected by pH [8]. The second part of the study focused on uptake measurements of Cs, Sr ions, which concluded that uptake of Cs was greater on Na/H_3O^+- Nb-Sitinakite than its Na form, and in contrast, Sr uptake was greater on Na-Nb-Sitinakite than its Na/H_3O^+ form [9]. The presence of K, Ba, Mg, and Ca ions had very little effect on uptake performance of this type of material [9].

Various studies have been undertaken to make AMP silica composite, which have shown very good selectivity and remarkable uptake for Cs ions in various acidic conditions [10 - 14]. A study on Cs ions sorption onto AMP-Silica gel concluded that the synthesised composite was crystalline in nature, possessed good acid stability and very high selectivity and favourable Cs sorption capacity [10]. A similar study was performed to make AMP-Silica gel into bead shape composite for column operation [11]. The experiment predicted that the composite's lengthy separation time for caesium from highly concentrated nitric acid (5 M) would be a disadvantage. The adsorbed caesium could be removed by simply washing the column by distilled water and 5 M ammonium chloride. The study also indicated that the composite had shown maximum rate of exchange at 80 °C [11]. Another bead shape composite has been studied which involved aluminium instead of silica as support and AMP for selective chromatographic

separation of caesium from barium ions [12]. The study suggested that the composite was stable up to 6 M HNO_3 and NH_4NO_3 solution. The optimum sorption capacity in column operation was found in 2 M HNO_3 [12].

Different studies have been undertaken to make mesoporous zeolite in which AMP was incorporated into MCM-41 type inorganic materials [13, 14]. The study used self-assembling route to synthesise MCM-41, which was further studied for its sorption capacity of lead, copper, and cadmium mixed ions aqueous solution. The study concluded that the composite had shown the highest selectivity towards lead in multi-element system [13].

A different approach to incorporate various heteroatoms into mesoporous MCM-41 and measurement of cations uptakes in various conditions has been reported. Part one of the series was to demonstrate one pot synthesis method of silica MCM-41 incorporating various hetero ions (Al, B and Zn), and their characterisation [15]. Part two of the series focused on determining possible cation selectivity [16] which was followed by measurements of uptake of Cs, Sr and Co ions in simulated ground water, with 0.1 M HNO_3, 0.1 M $NaNO_3$ and 0.1 M HNO_3/ NaOH media [17]. The research concluded that a one pot synthesis method was successfully employed to incorporate various hetero ions into the MCM-41 structure. The uptake studies of fission products suggest that only aluminium containing MCM-41 structure has ability to take up a small quantity of caesium ions from the aqueous media. The distribution coefficient studies of strontium in Si-MCM-41 showed remarkable uptake in pH value 6-8. Similar result was obtained in boron incorporated MCM-41. Zn incorporated material showed best performance in 0.1 M $NaNO_3$/OH however, no uptake was observed in presence of HNO_3 [18, 19].

Numerous studies have shown possibilities of impregnation of mesoporous materials with organic materials such as calixarenes, crown-ethers etc. to selectively remove Cs and Sr ions from the acidic media. However, their leaching and expensive synthesis procedures make them unsuitable for nuclear reprocessing and decontamination applications [20 – 22].

Selective separation of caesium ions from high level liquid waste using calix[4] + Dodecanol impregnated on silica surface showed excellent Cs ions adsorption compared to other metal ions. The research reported that the separation factor of Cs ions increased with increasing HNO_3 strength and found the optimum at 4 M [20].

Similar research was done by impregnating 1,3-[(2,4-diethylheptylethoxy)oxy]-2,4-crown-6-calix[4]arene (Calix[4]arene-R14) and methyloctyl-2-di-methylbutanemide (MODB) into the pores of silica gel for selective absorption of caesium from other metal ions in acidic media [21]. The result suggested that the optimum uptake of Cs ions was found in 3 M HNO_3 [21]. Similar to above ligands, macrocyclic ligand *cis*-dicyclohexano-18-crown-6 (*cis*-DCH18C6) was investigated to absorb Sr ions from high-level waste [22]. The study concluded that impregnated ligand had very high adsorption capacity and selectivity towards Sr ions in HNO_3 [22].

2.2 References

1. Panagiotis M., Application of natural zeolites in environmental remediation: A short review. Microporous and Mesoporous Materials, 2011. 144(1–3), p. 15 - 18.

2. Baxter M., Cooper J., Randle K., and Sokhi R., Radioactive Releases in the Environment: Impact and Assessment:, John Wiley & Sons Ltd, Chichester, UK, 2003, ISBN 0-471-89924-0, p. 50 - 147.

3. Collins E.D., The Three Mile Island accident and post-accident recovery – What did we learn? Chemical Technology Division, Oak Ridge National Laboratory, Conference Report CONF-820559-1, 1982.

4. Chelishchev N.F., Use of natural zeolites at Chernobyl, International Committee on Natural Zeolites, 1993. p. 525 – 532.

5. Popa K. and Pavel C., Radioactive wastewaters purification using titanosilicates materials: State of the art and perspectives. Desalination, 2012. 293, p. 78 - 86.

6. Chitra S., Viswanathan S., Rao S. and Sinha P., Uptake of caesium and strontium by crystalline silicotitanates from radioactive wastes. Journal of Radioanalytical and Nuclear Chemistry, 2011. 287(3), p. 955 - 960.

7. Chitra S., Sudha R., Kalavathi S., Mani A, Rao S., and Sinha P. K., Optimization of Nb-substitution and Cs^{+}/Sr^{2+} ion exchange in crystalline silicotitanates (CST). Journal of Radioanalytical and Nuclear Chemistry, 2013. 295(1), p. 607 - 613.

8. Dyer A., Newton J., O 'Brien L., and Owens S., Studies on a synthetic sitinakite-type silicotitanate cation exchanger. Part 1: Measurement of cation exchange diffusion coefficients. Microporous and Mesoporous Materials, 2009. 117(1-2), p. 304 - 308.

9. Dyer A., Newton J., O 'Brien L., and Owens S., Studies on a synthetic sitinakite-type silicotitanate cation exchanger. Part 2. Effect of alkaline earth and alkali metals on the uptake of Cs and Sr radioisotopes. Microporous and Mesoporous Materials, 2009. 120(3), p. 272 - 277.

10. Ingale S., Ram R., Sastry P., Wagh P., Kumar R., Niranjan R., Phapale S., Tewari R., Dash A., and Gupta S., Synthesis, and characterization of ammonium molybdophosphate–silica nano-composite (AMP–SiO_2) as a prospective sorbent for the separation of Cs-137 from nuclear waste. Journal of Radioanalytical and Nuclear Chemistry, 2014. 301(2), p. 409 - 415.

11. Doležal, J., Stejskal J., Tympl M., and Kouřím V., Improved inorganic ion-exchangers. Journal of Radioanalytical Chemistry, 1974. 21(2), p. 381 - 387.

12. Chakravarty R., Ram R., Pillai K.T., Pamale Y., Kamat RV., and Dash A., Ammonium molybdophosphate impregnated alumina microspheres as a new generation sorbent for chromatographic Cs-137/137mBa generator. Journal of Chromatography A, 2012. 1220, p. 82 - 91.

13. Naggar M., Aglan R., and Sayed M., Direct incorporation method for the synthesis of molybdophosphate/MCM-41 silica composite: Adsorption study of heavy metals from aqueous solutions. Journal of Environmental Chemical Engineering, 2013. 1(3), p. 516 - 525.

14. Narkhede N., Patel A., and Singh S., Mono lacunary phosphomolybdate supported on MCM-41: synthesis, characterization, and solvent free aerobic oxidation of alkenes and alcohols. Dalton Transactions, 2014. 43(6), p. 2512 - 2520.

15. Dyer A., Newton J., and Pillinger M., Synthesis and characterisation of mesoporous silica phases containing heteroatoms, and their cation exchange properties. Part 1. Synthesis of Si, Al, B, Zn substituted MCM-41 materials and their characterisation. Microporous and Mesoporous Materials, 2009. 126(1–2), p. 192 - 200.

16. Dyer A., Newton J., and Pillinger M., Synthesis and characterisation of mesoporous silica phases containing heteroatoms, and their cation exchange properties. Part 2. Cation exchange isotherms for MCM-41 phases. Microporous and Mesoporous Materials, 2009. 126(1–2), p. 201 - 212.

17. Dyer A., Newton J., and Pillinger M., Synthesis and characterization of mesoporous silica phases containing heteroatoms, and their cation exchange properties. Part 3. Measurement of distribution coefficients for uptake of Cs-137, Sr-89 and Co-57 radioisotopes. Microporous and Mesoporous Materials, 2010. 130(1-3), p. 56 - 62.

18. Dyer A., Newton J., and Pillinger M., Synthesis, and characterization of mesoporous silica phases containing heteroatoms, and their cation exchange properties. Part 4. Measurement of distribution coefficients for Am-241, Cr-51, Fe-59, Mn-54, Ni-63, Pu-263 and Zn-65. Microporous and Mesoporous Materials, 2010. 130(1-3), p. 63 - 66.

19. Dyer A., Newton J., and Pillinger M., Synthesis, and characterization of mesoporous silica phases containing heteroatoms, and their cation exchange properties. Part 5: Cation exchange isotherms and the measurement of radioisotope distribution coefficients, for an MCM-22 phase containing aluminium. Microporous and Mesoporous Materials, 2010. 135(1-3), p. 21 - 29.

20. Wu Y., Study on selective separation of caesium from high-level liquid waste using a macroporous silica-based supramolecular recognition absorbent. Journal of Radioanalytical and Nuclear Chemistry, 2012. 293(1), p. 13 - 20.

21. Zhang A., and Hu Q., Adsorption of caesium and some typical coexistent elements onto a modified macroporous silica-based supramolecular recognition material. Chemical Engineering Journal, 2010. 159(1–3), p. 58 - 66.

22. Bai F., Ye G., Chen G., Wei J., Wang J., and Chen J., New macrocyclic ligand incorporated organosilicas: Co-condensation synthesis, characterization, and separation of strontium in simulated high-level liquid waste. Reactive and Functional Polymers, 2013. 73(1), p. 228 - 236.

Chapter 3

Characterisation and experimental methods

3.1 Instruments

Table 3.1 List of instruments, manufacturer, models, and software

Instruments	Manufacturer	Model	Software	Location
XRD	Bruker	D2 Phaser	DIFFRAC.EVA v3.0	Coventry, UK
^{29}Si NMR	Bruker	Multinuclear 400 MHz NMR	TopSpin	Coventry, UK
Gas sorption	Micrometrics	ASAP2010	ASAP2010 v5.02	Hertfordshire, UK
SAXS	Anton Paar	SAXSpace	SAXSdrive™	St Albans
SEM	FEI	Quanta 200	XTMicroscopeControl	Eindhoven, ND
ATR-IR	Thermo scientific	Nicolet IR200	OMNIC	Warrington, UK
TEM	JEOL	JEM200EX	Gatan Digital	Hertfordshire, UK
TGA	Mettler Toledo	TGA 1	STAR Default DB V13.00	Leicester, UK
ICP-MS	Thermo Electron Corporation	X Series	Plasma Lab	Warrington, UK
Laser Diffraction	Malvern	Master sizer 2000	-	Malvern, UK
Stainless steel autoclave	Parr	Model No 4748		Stockport, UK
Water bath Shaker	Jalubo	SW22	-	Peterborough, UK
Balance	VWR	LA314i	-	Lutterworth, UK
Furnace	Vecstar Ltd	Temperature controller	-	Chesterfield, UK
Pipettes	Bioline	Biopette	-	London, UK
pH meter	Hanna Instruments	HI 2215	-	Leighton Bizzard, UK
Conductivity meter	Jenway	470	-	Stone, UK
Oven	Binder	-	-	Bedford, UK
Hot Plate and stir plate	IKA	C-MGG HS7	-	Staufen, DE
Peristatic pump	Watson Marlow	-	-	Cornwell, UK
Water Bath	Clifton	-	-	Somerset, UK
Centrifuge	Jouan	B4	-	Newport, UK

3.2 Analytical Techniques

3.2.1 Powder X-Ray Diffraction Spectroscopy (PXRD)

X-Ray diffraction has been widely accepted as an analytical technique to characterise different materials at atomic level [1, 2]. This technique has been developed in past 100 years based on the understanding that the wavelength of the x-rays are in order of 1Å, which are scattered from atoms to produce a diffraction pattern when subjected to a radiation beam [1]. The pattern is the product of scattered x-rays by a periodic array with long-range order, producing constructive interference at specific angles [1, 2]. The basic understanding was explained by Bragg who established the relationship between the crystal structure and diffraction pattern since termed as "X-ray diffraction" (XRD) [1, 2].

Bragg's Law

Bragg diffraction occurs when radiation, with wavelength comparable to atomic spacing, is scattered in a specular fashion by the atoms of a crystal system and undergoes constructive interference. Bragg's law is represented as;

$n\lambda = 2d_{hkl}\sin\theta$……..... **Equation 3.1 [1]**

Where, n= 0, ±1, ±2, ±3…

λ = Wavelength of the x-ray

d_{hkl} = Spacing between crystallographic plane

θ = diffraction angle

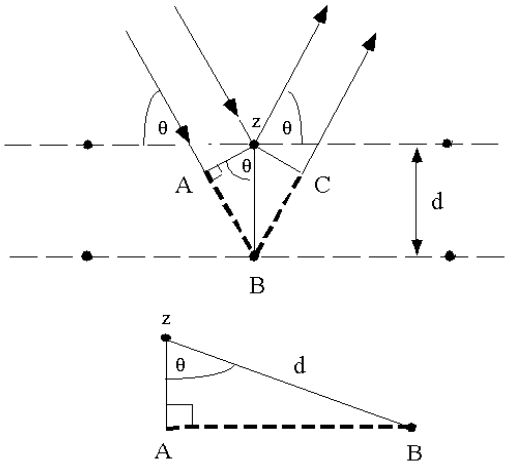

Figure 3.1 Bragg's Law [1]

The technique is extremely useful for crystalline materials as each material has its own specific crystal structure, which can be compared with library of such patterns to identify the crystalline phase. It can also be useful in identifying the unit cell parameters, crystal structure, crystallite size etc. [1, 2].

Figure 3.2 represents the basic construction of typical XRD instrument. A typical XRD experiment includes five major steps. (1) Sampling, (2) X-ray production, (3) diffraction, (4) detection, and (5) interpretation.

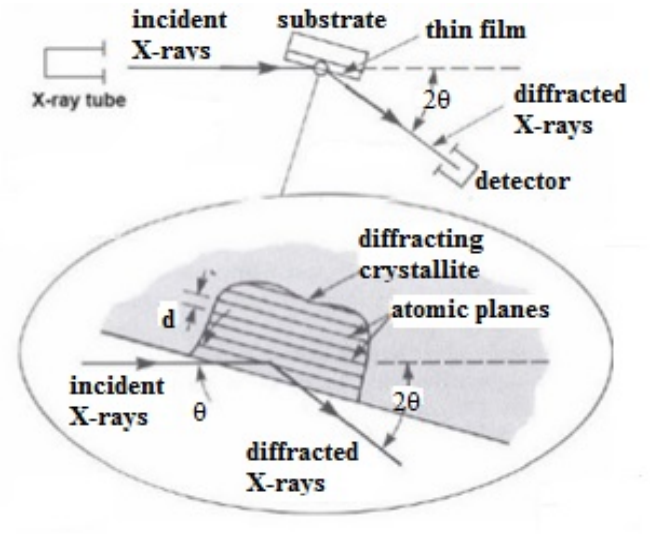

Figure 3.2 Basic construction of typical XRD instrument [1]

Experimental procedure

The powder samples were ground lightly in a pestle and mortar; the resulting powder, approximately 5 mg, was densely packed into a sample holder and the surface was smoothed by a clean flat glass slide. The experiment was performed on Bruker D2 Phaser, which uses X-ray generator producing monochromatic Kα X-rays from a copper source (wavelength 1.54 Å) along with nickel filter. The instrument operating conditions were set at 30 kV, 10 mA and with the step width 0.02° at room temperature. To analyse various samples, scattered x-rays were allowed to pass through 0.1 mm and 0.6 mm divergence slit for mesoporous MCM-41s (chapter 4) and zeolites (chapter 5) respectively. The LYNXEYE detector (provide by Bruker) was used to collect scattered radiation from the samples and software DIFFRAC.EVA v3.0 was used to report high quality data. The data was collected between 1.5 - 40° and 5 - 90° 2θ region for MCM-41s and zeolites respectively.

3.2.2 Small Angle X-ray scattering (SAXS)

SAXS is a non-destructive technique, which works on a similar principle as XRD and enables the study of correlations at the mesoscopic scale. SAXS is a technique performed on liquid and/or powdered sample between 0.3 - 10° 2θ region [2]. In a typical SAXS experiment, an X-ray beam is bombards on the sample, which interacts with electrons of the sample and is subsequently scattered [2]. The detected scattering pattern at low angle can be used to determine the size, shape, internal structure, and porosity of the sample.

The detected scattering pattern is generally represented as scattering vector q and the equation is represented as

$$q = 4\pi \frac{sin\theta}{\lambda}$$ **Equation 3.2 [2]**

$$d = \frac{2\pi}{q}$$ **Equation 3.3 [2]**

Where, q = scattering vector,

θ = scattering angle,

λ = Wavelength of the x-ray

d = change in the electron density

Figure 3.3 represents the difference between two techniques (SAXS and XRD).

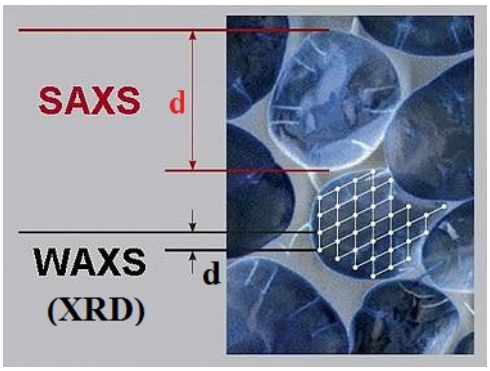

Figure 3.3 Difference between SAXS and WAXS (XRD) techniques [2]

Experimentation

SAXS analysis was performed on Anton Paar SAXSpace instrument by Dr Amin Dilmaghani in School of Food Science & Nutrition, University of Leeds. Synthesised mesoporous zeolite samples (chapter 5) were deposited on the sample holder and scattering pattern was analysed by SAXSdrive™ software. The instrument parameters were set as following:

Table 3.2 SAXS experiment set up parameters

Measuring temperature	25 °C
Acquisition time	300 Seconds
Number of frames	3
Vacuum	1.4 mbar
Wavelength	1.54 Å
Voltage	40 kV
Current	50 mA

3.2.3 Surface area and Pore analysis

Surface area and texture (pore size, volume, and shape) of materials are fundamental properties to analyse in material science, the surface properties can be analysed by various adsorption techniques such as gas sorption and non-wetting method (mercury porosimetry) [3]. Gas sorption is a widely acceptable technique due to its versatile use to characterise wide range of pore sizes (micro-, meso-, and macropores), non-destructive and cost effective method [3]. Various gases (e.g. argon, krypton, nitrogen) can be used depending on the nature of the material [3]. Nitrogen (N_2) gas sorption has been used for the analysis of various materials in this thesis.

Adsorption is a consequence of the field force at the surface of the solid (adsorbent), which attracts the gas molecules (adsorbate) [3]. An adsorption isotherm is produced, by varying the partial pressure of the gas, which reflects the adsorption of the gas on the surface of the material. This technique is crucial for characterising various information such as surface area, pore size, pore size distribution, pore shape, and pore volume.

Figure 3.4 (a) represents six common types of gas sorption profiles as classified by IUPAC [4]. Type I and IV (represents microporous and mesoporous respectively) are the most relevant types for this thesis. Type I isotherm, for pore sizes of less than 2 nm in diameter reflects adsorption of a high volume of N_2 at very low relative pressure [3, 4]. Type IV represents an isotherm of mesoporous materials, which have pore diameter of 2 - 50 nm [3]. This isotherm is similar in profile to isotherm I until point B (figure 3.3 (a)) which then further extends with a loop profile at higher relative pressure. This is called “hysteresis loop” [3, 4]. Figure 3.4 (b) represents adsorption/desorption at various stages of a cylindrical-shape mesopore. The gas sorption in mesoporous materials are initiated by the formation of an adsorbate monolayer across the surface, which results in a rise in adsorbed volume (stage A).

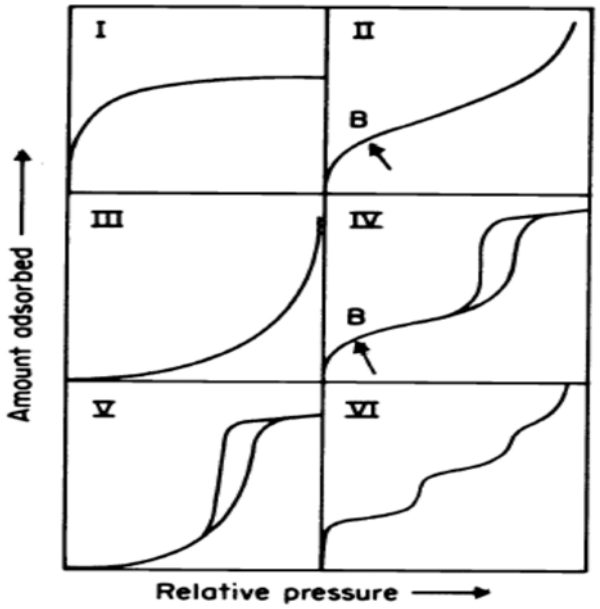

(a)

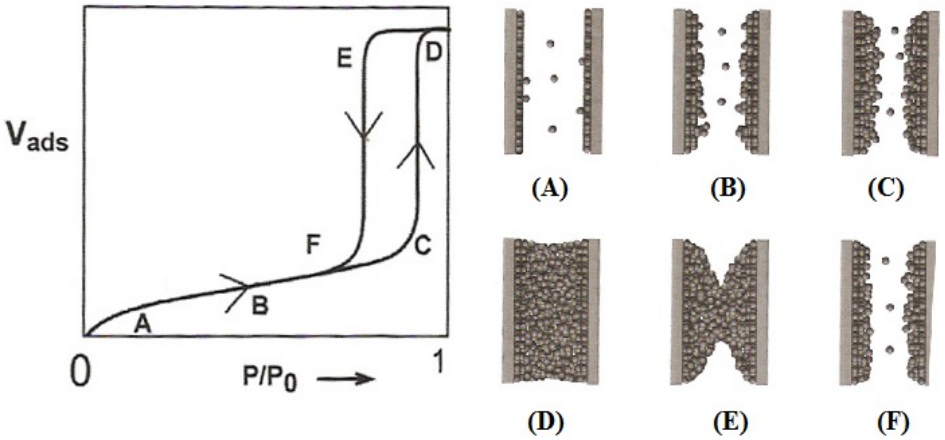

(b)

Figure 3.4 N_2 gas sorption, (a) six types of adsorption isotherm, and (b) hysteresis loop of type IV isotherm [3]

Further increase in the relative pressure, results in multiple layer adsorption on the surface due to large pore size (stage B). After reaching a critical point (stage C), capillary condensation takes place (transition from stage C to D). Stage D represents the position where the pore is completely filled. Stage E is the representation of cylindrical pore with both ends open. Pore evaporation begins by lowering the relative pressure (Stage E-F). The point at which the loop ends corresponds to the multilayer. The occurrence of the hysteresis loop is due to condensation at both ends of the pore at different relative pressures. The loop will be absent in the situation where one end is open and the other is closed since condensation takes place at only one end (open end)

which further expands to the end of the pore. The process occurs at the same relative pressure hence no hysteresis loop [3, 4].

3.2.3.1 Brunauer-Emmett-Teller (BET) Method

Brunauer, Emmett, and Teller, first explained the Langmuir's theory to multilayer adsorption [3]. The theory assumes that the uppermost layer of the adsorbed gas molecules are in equilibrium with the vapour. In other words, there is always an equilibrium between layers and vapour despite the number of layers and the number of adsorbed molecules in each layer.

The equation for BET is presented as,

$$\frac{1}{\vartheta\left[\left(\frac{po}{p}\right)-1\right]} = \frac{c-1}{\vartheta m\, C}\left(\frac{p}{po}\right) + \frac{1}{\vartheta m\, C} \quad \text{..... Equation 3.4 [3]}$$

Where, ϑ = number of moles adsorbed

p/p_0 = relative pressure

ϑ_m = monolayer capacity

All the surface area measurements were calculated by using equation 3.4

3.2.3.2 Barrett-Joyner-Halenda (BJH) Method

The pore analysis of various mesoporous materials were calculated by Barrett-Joyner-Halenda (BJH) method. The method is based on the modified Kelvin equation (3.5) which examine the correlation between pore diameter and pore condensation pressure, i.e. Pore diameter (Dp) is directly proportional to relative pressure (P/P_o) [3].

The pore size and pore size distribution of all the materials studied were analysed by this method.

$$ln\left(\frac{P}{P_0}\right) = \frac{-2\gamma\cos\theta}{RT\Delta\rho(r_m - t_c)} \quad \text{..... Equation 3.5 [4]}$$

Where, R = universal gas constant,

γ = surface tension

Θ = contact angle of the liquid against the pore wall

$\Delta \rho$ = change in the density

T = temperature

r_m = radius of the mean curvature

t_c = statistical thickness prior to condensation

3.2.3.3 Horvath-Kawazoe (HK) method

The HK method is more suitable to analyse micropores (< 2 nm). The technique estimates the pore size distribution in microporous region by considering the relative pressure (P/P_o) required for the filling of micropores [3]. In other words, micropores are progressively filled with an increase in adsorbate pressure.

The pore size distribution of Zeolite 5A (chapter 5) were performed by this method.

Experimental procedure

The surface area and pore analysis was performed by Micromeritics ASAP 2010. All physisorbed species were removed from the adsorbent surface prior to the determination of the various properties, this was performed by using a small amount of sample (e.g. 200 mg) that was carefully weighed in a clean glass tube with a stopper at the open end of the tube and outgassed at low pressure for 24 hours at 150 °C. The change in weight after degassing was used in calculating the various properties of the material using ASAP2010 v5.02 software (provided by Micromeritics) and data reported with ± 1% error.

3.2.4 Attenuated Total Reflectance – Infrared spectroscopy (ATR - IR)

Infrared (IR) spectroscopy a vibrational spectroscopic technique based on the interaction between electromagnetic radiation and sample in the infrared region (4000 – 400 cm^{-1}) [5, 6]. The technique is used to identify functional groups of materials as they absorbed IR radiation at selected frequencies, which corresponds to

vibration of bonds [5, 6]. The vibration in the functional group can be either stretching (changes in the bond length) or bending (change in the bond angle) [5, 6].

ATR is a tool of IR spectroscopy, which measures the changes that occur in a total internally, reflected IR radiation when the beam of IR is exposed to a sample [5, 6]. Figure 3.5 represents the principle of ATR-IR spectroscopy.

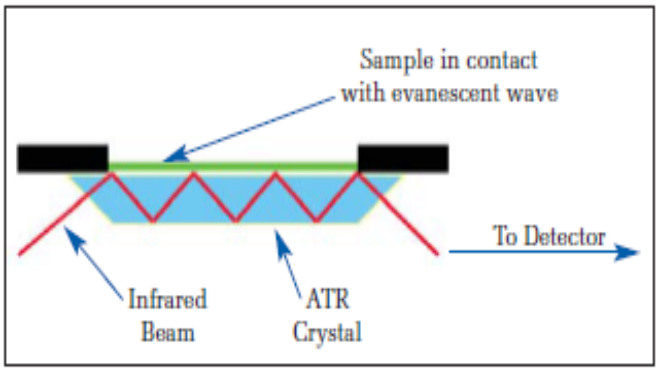

Figure 3.5 Principle of ATR-IR [6]

Experimental procedure

Nicolet IR200 from Thermo Scientific Instrument was used for qualitative analysis of functional groups of various materials. A small amount (~1 mg) of the sample was placed in a direct contact with a diamond crystal that has higher reflective index than the sample. The transmission of the reflected IR beam was recorded by the detector. To establish the consistency of the recorded data, a blank curve was recorded prior to every analysis followed by 64 scans on each sample and the reflected beam data analysed by OMNIC software.

3.2.5 Scanning electron Microscopy (SEM) and Transmission Electron Microscopy (TEM) imaging

SEM and TEM are two similar techniques, used to produce high-resolution images [7]. Both techniques produces an image by scanning and recording the scattered electrons from a thin layer of sample when bombarded with a beam of electrons.

In a SEM imaging, secondary electrons (SE) and back-scattered electrons (BSE) are reflected form the sample and detected [7]. The most common technique is to detect SE which are low energy electrons emitted from the surface of the sample. The local variations in the detected secondary electron density produces the SEM image.

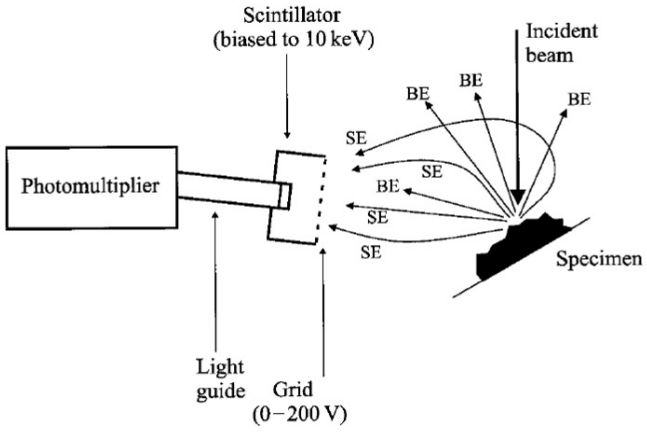

Figure 3.6 A schematic representation of Everhart-Thornley secondary detector in SEM [7].

SEM experimental procedure

SEM imaging was performed on Quanta 200, SW39 with an Everhart-Thornley detector accompanied by XT Microscope Control software. Sticky carbon tape was placed on the specimen stub and a small amount of sample was deposited on the surface of the carbon tape, for AMPPAN composites, a bead was bisected to analyse the core morphology. The SEM imaging was performed under 3.4×10^{-5} Torr pressure and 20 kV conditions for all samples. The area of interest was focussed and images were recorded.

In TEM, the scattered and un-scattered electrons transmitted through a thin layer of sample were analysed [7]. In the image, denser areas of atoms and heaver elements appear darker due to increased scattering of electrons [7]. This technique was used to produce images at nanometre scale.

TEM experimental procedure

TEM images were analysed by JEOL, JEM200EX with Gatan Digital software. A small amount of sample (a few particles) was suspended in 1 ml Eppendorf filled with absolute ethanol. The sample was prepared by placing a drop of this suspension on a carbon grid. The prepared grid was allowed to dry for 15 minutes and inserted into the sample chamber, which was under vacuum for analysis.

3.2.6 Thermogravimetric analysis (TGA) and Differential Thermal Analysis (DTA)

TGA is a technique, which monitors the amount and rate of change of mass of a sample as a function of temperature or time in a controlled environment [8]. The DTA is a plot of differential temperature against time, or temperature [8].

The technique primarily is used to analyse composition of materials and predict their thermal stability within the required range (up to 1100 °C).

A TGA instrument consists a sample pan that is supported on a precision balance. The sample pan placed in a furnace, which is linked with purge gas and sample gas inlets. The furnace is heated and cooled in controlled manner (i.e. 5 °C/min) up to the desired temperature. The sample gas is fed in a controlled manner (i.e. 20 ml/min) which regulates the furnace environment during the experiment and further purge gas (nitrogen) is used to prevent any contamination. The rate of change in mass upon heating is recorded by the balance and the weight loss data analysed.

Experiment Procedure

A TGA 1 from Mettler Toledo was used with data recorded on STAR Default DB V13.00. The ultra-micro balance was capable of 0.0025% and 0.005% weighing accuracy with a measurement range 1 µg - 5 g. The furnace chamber was purged with nitrogen gas for 5 minutes at 20 ml/min before and after each experiment. A known amount of sample was weighed in a 90 µl aluminium pan and the experiment was performed at 10 °C/min from 25 - 1000 °C in 20 ml/min airflow. For consistency the blank curve was produced which was deducted from the measured sample curve for all samples.

3.2.7 Solid State Nuclear Magnetic Resonance Spectroscopy (NMR)

Nuclear magnetic resonance, an analytical technique used to characterise structural arrangements (chemical bonds) in the sample. This technique is based on the principle that when a magnetic field is applied to a molecule, which contains a magnetic nucleus, a resonant electromagnetic field is produced, which is analysed [9]. The NMR is conducted on elements, which have an odd number of protons and neutrons such as ^{1}H, ^{11}B, ^{13}C, ^{15}P, ^{19}F, ^{29}Si etc., this property allows a spin, or magnetic moment which can interact with an external magnetic field [9]. The recorded frequency can be further interpreted as spectra, often called chemical shift where characteristic peaks are identified according to their local magnetic field [9].

^{29}Si NMR has been used for chemical analysis within the thesis (Chapter 4).

Experiment Procedure

Analysis was performed on Bruker solid-state 400 MHz instrument. A small amount (1 mg) of sample powder was finely ground and packed tightly into the rotor. The sample was rapidly spun (7 kHz) at a magic angle (54.74°) with respect to magnetic field. The chemical shift was recorded and compared with other samples.

3.2.8 Laser diffraction

This technique is used to measure particle size distribution in the range 0.02 – 2000 µm by measuring the intensity variation of light scattered when a laser beam passes through a dispersed particulate sample [10]. In general, large particles scatter light at small angle and small particles vice versa [10]. Laser diffraction uses Mie theory of light scattering, which assists in the calculation of the degree of light scattered and produces a particle size distribution, based on an equivalent volume of a sphere [10].

Experiment Procedure

Particle size distribution was performed on a Malvern Mastersizer 2000. A small amount of sample (~5 mg) was dispersed in deionised water (reflective index 1.330) in a 2 ml Eppendorf. A vortex mixer was used to disperse particles homogeneously, few drops of this prepared suspension was dropped into the sampling chamber, and particle size distribution was recorded which is an average of three measurements.

3.2.9 Inductively Coupled Plasma Mass Spectrometer (ICP-MS)

ICP-MS is a multi-element analytical technique, which is capable of analysing very low concentrations of elements (ppb), based on the elements' isotopic compositions [11]. Figure 3.7 represents a schematic diagram of the important components of ICP-MS. In a typical experiment, a small amount (10 µl) of sample diluted in ~1% nitric acid is introduced into the ICP via the nebuliser-spray. The plasma has a high electron flux and temperature, which act as both atomiser and ioniser on the sample. The resulting sample passes through a most common quadrupole mass spectrometer (MS). This MS acts as a filter, allowing the pre-selected mass/charge ratio of the element of interest to pass, which is eventually detected [11]. Diluted acidic sample (1% HNO_3) was used due to high sensitivity of the instrument.

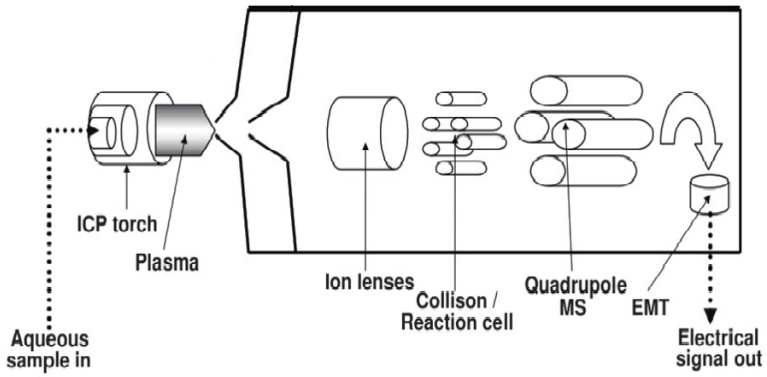

Figure 3.7 A schematic representation of ICP-MS [11]

Experiment Procedure

All measurements were carried out on Thermo Electron Corporation; X Series ICP-MS. Samples were prepared by measuring 10 µl aliquot using previously calibrated micropipettes and diluted in a 10 ml plastic tube. In order to ensure a consistency, 100 µl of 1 ppm Be and Ba as internal standards for B and Cs, Sr and Ce measurement respectively was used. The remaining volume of the sample was made up by analytical grade 1% v/v nitric acid and shaken thoroughly.

Prior to the measure of samples, the detection chamber was cleaned with 1% nitric acid followed by calibration for each ion of interest with a blank, which consisted of 100 µl of the respective internal standard and 1% nitric acid. The standards were prepared by estimating highest and lowest concentration of each ion in the solution and set as 0.5, 1, 3, 5, 7, and 9 ppm. The regression analysis of this calibration curve was considered when $r^2 \geq 0.998$ for all the measurements in this thesis.

Each sample was analysed three times and carried out in duplicate (n = 6 samples) for further consistency. The analytical procedure required for every third sample fresh 1% v/v nitric acid was sprayed into the instrument. All the results were reported with 95% confidence limit. The measured errors are very low and consequently no error bars are shown on the appropriate figures.

The elemental analysis were performed on natural occurring isotopes; B-11, Cs-133, Sr-88, Ce-140, Ba-137, Be-9, Mo-95, and Al-27.

3.2.10 Uptake Measurements

The performance of various synthesised materials was measured by contacting a known quantity of sample with single ions and mixed ion solutions of different nitric acid strength.

In a typical nuclear waste,

Cs^{+}, Sr^{2+}, and Ce^{4+} cations were selected as:

1. Their chemistries and behaviour are different,
2. Cs and Sr ions account for a significant amount of β/γ activity present in spent fuel dissolver liquor [13],
3. Ce is a good inactive simulant for Pu and/or U in the PUREX process [14, 15].

Cs, Sr and Ce are present as Gp1, Gp2 and lanthanide elements respectively in the periodic table; consequently their hydrated ionic radii, complexation behaviour and general chemistry are different for example the Ce^{4+} forms relatively weak nitrato complexes in nitric acid solution (~1 M), with the Ce^{4+} ion predominating but with $Ce(NO_3)_3^{+}$ and $Ce(NO_3)_2^{2+}$ ions increasing in stronger nitric acid [12], neither Cs or Sr exhibit such behaviour.

Caesium and strontium isotopes account for about 50% of the total activity (TBq/t) from fission products for 10-year cooled fuel, with a burn-up of 33 GWd/t [13]. At cooling times 10 - 1,000 years the activities of strontium-90, a strong β emitter with a half-life of 28.8 years, and caesium-137 with a half-life of 30.2 years, a strong β/γ emitter dominate among the fission products [13]. They are the two most important fission products when considering reagent stability in a reprocessing flowsheet.

Cerium ions (3+/4+) have been used as a surrogate for Pu in a variety of studies ranging from reprocessing, fuel fabrication to waste management [14]. The liquid-liquid extraction of cerium ions from nitrate solution using Tri- Butyl Phosphate was well established even before the conception of the PUREX process [15].

The salts chosen to prepare the solutions for various batch studies were caesium nitrate ($CsNO_3$), strontium nitrate ($Sr(NO_3)_2$) and ammonium cerium nitrate $Ce(NH_4)_2(NO_3)_6$. All the ion exchange work was performed in a non-radioactive environment.

The various stock solutions of different cations used along with different nitric acid strength are reported in table 3.3.

Table 3.3 Composition of various cationic solutions

Acidity (M)	Single ion			Mixed ion
	$CsNO_3$	$Sr(NO_3)_2$	$(NH_4)_2Ce(NO_3)_6$	
Weakly acidic (D.W)	✔	✔	✔	✔
0.5	✔	✔	✔	✔
1	✔	✔	✔	✔
3	✔	✔	✔	✔

Mixed ion solutions contained approximate 5 mM $CsNO_3$, 5 mM $Sr(NO_3)_2$ and 50 mM $(NH_4)_2Ce(NO_3)_6$.

Single ion solutions contained approximate 5 mM of respective nitrate salt. The stock solutions were prepared by dissolving relevant metal salt in relevant acidic or D.W media. The concentration of ions (Cs, Sr and Ce) were measured quantitatively by ICP-MS, which were found as approx. 675 ppm for Cs, 450 ppm for Sr and between 4300 - 6900 ppm for Ce. The elemental concentrations of the various solutions were achieved by dissolving appropriate qualities of respective salts in either HNO_3 or in d.w.

0.5 g sample of the synthesised material was contacted with 25 ml of chosen stock solution in a 50 ml Duran glass bottle. The bottles were placed in a water bath for 24 hours at 25 °C. A sample of liquor was taken after 24 hour (assumes equilibrium has been attained) and analysed by ICP-MS.

The result are reported by measuring the cation concentration of the stock solution and after equilibration with the exchange material.

The distribution coefficient (Kd) was calculated by

$$Kd = \frac{C_o - C_e}{C_e} \times \frac{v}{m} \text{ (ml/g)} \quad \text{..... Equation 3.6}$$

The capacity (q) was calculated by

$$q = \frac{C_o - C_e}{1000} \times \frac{v}{m} \text{ (mg/g)} \quad \text{..... Equation 3.7}$$

Where, Co = Initial concentration (ppm)

Ce = Final concentration (ppm)

v = volume of the liquor (ml)

m = mass of the sample (g)

3.2.11 Rate of Uptake Measurements

The cation rate of uptake measurement of the synthesised materials was performed in a similar manner as capacity measurement but 100 µl liquid samples were removed at specific times during the equilibration. These measurements were performed mainly on AMPPAN composites due to their high Cs capacity compared to other synthesised materials reported in this thesis.

1 g of composite was contacted for 2880 minutes (48 hours) with 100 ml of 5 mM $CsNO_3$ liquor in a 150 ml Duran glass bottle. The experiment was conducted in two groups, (1) different acidity (1 M and 3 M nitric acid) at 25 °C, and (2) different temperature (25 °C and 50 °C) in 1 M nitric acid. 100 µl liquid samples were removed after 10, 30, 60, 180, 1440 and 2880 minutes and the concentration of Cs ions determined. The rate of percentage uptake was calculated by setting the 48-hour Cs concentration as 100% uptake.

The rate of uptake expression is represented as:

$$percentage\ uptake\ (\%) = \frac{Kd\ (t)}{Kd\ 2880} \times 100 \quad \text{..... Equation 3.8}$$

Where, K_d = distribution coefficient (Equation 3.6)

t = sampling time (0, 10, 30, 60, 180, 360, 1440 minutes)

K_d 2880 = K_d value of sample 2880 minutes (48 hours)

3.3 References

1. Dinnebier R., Powder Diffraction: Theory and Practice. Royal Society of Chemistry, 2008. ISBN: 978-1-84755-823-7, p. 1 - 19.
2. Bruce D., O'Hare D., and Walton R., Inorganic Materials Series: Structure from Diffraction Methods. Wiley, 2014. ISBN: 978-1-119-95322-7, p. 1 - 98.
3. Lowell S., Shields J.E., Thomas M.A., Thommes M., Characterization of Porous Solids and Powders: Surface Area, Pore Size, and Density, Springer 2006. ISBN: 978-1-4020-2303-3, p. 1 - 154.
4. Sing K.S.W., Reporting physisorption data for gas solid systems with special reference to the determination of surface area and porosity. Pure and Applied Chemistry, 1982. 54 (11), p. 2201 - 2218.
5. Koenig J.L., Infrared, and Raman Spectroscopy of Polymers. Shrewsbury 2001. ISBN : 9781859572849, p. 1 - 132.
6. Rees O.J., Fourier Transform Infrared Spectroscopy: Developments, Techniques and Applications. Nova 2010. ISBN: 978-1-61324-383-1, p. 1 - 204.
7. Goodhew P., Humphreys J., and Beanland R., Electron Microscopy and Analysis. Taylor & Francis Ltd, 2000. ISBN: 9780748409686, p. 16 - 213.
8. Brown M., Introduction to Thermal Analysis, Volume 2: Techniques and Applications (2^{nd} Edition). Springer 2001. ISBN: 978-0-306-48404-9, p. 1 - 90.
9. Duer M., Solid State NMR Spectroscopy: Principles and Applications. Wiley, 2008. ISBN: 9780632053513, p. 1 - 56.
10. Xu R., Particle Characterization: Light Scattering Methods. Hingham, Kluwer Academic Publishers, 2000. ISBN: 9780792363002, p. 1 - 96.
11. Dean J.R., Environmental Trace Analysis: Techniques and Applications. Somerset, John Wiley & Sons, Incorporated, 2013. ISBN: 978-1-119-96270-0, p. 157 - 176.
12. Bayulken S. and Sarac A., Distribution of Ce (IV) species in HNO_3-$HClO_4$ Media and Determination of Stability Constants of the Nitrato Complexes, Turkish Journal of Chemistry, 1996. 20, p. 111 - 117.

13. Choppin G., Liljenzin J.O., and Rydberg J., Radiochemistry and Nuclear Chemistry Chapter 21 Nuclear fuel Cycle, 3rd edition, Publ. Butterworth Heinemann. 2002, ISBN-13: 978-0124058972, p. 608 - 739.
14. Lopez C., Deschanels X., Bart J.M., Jollivet P., Denauwer C., Structural study of plutonium surrogates in nuclear glasses, Ceramic Transactions, 1996. 72, p. 399 - 408
15. Warf J.C., Extraction of Cerium (IV) nitrate by Butyl Phosphate, Journal of American Chemical Society. 1949, 71 (9), p.3257 - 3258.

Chapter 4

Preparation of modified mesoporous MCM-41

4.1 Introduction

MCM-41 (Mobile Composition of Matter No 41) is often referred as a model mesoporous adsorbent. The main characteristics of MCM-41 are:

(1) it consists of an array of uniform hexagonal channels,

(2) the pore length is greater than pore diameter,

(3) the absence of pore channel intersections,

and (4) it has high surface area and narrow pore size distribution [1-4].

The only route to synthesise this type of material is by using templates or structure directing agents (SDA) [2, 4]. These templates can be anionic, cationic, or neutral surfactant or non- surfactant. The basic idea of preparing MCM-41 is to form a central structure about which oxide moieties organise into a crystalline lattice. Further, when the templates are removed it leaves behind a mesoporous skeleton.

Researchers at Mobile Oil Corporation proposed a mechanism for how typical MCM-41, assemblies of surfactant micelles (e.g. alkyltrimethylammonium surfactants) play a role of a template or SDA for the formation of mesopores [5]. In figure 4.1, pathway-1, rod shaped micelles self-organise into an hexagonal array, further condensation of silicate species (formation of a sol-gel) around templates results into hexagonal ordered rod-like structure [1]. In pathway-2, condensation of silicate species occurs before formation of hexagonal arrays and further self assembles, which leads to hexagonal structure shown in figure 4.1 and figure 4.2 [4]. It is very difficult to confirm by which pathway this material is synthesised. Further calcination of templates results into highly ordered hexagonal structure.

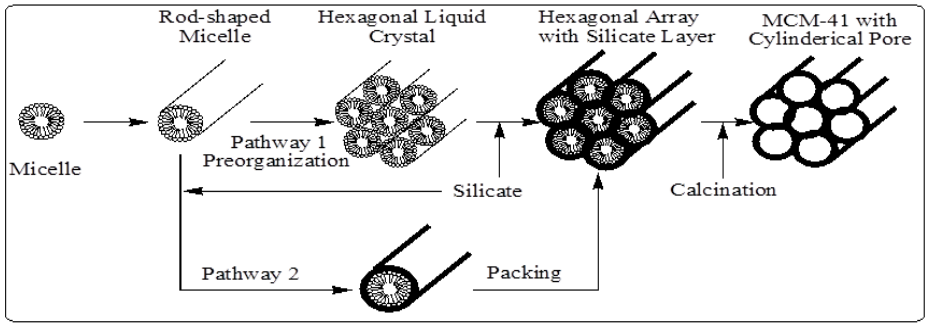

Figure 4.1 Schematic representation of liquid crystal templating mechanism in two possible pathways [1]

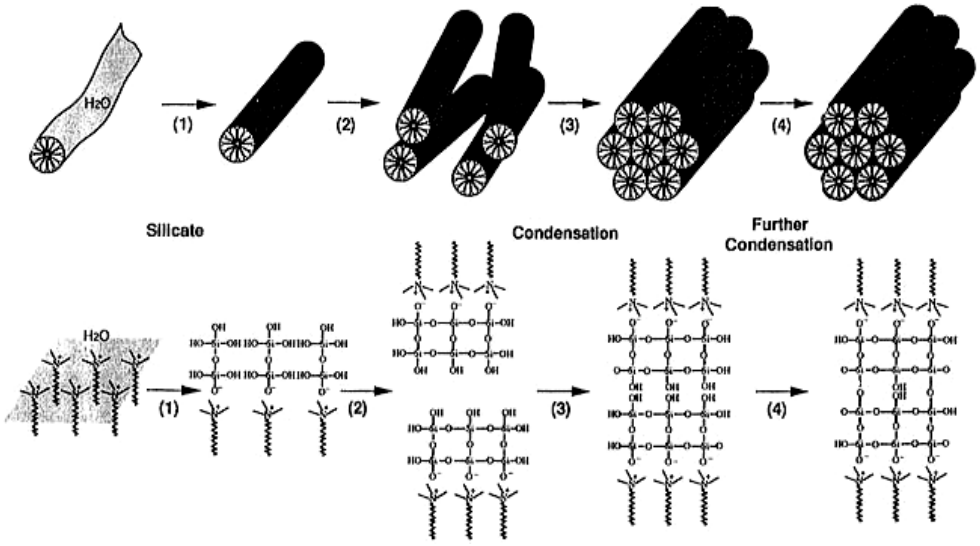

Figure 4.2 Mechanism of formation of MCM-41[4]

4.1.1 Role of surfactant during MCM-41 synthesis

Surfactants or surface directing agents play a crucial role in the formation of mesoporous structure. A surfactant consists of a hydrophobic tail and hydrophilic head. At a low concentration, surfactant molecules carry very low energy hence exist as monomers. Further increase in concentration, these monomers self-assemble together and form micelles. The degree or point at which micelles form is called critical micelle concentration (CMC) [1, 3].

The formation of a particular phase (hexagonal, cubic or lamellar) depends on the concentration of surfactant and the nature of the surfactants such as the length of the hydrophobic carbon chain, head group, and counter ions for ionic surfactants. It also depends on external factors such as pH, temperature, ionic strength, and other additives.

It is important to note that in the case of MCM-41 structure formation, a high surfactant concentration, high pH, low temperature and slow silicate polymerisation leads to cylindrical micelles and hexagonal mesophase as shown in figure 4.3[1 - 3].

The interaction of organic parts and inorganic parts play a very important role in the assembly [1]. There are various possible types of interactions depending on the charge of surfactant (S) S^+ or S^-, on inorganic species (I), I^+ or I^-, and the presence of mediating ions, i.e. X^- or M^+ as shown in figure 4.4 [1, 4] . The size of the pores can be controlled by selecting different size of the surfactant chain length and addition of organic compounds [1].

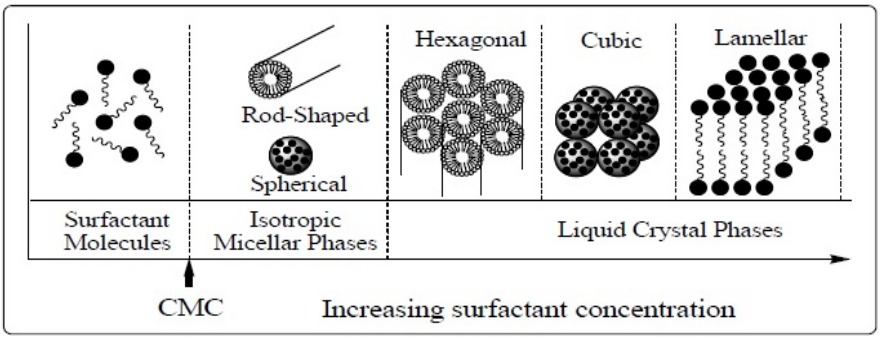

(1)

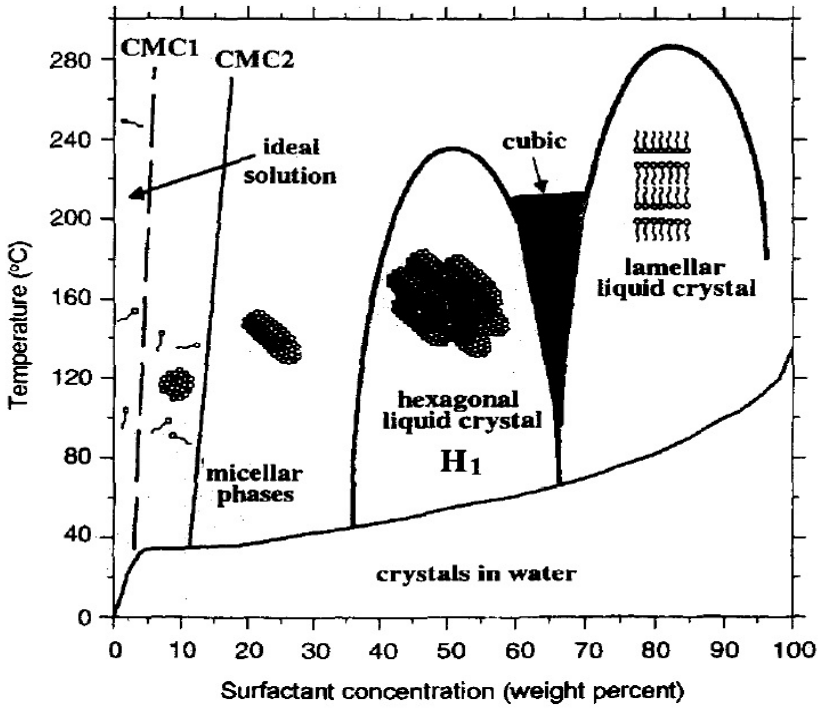

(2)

Figure 4.3 (1) Schematic representation of micelles formation and sub sequentially transformation into different mesoporous phases [1], (2) Schematic representation of C_{16}TAB in water and its transformation into different phases [3].

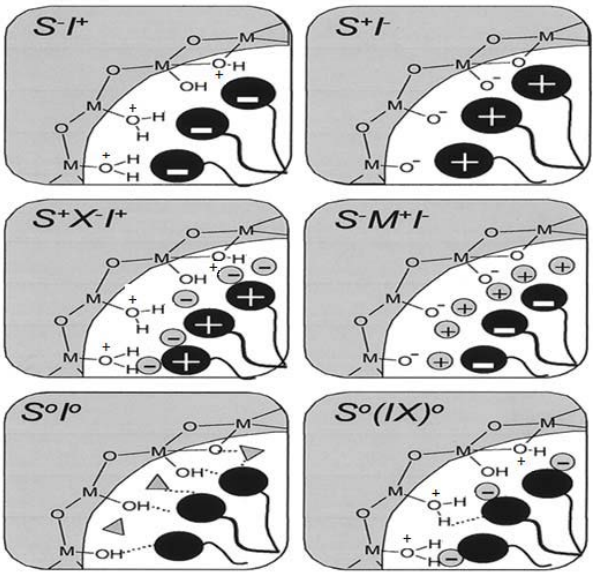

Figure 4.4 Schematic representation of possible interaction between types of silicate species to surfactant molecules [1].

4.1.2 Silicate chemistry during MCM-41 synthesis

There are different silica sources such as sodium silicate, tetramethoxysilane (TMOS), tetraethoxysilane (TEOS), fumed silica etc. that can be employed as an inorganic species during synthesis [2, 4].

In a typical synthesis procedure,

Step 1- The source of the silica undergoes hydrolysis in presence of water, which leads to production of silanol group (Si-OH)

Step 2- Further, silanol group condense with another silanol group, building strong siloxane (Si-O-Si) bonds, and produces water as a by-product. As the reaction proceeds the number of siloxane bonds increase, the particles tends to aggregate into a sol, which appears in the solution as small silicate clusters. Further condensation of these silicate clusters forms a thick gel along with water molecules.

Step 3 - The removal of these trapped molecules by heat treatment leads to formation of hard network. The whole process is termed as sol-gel as the species starts from solution (Sol) and leads to thick gel network (Gel).

4.1.3 Role of Catalyst

As explained in silicate chemistry above, in general hydrolysis and condensation of inorganic alkoxides (Si-O-R) are very rapid in absence of catalysts (acid or basic). However, hydrolysis of alkoxysilanes $(RO)_4$-Si is very slow hence, catalysts are needed. In the presence of acid catalyst, nucleation is the rate-controlling step where hydrolysis is very rapid. This process leads to less siloxane bonds and high number of silanol groups; in presence of base catalyst, hydrolysis is faster than acid catalyst and inhibit quick aggregation of particles, which produces dense materials with few silanol groups in the structure [1].

4.1.4 Boron substituted MCM-41

The idea of doping or substitution of silicate materials with boron (B^{3+}) ions is to create chemical and cation diversity in the framework. For example doping with trivalent cation (B^{3+}) into silicate network creates a negative charge around the network hence, it now becomes suitable host to adsorb cations such as caesium. In other words, it forms a Bronsted acid site depending on the nature of the trivalent cation [7, 8]. Boron containing MCM-41 structure carries [BO_4^-] tetrahedral units in the silicate network. It has been observed that boron changes its coordination to trigonal planar after calcination in which boron removed from the framework now resides within pores and is hydrated upon exposure to atmospheric humidity [7]. The study also revealed that calcined B-MCM-41 if brought into atmospheric moisture changes its trigonal coordinated geometry to a four- coordinate state and it removes another part of the boron from the framework [9]. Moreover, it demonstrate that low boron containing samples carry significant part of the boron presence in a strongly coordination state which is not removable by further thermal treatment [9]. Further, boron is an excellent natural neutron absorber [10] hence, this property could be ideal for stationary phase treating high level radioactive waste if fissile material is present provided its uptake and kinetics are good enough.

4.2 Material and Methods

4.2.1 Materials

All the reagents were purchased in the reasonably purest form and used without any prior treatment. The source and purity of the reagents used are presented in table 4.1.

Table 4.1 Reagents, their purity and source of purchase

Reagents	Company	Purity/Grade
Sodium Silicate ($Na_2O_7Si_3$)	Sigma Aldrich	Reagent Grade
Hexadecyltrimethylammonium bromide (CTAB)	VWR	≥98%
Boric Acid (H_3BO_3)	VWR	≥99%
Sodium Hydroxide (NaOH)	Sigma Aldrich	≥98%
Sulfuric Acid (H_2SO_4)	Fisher	≥95%
Nitric Acid (HNO_3)	Sigma Aldrich	Reagent Grade (≥69%)
Deionised Water (H_2O)	NA	≥18.2 $M\Omega.cm^{-1}$
Caesium nitrate ($CsNO_3$)	Sigma Aldrich	≥99.999%
Strontium nitrate ($Sr(NO_3)_2$)	Sigma Aldrich	≥99.995%
Ammonium cerium nitrate ($Ce(NH_4)_2(NO_3)_6$)	Sigma Aldrich	≥99.9%

4.2.2 Synthesis Method

4.2.2.1 Synthesis of Si- MCM-41 with different quantities of Na ions

Pure silica MCM-41 (Si-MCM-41) was synthesised from aqueous solution of sodium silicate ($Na_2O_7Si_3$) as the silica source and hexadecyltrimethylammonium bromide (CTAB) as pore forming agent. The materials were synthesised in the same molar ratio as describe by Dyer *et al*. [8] but different amount of Na ions in the following molar ratio X Na_2O: 0.53 CTAB: 1 SiO_2: 100 H_2O. The required quantity of chemicals are listed in table 4.2 and the synthesised samples were denoted as the mole ratio of Na_2O. As shown in table 4.2, 1.27 - 2.55 g of NaOH were dissolved in 80 ml of water, which was stirred at 50 °C until complete dissolution. 10.72 g of CTAB was mixed into the above solution and stirred until a clear solution was obtained (solution A). In a separate 50 ml glass beaker, 12 ml of sodium silicate ($Na_2O_7Si_3$) solution and 20 ml of deionised water were mixed by stirring at room temperature (Solution B). Solution B was mixed with solution- A dropwise with constant stirring and continued stirring for 2 hours at 50 °C. The pH of the mixture was then adjusted to between 9 and 10 from 12 by adding concentrated sulfuric acid (H_2SO_4) dropwise. The cloudy white gel was transferred to a 125 ml Teflon-lined autoclave and heated to 150 °C for (72 hours) in an oven. The vessel was allowed to cool to room temperature and the gel was gravity filtered through a Whatman No 6 filter paper. The solids were washed with 500 ml of deionised water and further drying at 50 °C for 24 hours. The dry solids were ground and subsequently calcined at in a furnace from room temperature to 560 °C at heating rate 2 °C/min before being held at the final temperature for 6 hours.

Table 4.2 Amount of reagents used for Si-MCM-41 synthesis

Samples	$Na_2O_7Si_3$ (ml)	CTAB (g)	X (NaOH) (g)	H_2O (ml)
0.29 Si-MCM-41	12	10.72	1.27	100
0.43 Si-MCM-41			1.89	
0.58 Si-MCM-41			2.55	

4.2.2.2 Synthesis of boron substituted MCM-41

Different weight percentages of boron substituted MCM-41s were prepared by similar technique as mentioned above, with increased (3 times) the quantity of starting reagents and only modification of adding boric acid. Y amount (table 4.3) of boric acid (H_3BO_3) was carefully weighed and dissolved in 20 ml of deionised water (Solution C) and

added dropwise after addition of sodium silicate (Solution B). The washed liquor was collected for boron analysis. The required quantity of chemicals are listed in table 4.3.

Table 4.3 Amount of reagents used for B-MCM-41 synthesis

Samples	$Na_2O_7Si_3$ (ml)	CTAB (g)	NaOH (g)	H_2O (ml)	Y (H_3BO_3) (g)
5% B-MCM-41	37.32	32.16	5.67	300	0.51
10% B-MCM-41					1.03
20% B-MCM-41					2.06
30% B-MCM-41					3.09

4.2.3 Characterisation

The structural characterisation of all the samples was achieved by low angle PXRD. The textural characteristics were evaluated by nitrogen sorption. Different physical properties were analysed by SEM, TEM, FTIR, ^{29}Si NMR, and TGA. These techniques have been explained in chapter 3.

The amount of boron in the structure was calculated by measuring amount of boron present in the synthesis gel and amount found in the washed liquor by ICP-MS. The difference was assumed to be substituted in the structure. The detailed measurement experiment has been described in ICP-MS experimentation section in chapter 3.2.9

The uptake measurement of various ions by ICP-MS has been explained in chapter 3.2.9

4.3 Results and Discussion

The synthesised materials were white powders and approximately 10 g (from four 125 ml autoclaves), approximately 66% yield obtained after calcination, with particle size ≤ 2 µm. It was noted that during the addition of silica source to the surfactant solution a cloudy solution was produced; this was believed to be due to the interaction of hydrolysed silica with micelles. Further condensation was taking place whilst the pH of the final gel mixture was being adjusted from 12 to 9 – 10 producing hydrolysed silica. These observations support the theory explained earlier in figure 4.1 and 4.2 and found by previous work [2, 5, 7, 8].

The structural and physiochemical data will now be discussed.

4.3.1 PXRD

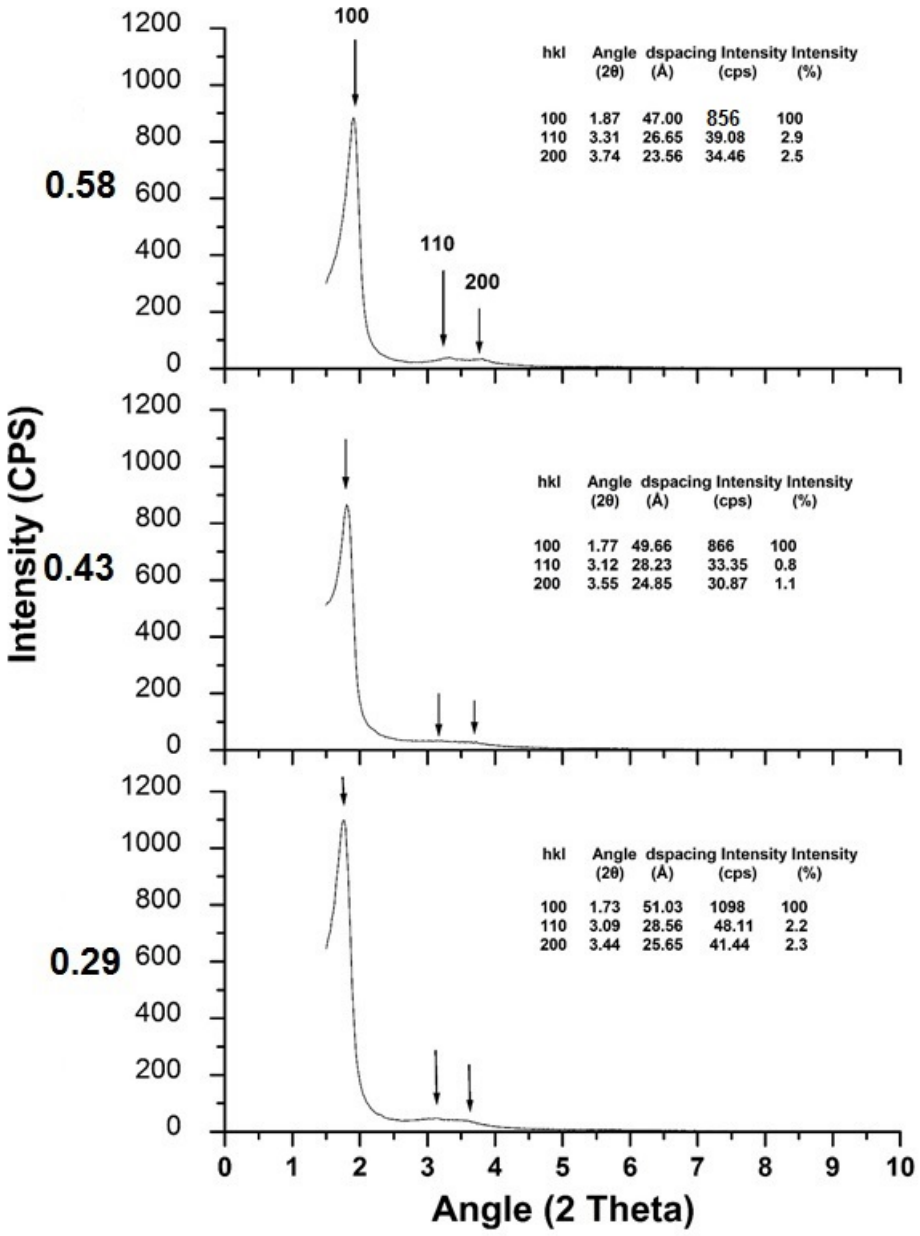

Figure 4.5 Low angle PXRD comparison of different amount of NaOH synthesised Si-MCM-41

The Powder X-ray powder diffraction pattern of the different sodium ratios materials are shown in figure 4.5. Each diffraction pattern was the same as those of MCM-41 previously described elsewhere [2, 7-9, 11]. A sharp Bragg peak ascribed to the (100) reflection of the structure was observed between 1.7 – 1.8° which corresponds to d spacing 47 – 51 Å. Besides the strong peak, two weak peaks were also recorded which were ascribed to (110) and (200) reflections. The three clear peaks (one strong and two

peaks) indicate that the long-range order in the structure had been achieved which was similar to previously reported data [2, 5, 7-9, 11].

Increased amounts of sodium content had a little effect on the XRD pattern. The d spacing of reflection (100) was reduced with increasing sodium content. Subsequently the reflection angle was also changed and hence their overall lattice parameter (figure 4.5) (table 4.4).

Table 4.4 Lattice parameters in Si-MCM-41

Samples	**Lattice parameter ($a_0=2d_{100}/\sqrt{3}$) (Å)**
0.29	58.92
0.43	57.34
0.58	54.27

The PXRD profiles of different quantities of boron as a hetero-cation substituted in MCM-41 framework are presented in figure 4.6. There were again three reflections observed which are characteristic x-ray profile for hexagonal MCM-41 structure as reported by previous work [1, 7, 11]. The profile contained three broad but separated reflections between 1 – 6° 2θ regions which was consistent with previous results [1, 7, 11] and that indicates high ordering in the material at atomic level even after boron ions substitution.

Substitution of various cations into the framework could affect size of the unit cell [8]. Boron substituted MCM-41 had shown similar (100) reflection intensities compared to Si-MCM-41, which indicates the higher atomic distribution in the synthesised material.

Increased quantities of boron resulted in decreased d spacing which is compared and shown in figure 4.6 (100 reflection) except 10%B sample. The lattice parameter calculations has also shown decrease in the unit cell, which was consistent due to decreased d spacing and hence overall structure.

The intensities of peak 1 in all boron substituted MCM-41 samples were similar except for 10%B constituent, which was slightly less. Comparison of overall lattice parameter of boron substituted MCM-41 structures revealed that 10%B has the biggest lattice

parameter (Table 4.5). Pore analysis has shown highest total pore volume of this structure (table 4.8). The variation in 10%B MCM-41 structure was attributed to highest amount of boron that had been incorporated into the structure measured by ICP-MS (Table 4.6). Hence, the loss of intensity could be defined by the loss of structural integrity due to increased substitution of boron in the structure compared to other boron substituted MCM-41 materials. Similar evaluation also reported by Dyer *et. al*. [8]

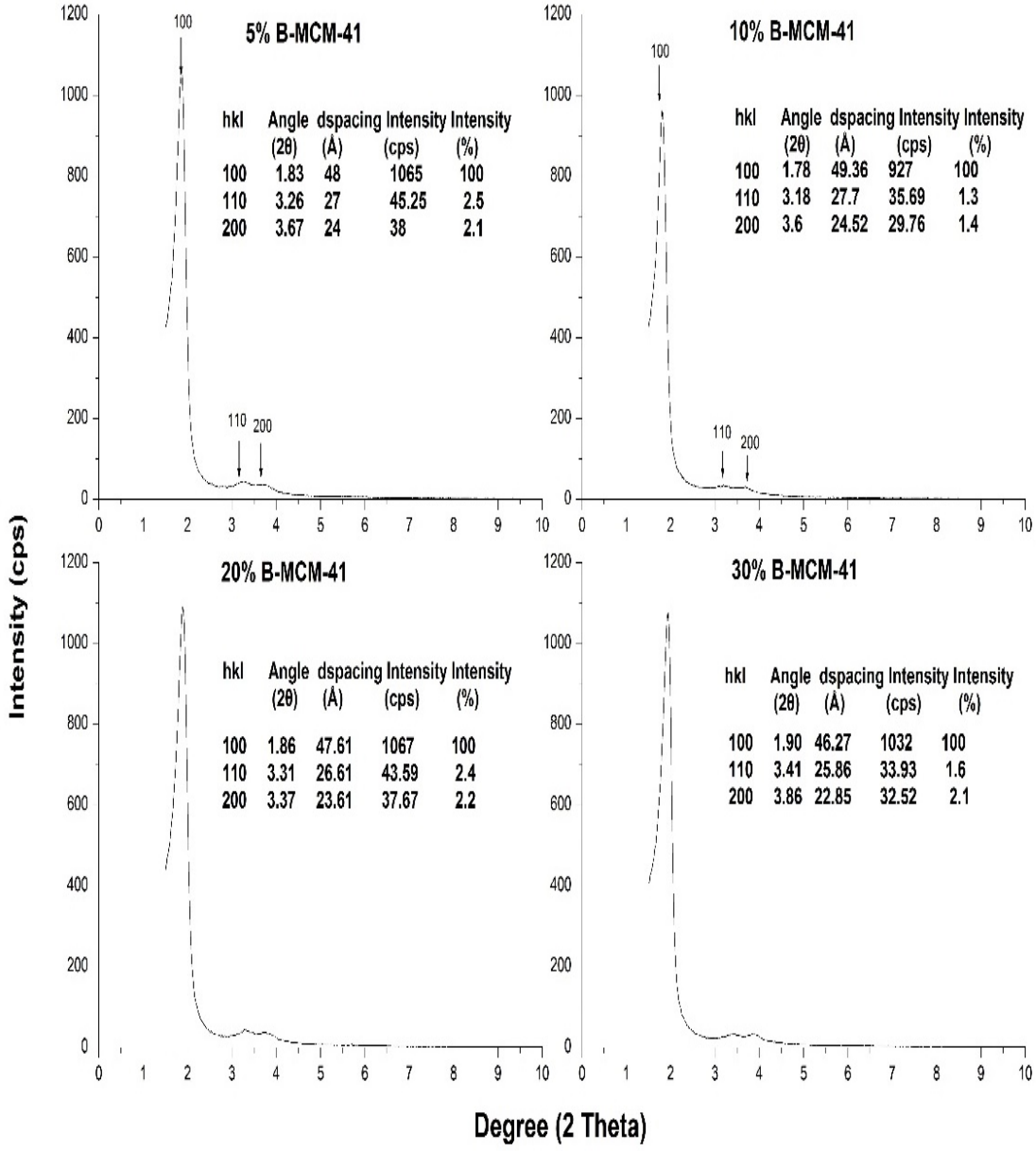

Figure 4.6 Low angle PXRD pattern of boron substituted MCM-41

Table 4.5 Lattice parameters of boron incorporated MCM-41

Samples	Lattice parameter ($a_0=2d_{100}/\sqrt{3}$) (Å)
5% B-MCM-41	55.47
10% B-MCM-41	57.06
20% B-MCM-41	55.04
30% B-MCM-41	53.49

Table 4.6 Amount of boron in MCM-41 structure measured by ICP-MS

Samples	Amount of Boron during synthesis (ppm)	Amount of Boron in filtrate (ppm)	Difference (ppm)	Boron content in structure (%)
5% B-MCM-41	290	56	233	80%
10% B-MCM-41	580	7	572	98%
20% B-MCM-41	1161	320	841	72%
30% B-MCM-41	1731	466	1265	73%

4.3.2 Surface area and Pore analysis

The textural properties of porous MCM-41 and heteroatoms (boron) substituted MCM-41 structures were characterised by gas (Nitrogen) sorption method by analysing their surface area, pore size distribution, and pore volume. The method of gas sorption has been explained in chapter 3.

Nature of isotherm

The isotherms obtained from siliceous and boron substituted MCM-41 were very similar to type IV isotherm according to classification of IUPAC [14]. The type IV isotherms exhibit characteristic hysteresis loop between 0.3 - 0.5 relative pressure which is associated with capillary condensation taking place in mesoporous and limiting uptake over a range of high relative pressure (P/P_o) (figure 4.7 and 4.8) [14]. The starting point of the isotherm of this kind is attributed to monolayer-multilayer adsorption [14].

Figure 4.7 represents the comparison of Si-MCM-41 different sodium ratios. As the concentration of Na ions increased, the volume of gas adsorption decreased. There is very marginal difference between sample 0.29 and 0.43 Si-MCM-41 samples.

Figure 4.8 represents the comparison of 0.43 MCM-41 to boron substituted MCM-41. The study revealed that boron substituted samples had shown similar gas sorption profile to Si-MCM-41 (For comparison 0.43 Si-MCM-41 was used as a benchmark).

The shape of the hysteresis loops can be associated with specific pore structures [14]. Si-MCM-41, 5%, 10%, 20% B-MCM-41 show similar hysteresis loops where 30%B MCM-41 has shown a narrow loop which could be due the size and the geometry of the pore structure affected by amount of boron incorporated into the lattice.

All the samples show absence of extension in the relative pressure region 0.9 - 1 which also indicate absence of macro pores. Hence, materials have a well-ordered mesoporous structure as already established from PXRD studies.

Surface area, pore volume and poresize distribution

BET analysis was performed to determine the specific surface area. As shown in table 4.7, the specific surface area was affected by increased quantities of Na ions. The surface area decreased as amount of Na ions increased, which supports isotherm evaluation results.

In the case of boron-substituted samples, 5% and 10% samples show increased surface area where 20% and 30% samples had diminishing effect (table 4.8). Similar trend was observed with 20% and 30% samples that had the boron content 72% and 73% (table 4.6). Hence, amount of boron in the structure can be very important in the preparation of this kind of material. This was possibly due to bond length of Si-O and B-O as it affects the overall structure. The mean Si-O and B-O bond length were estimated to be 1.59 Å and 1.20 Å respectively [15, 16]. The study was not intended to measure actual bond length.

BJH calculations were performed to measure pore size and pore size distributions in the synthesised samples. Figures 4.9 and 4.10 illustrate the narrow pore size distribution, which confirms the uniform and highly ordered structure. Pore volume analysis also revealed the effect of Na ions, which was consistent from isotherm and surface area evaluations. 0.29 Si MCM-41 has highest pore volume and biggest pore size. In the case of boron substituted samples, 10%B sample has highest pore volume and biggest pore size while others gradually decreased (table 4.8).

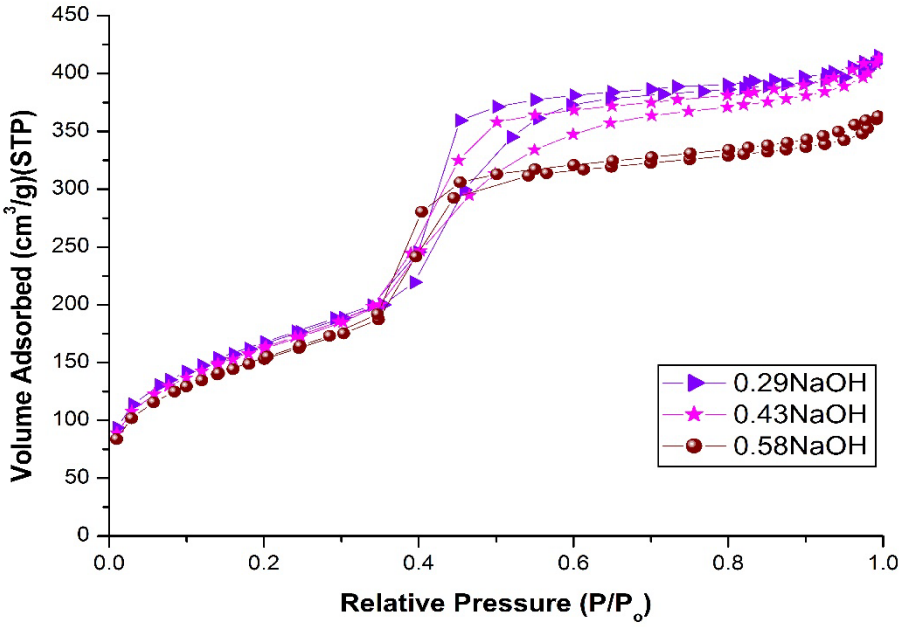

Figure 4.7 Isotherm comparison of different amount of Na synthesised Si-MCM-41

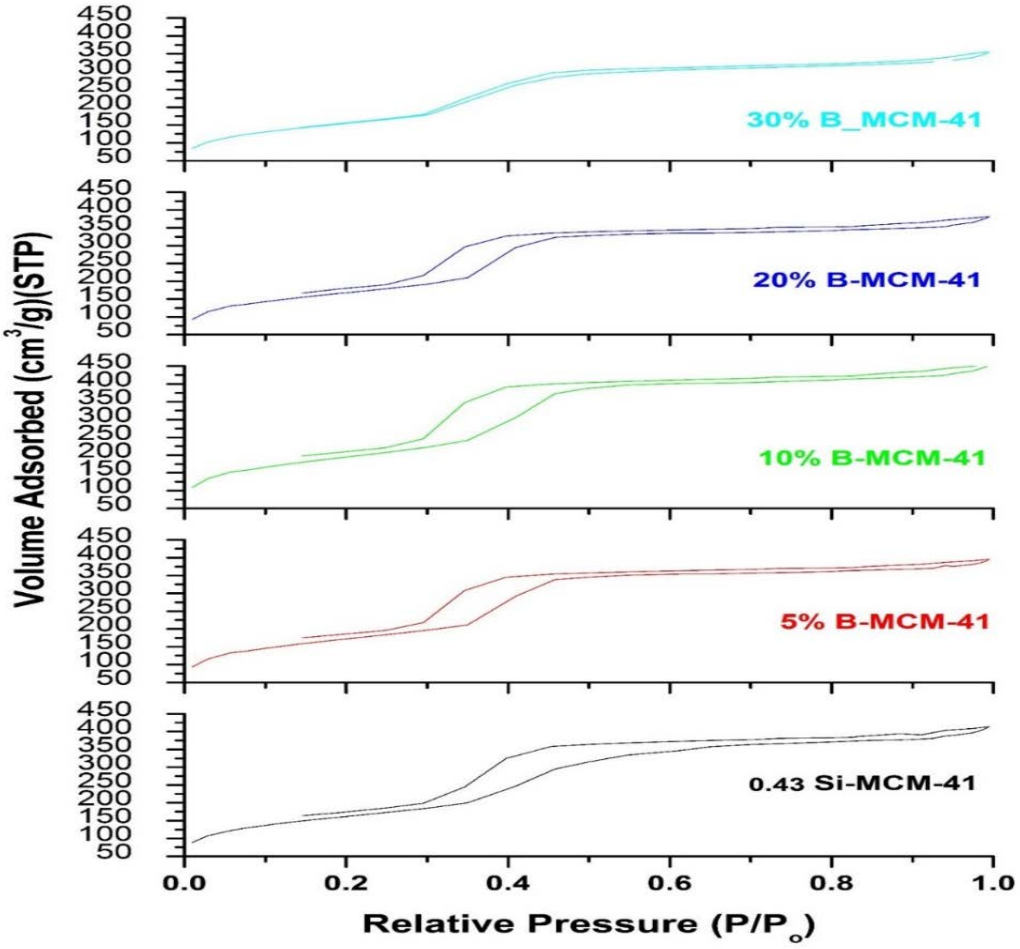

Figure 4.8 Isotherms comparison with 0.43 Si-MCM-41 and boron substituted MCM-41

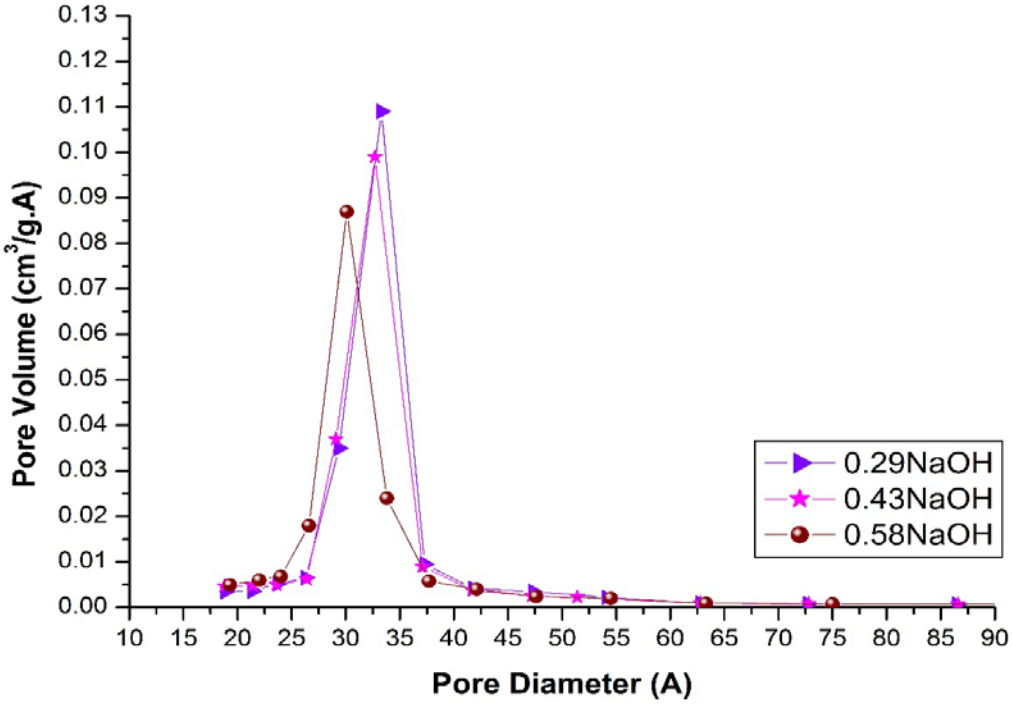

Figure 4.9 Comparison of pore size distribution of different amount of Na synthesised Si-MCM-41

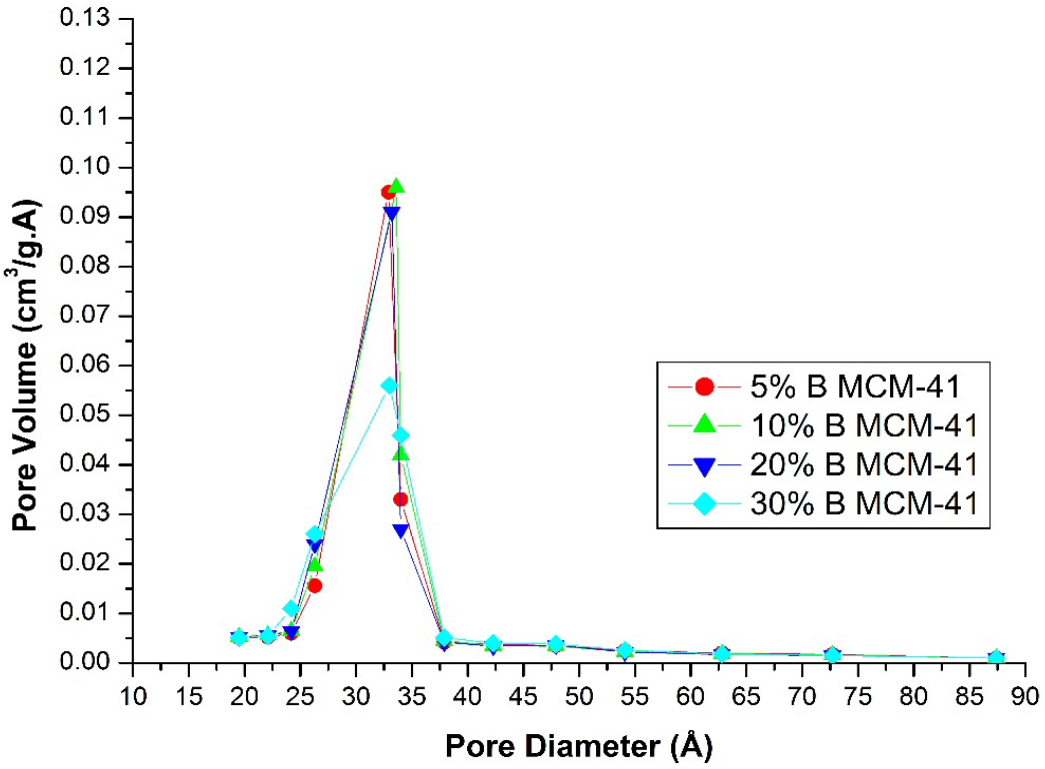

Figure 4.10 Comparison of pore size distribution in boron substituted MCM-41

Table 4.7 Surface area and Pore analysis of Si-MCM-41

Samples	Specific Surface area (BET) "S_{BET}" (m^2/g)	Total Pore Volume "V_P" (cm^3/g)	Av. Pore diameter "D_P" (Å)
0.29Si-MCM-41	585	0.620	34.74
0.43Si-MCM-41	577	0.613	34.68
0.58Si-MCM-41	545	0.538	33.40

Table 4.8 Surface area and Pore volume analysis of boron substituted MCM-41

Samples	Specific Surface area (BET) (m^2/g)	Total Pore Volume (cm^3/g)	Av. Pore diameter "D_p" (Å)
5% B-MCM-41	613	0.589	32.96
10% B-MCM-41	690	0.674	33.68
20% B-MCM-41	596	0.564	33.22
30% B-MCM-41	557	0.524	33.02

4.3.3 ATR-IR

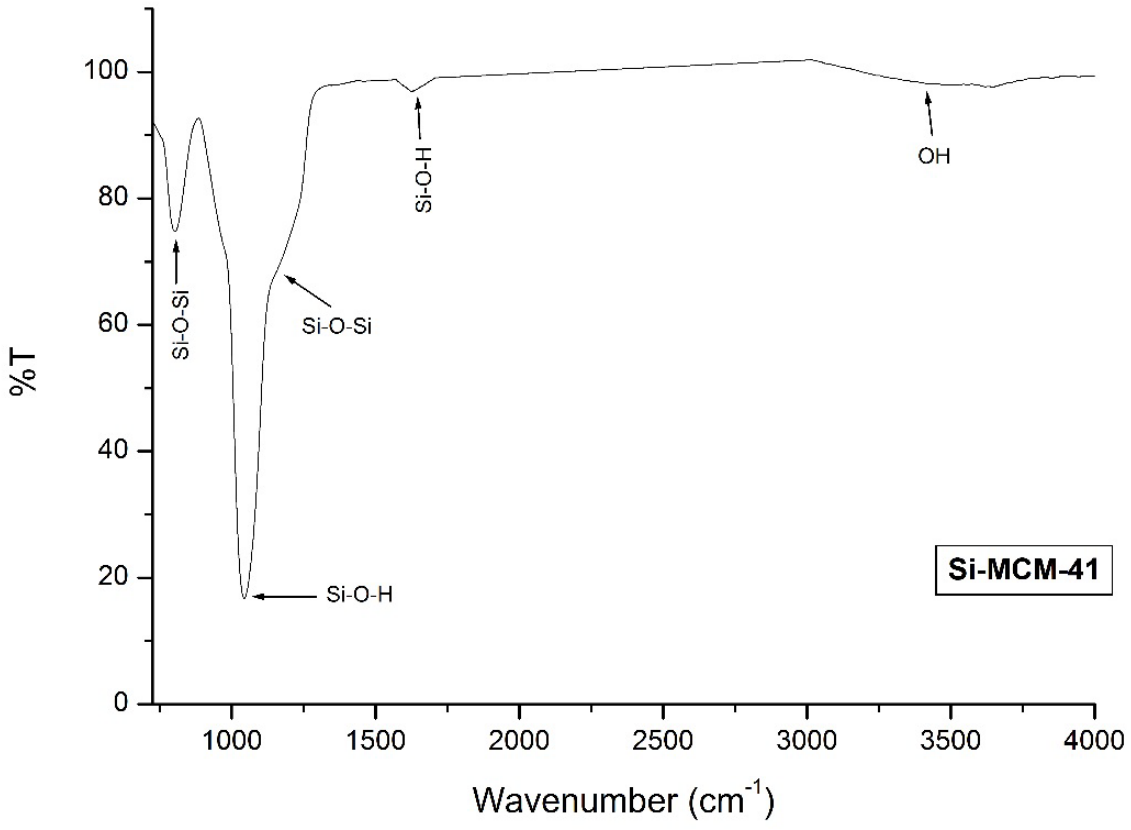

Figure 4.11 ATR-IR Study of 0.43 Si-MCM-41

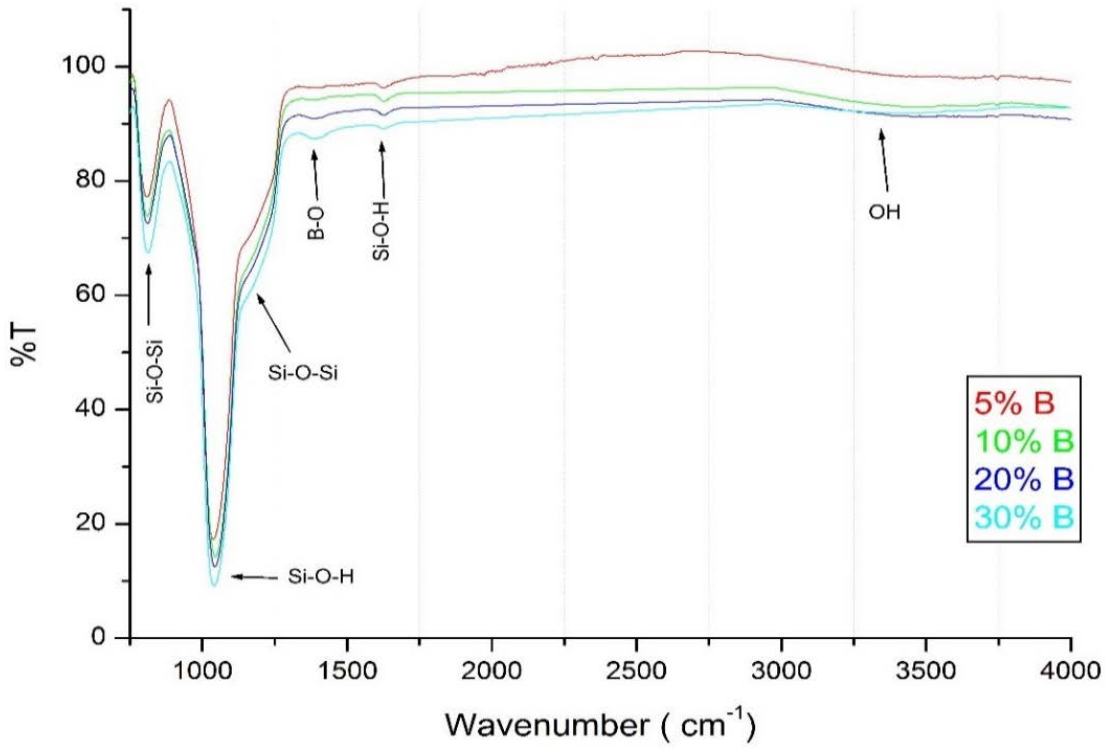

Figure 4.12 ATR-IR Study of boron substituted MCM-41

Table 4.9 Observed IR band position in MCM-41

Sample	Symmetrical Stretching Si-O-Si (cm^{-1})	Si-O-H (cm^{-1})	Asymmetrical (external Stretching) Si-O-Si (cm^{-1})	Si-O-H (cm^{-1})	B-O (cm^{-1})	O-H (cm^{-1})
0.43 Si-MCM-41	806	1030	1200	1630	NA	3250-3700
5% B-MCM-41	807	1037	1200	1623	1375.	3250-3700
10% B-MCM-41	809	1045	1200	1626	1387	3250-3700
20% B-MCM-41	810	1043	1200	1626	1384	3250-3700
30% B-MCM-41	812	1040	1200	1625	1387	3250-3700

4.3.4 ^{29}Si NMR

Table 4.10 Observed chemical shifts in solid state NMR

Samples	^{29}Si (ppm)			Figure No.
	Q_4 $(Si–O–)_4Si$	Q_3 $(Si–O–)_3Si$	Q_2 $(Si–O–)_2Si(OH)$	
Si-MCM-41	-111	-103	-99	4.13 (a)
5%B MCM-41	-111	-101	-96	4.13 (b)
10%B MCM-41	-112	-102	-95	4.13 (c)
20%B MCM-41	-111	-101	-92	4.13 (d)
30%B MCM-41	-111	-101	-94	4.13 (e)

ATR-IR and ^{29}Si NMR studies were carried out to understand chemical interaction between the species in synthesised materials. Figures 4.11 and 4.12 represent a typical profile of vibration bonds between the chemical species in Si-MCM-41 and boron substituted MCM-41 respectively.

For NMR, these species have been designated as Q_n where n = 0 - 4 and the number of next nearest adjacent Si atoms. High percentage of Q_3 and Q_4 had been identified previously for these kind of silica based mesoporous materials by ^{29}Si NMR [17, 18]. It has been generally agreed that bands found in IR spectroscopy at ≈1200 cm^{-1} were caused by asymmetrical *Si-O* (external stretching vibrations) and those between 1100-1000 cm^{-1} were by internal vibrations of the Q_3 and Q_4 species which were assigned to *$(Si–O–)_3SiOH$ and $(Si–O–)_4Si$* respectively [7, 8, 12, 17, 18]. Further, a broad absorption band has been observed in the range of 3554 cm^{-1}, which can be assigned to hydrogen bonded OH group shown in ATR-IR results (figures 4.11 and 4.12).

As seen from table 4.10, Q_2, Q_3 and Q_4 species were found in all the MCM-41 materials where Q_4 species dominates. This represents high order of polymerisation in the material.

For boron substituted MCM-41, it has been observed that the small peak at 1391 cm^{-1} could be assigned to boron-oxygen (*B-O*), measured by ATR-IR studies of all B-Si-MCM-41,which was consistent with previous result [19]. The later study observed that boron changes its coordination to trigonal planar after calcination in which boron when removed from the framework now resides within pores and becomes hydrated upon exposure to atmospheric humidity [7]. Studies also revealed that calcined B-MCM-41 if brought into the presence of atmospheric moisture, it changes its trigonal coordinated geometry to a four- coordinate state, and it removes another part of the boron from the framework [9]. This could be verified by ^{11}B NMR, which should show sharp boron peaks indicating position of B-O in various arrangements, however this was not performed.

From the ATR-IR and ^{29}Si NMR results, it is reasonable to conclude that:

1) The impregnation of boron in silica network was successfully achieved

2) As the intensity of Q_4 species were dominating in all the synthesised materials possibly indicates the higher degree of polymerisation of silica network had been successfully accomplished (figure 4.13). This was confirmed by the 1030 cm^{-1} peak in the IR spectra.

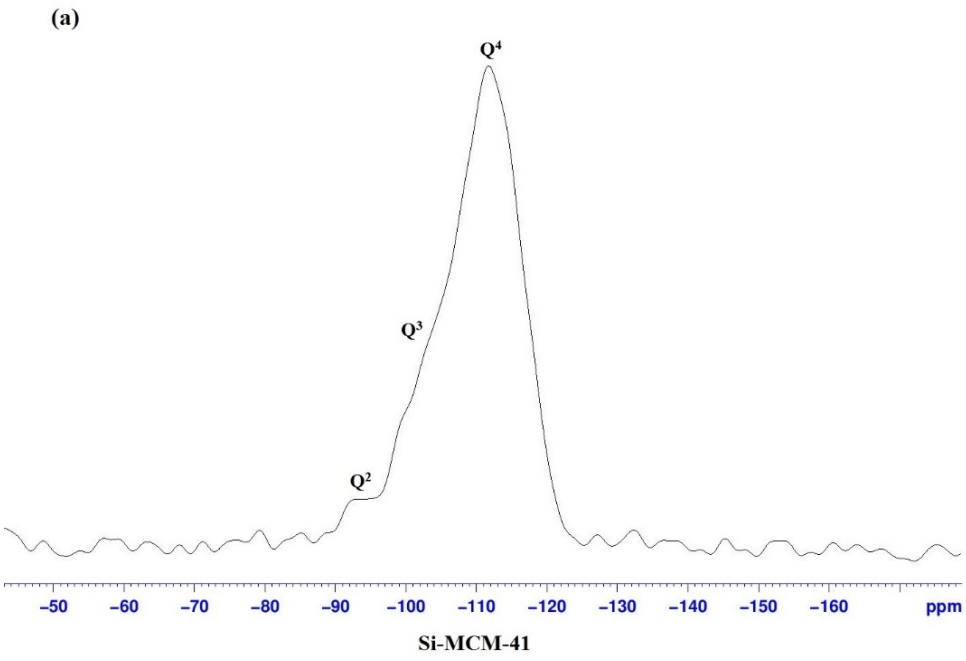

Figure 4.13 (a) ^{29}Si NMR peaks analysis on of Si-MCM-41

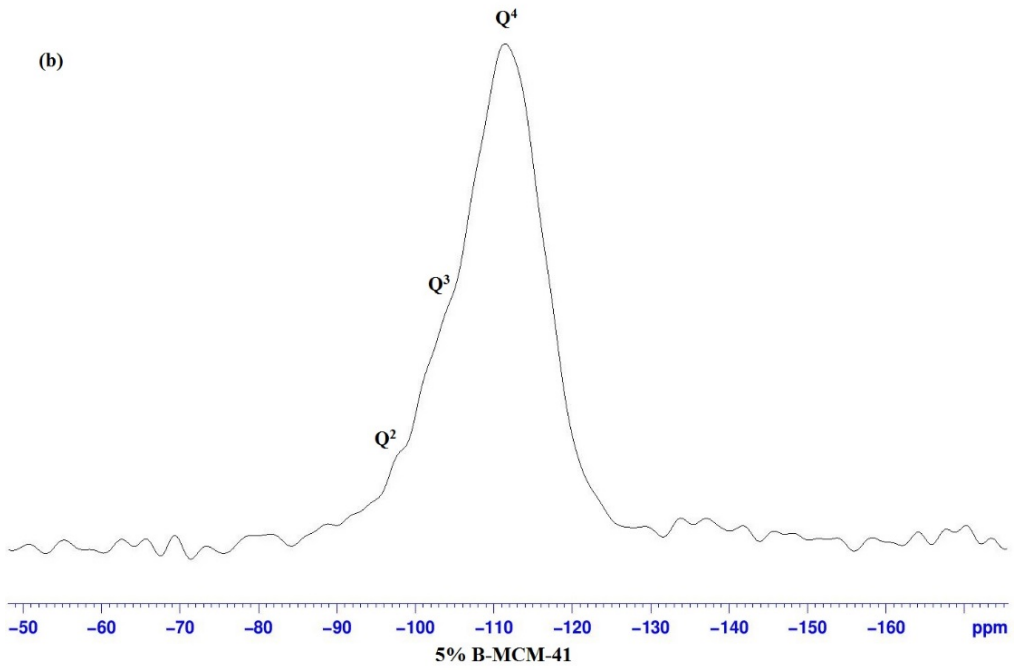

Figure 4.13 (b) ^{29}Si NMR peaks analysis of 5% boron substituted MCM-41

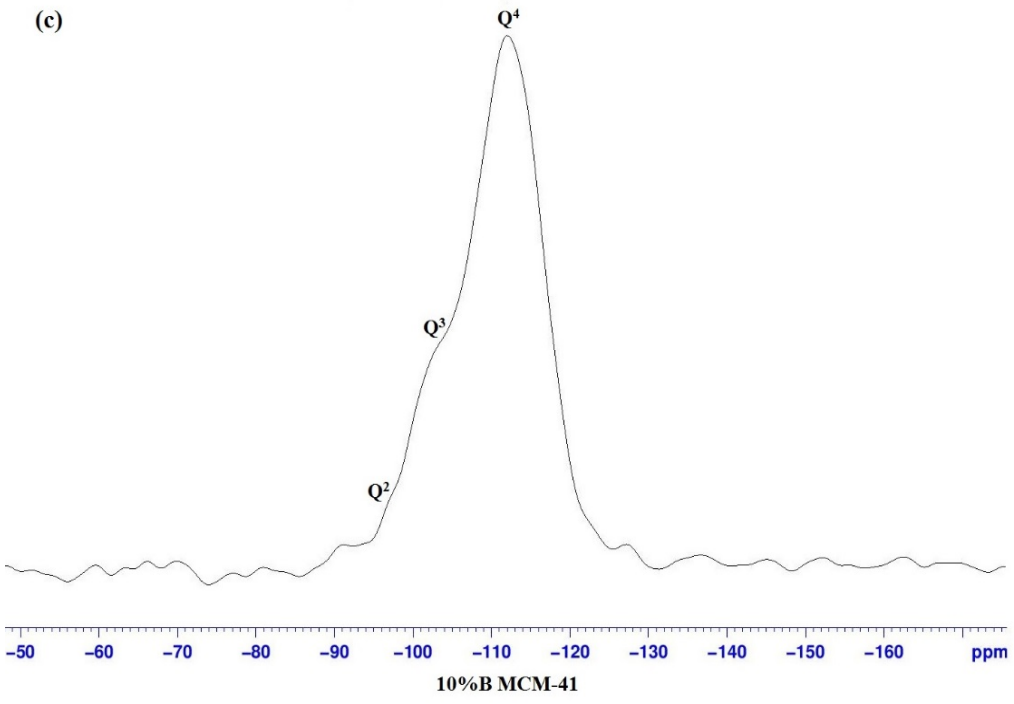

Figure 4.13 (c) ^{29}Si NMR peaks analysis of 10% boron substituted MCM-41

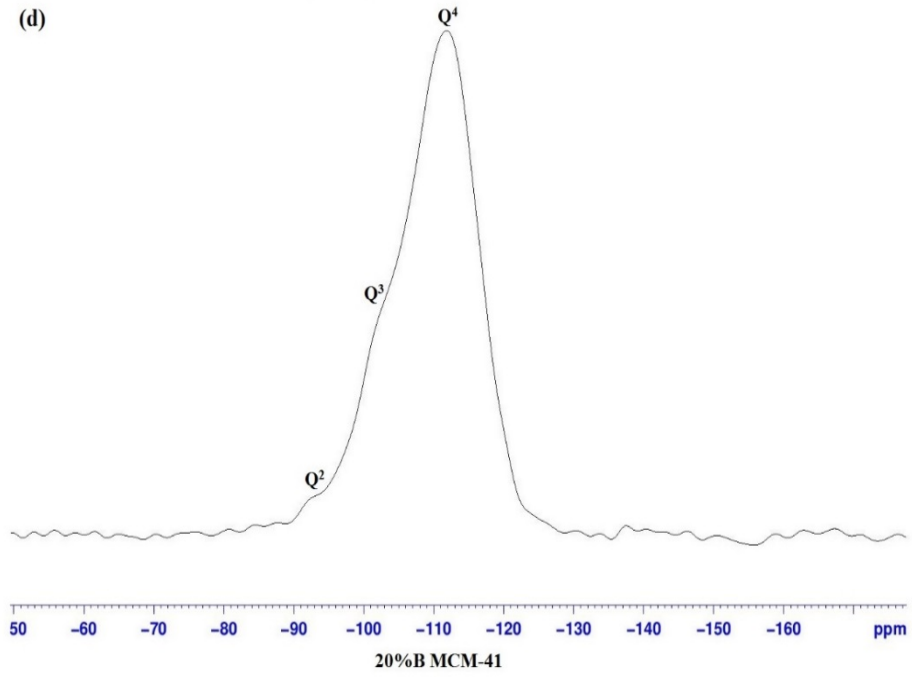

Figure 4.13 (d) ^{29}Si NMR peaks analysis of 20% boron substituted MCM-41

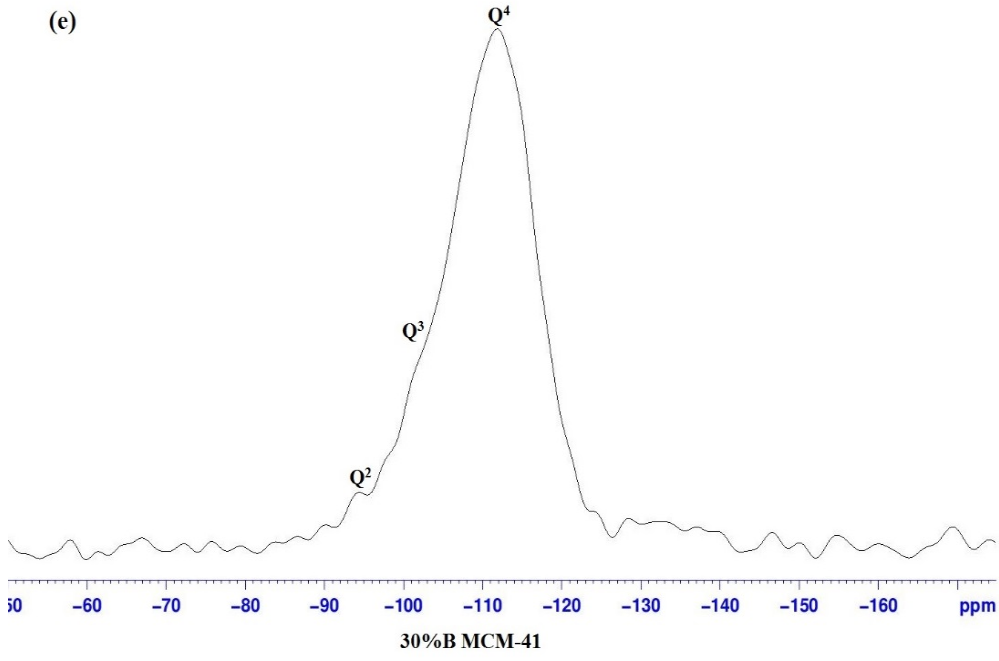

Figure 4.13 (d) ^{29}Si NMR peaks analysis of 30% boron substituted MCM-41

4.3.5 SEM

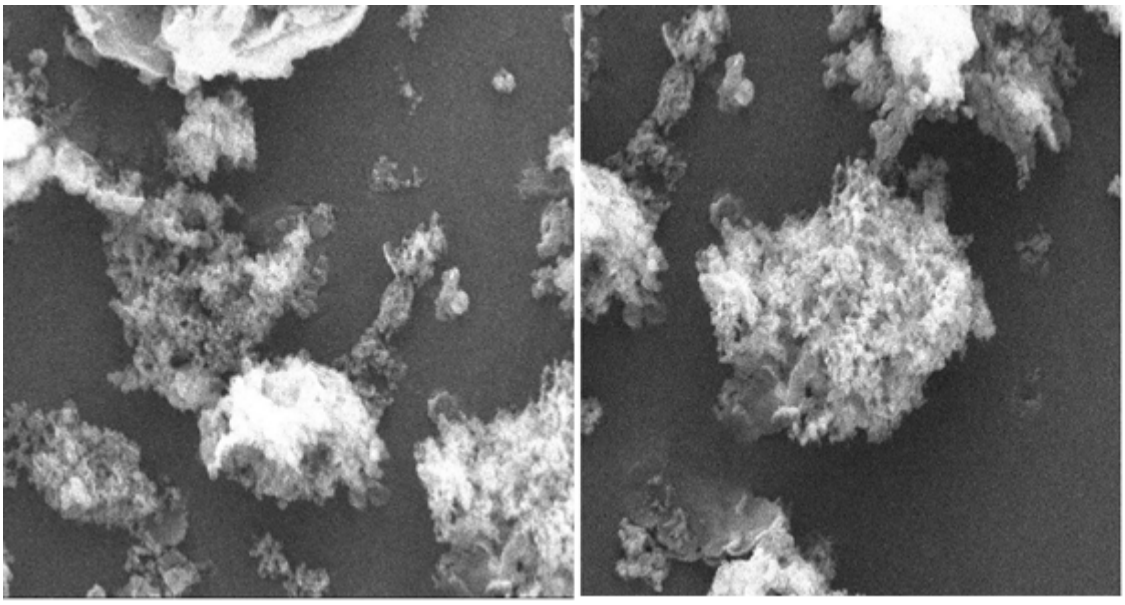

Figure 4.14 SEM Image of Si-MCM-41 with 4000X magnification

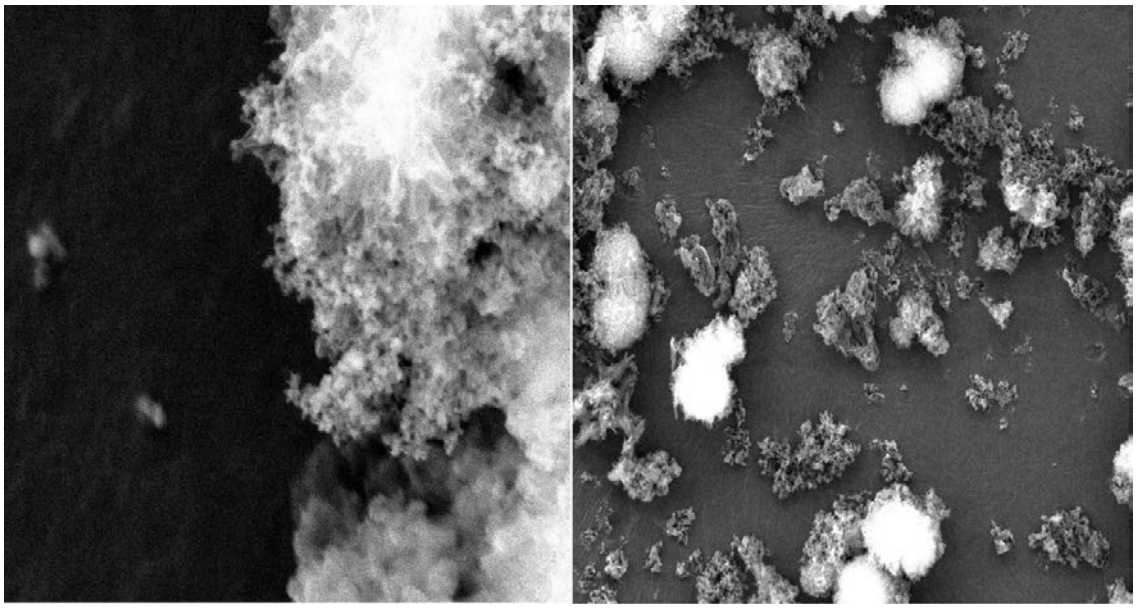

Figure 4.15 SEM Image of boron substituted MCM-41with 4000X magnification

4.3.6 TEM

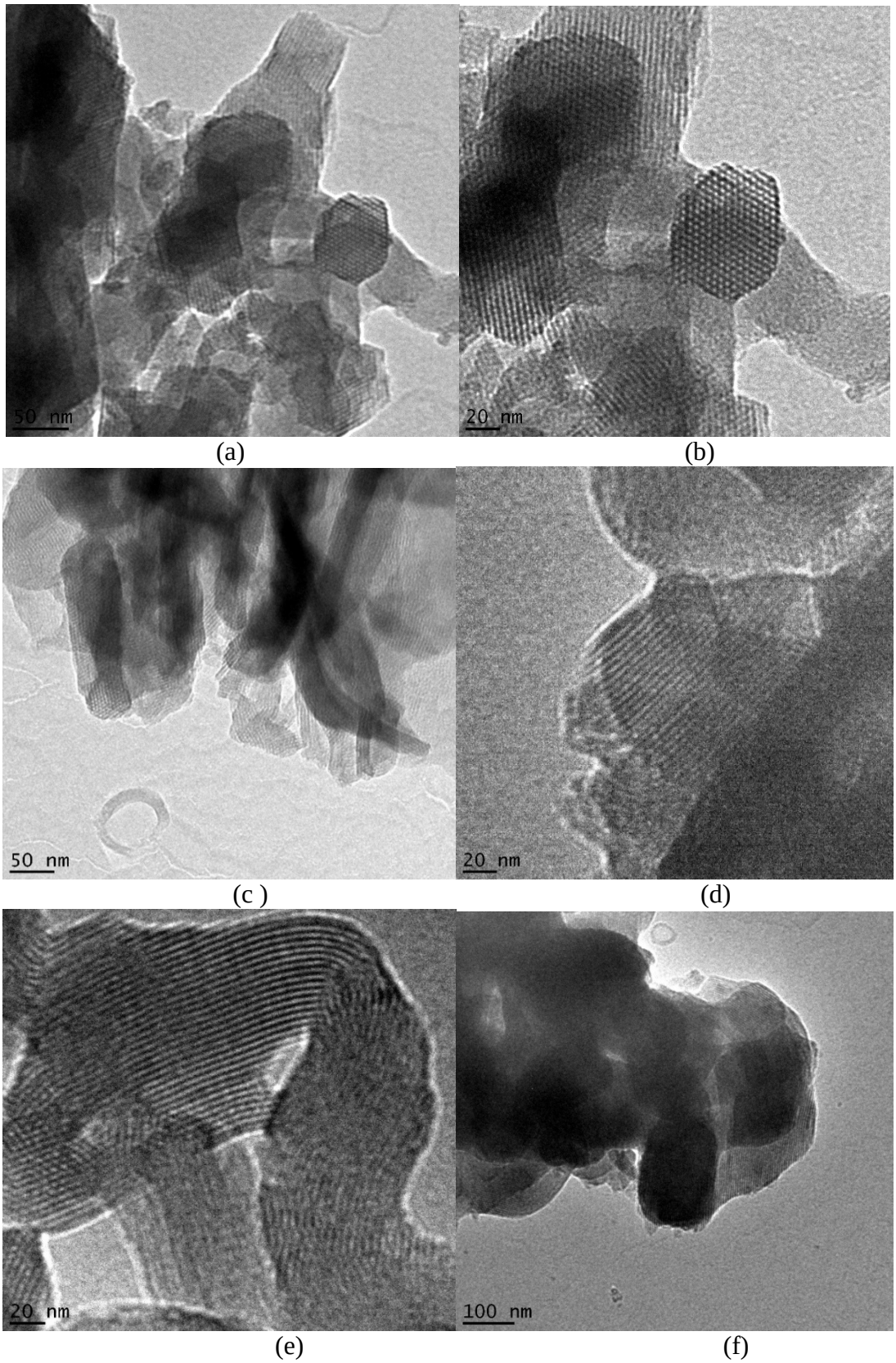

(a) (b)

(c) (d)

(e) (f)

Figure 4.16 TEM images of (a and b) Si-MCM-41, (c, d, e and f) boron substituted MCM-41

The morphology, shape, and size of the mesoporous Si-MCM-41, and B-Si-MCM-41 materials were characterised by high resolution scanning electron microscopy (SEM) and Transmission Electron Microscopy (TEM). The micrographs in figures 4.14 and 4.15 show agglomerated porous framework of the material. High-resolution TEM images of all MCM-41 particles show well-ordered hexagonal structure. Similar material and textural properties have been previously reported [2, 5, 7 - 9, 12]. TEM images of mesoporous MCM-41 show well defined channels and walls (figure 4.16). The study revealed the consistency of the materials previous evaluated in this research by PXRD, and gas sorption.

4.3.7 TGA analysis

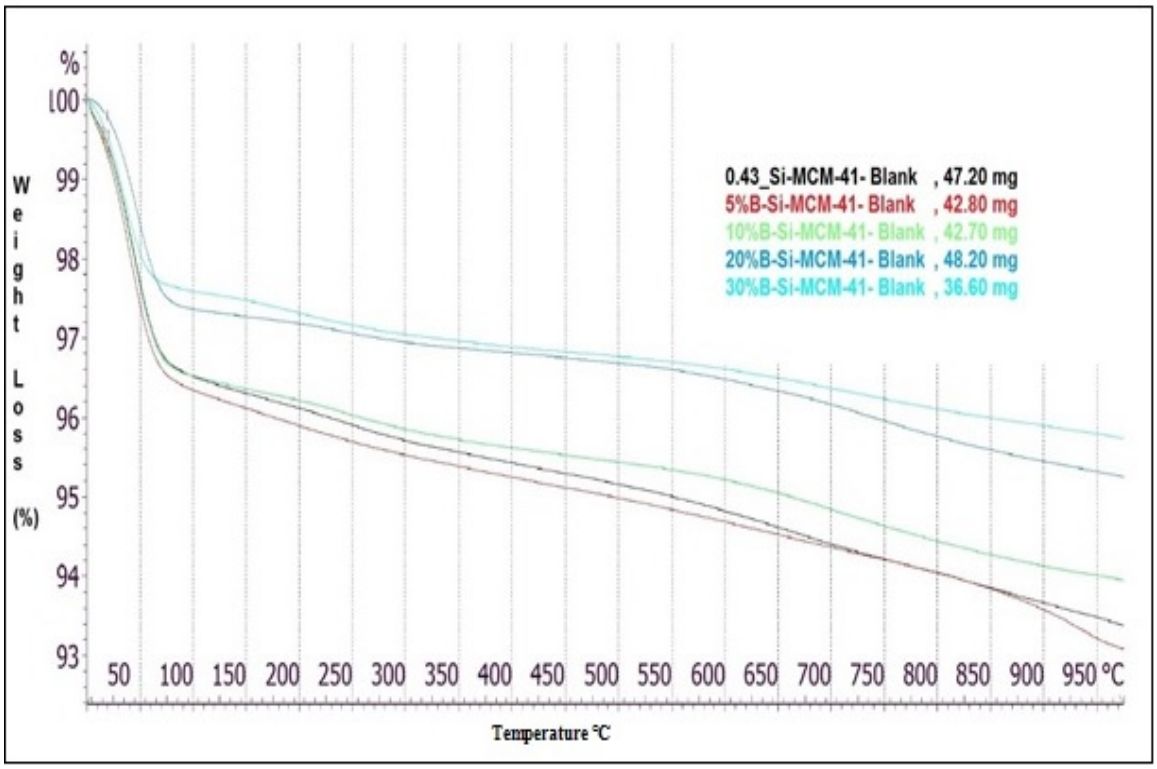

Figure 4.17 TGA evaluation of MCM-41

Thermal stability of MCM-41 materials were found to be very robust up to 1000 °C in air, losing only maximum 7% by weight. The initial weight loss up to 100 °C was due to loss of moisture. The weight loss was inversely proportional to the boron content of the structure; higher the boron quantity, lower the weight loss (figure 4.17). This evaluation suggests that loss of water at higher temperature originated from hydroxyl groups in pure Si-MCM-41, but in the reduced presence of these groups in higher boron substituted MCM-41 resulted into lower weight loss. This study may have more value for characterisation of catalysis rather than ion exchange materials.

4.3.8 Cation uptake measurements

The main objective of preparing and characterising these materials was to understand the separation of different cations by creating negative imbalance in an ordered structure. Different cation simulants were used to mimic the radionuclide concentration in high-level nuclear waste. Ce^{4+} ions was used as surrogate for Pu and/or U ions. High-level waste is usually in 1 - 3 M HNO_3 condition however, the study was extended to weakly acidic (D.W) system as the materials may have potential for treating other liquid nuclear wastes.

Table 4.11 Caesium ion concentrations in various aqueous systems

Samples	Initial (ppm)	Final (ppm)	Volume (ml)	Weight (g)	Kd (ml/g)
1 M HNO_3					
Si-MCM-41	654±8	642±6	25	0.50	0.93
5%B-MCM-41		644±8			0.78
10%B-MCM-41		640±6			1.09
20%B-MCM-41		645±10			0.70
30%B-MCM-41		640±6			1.09
0.5 M HNO_3					
Si-MCM-41	680±8	664±7	25	0.50	1.20
5%B-MCM-41		680±15			0.00
10%B-MCM-41		664±9			1.20
20%B-MCM-41		671±13			0.67
30%B-MCM-41		670±10			0.75
Deionised water (pH 4.60)					
Si-MCM-41	691±11	642±14	25	0.50	3.82
5%B-MCM-41		624±12			5.37
10%B-MCM-41		632±8			4.67
20%B-MCM-41		641±10			3.90
30%B-MCM-41		608±9			6.83

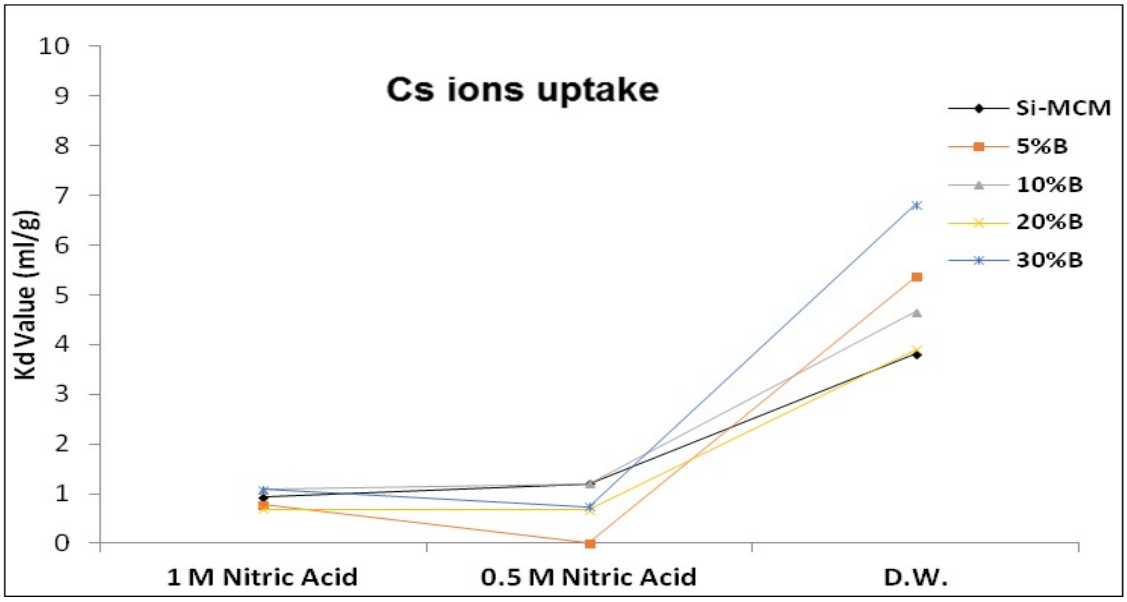

Figure 4.18 Cs ion Kd value for various aqueous systems

Table 4.12 Strontium ion concentrations in various aqueous systems

Samples	Initial (ppm)	Final (ppm)	Volume (ml)	Weight (g)	Kd (ml/g)
1 M HNO_3					
Si-MCM-41	464±6	439±6	25	0.50	2.85
5%B-MCM-41		450±7			1.56
10%B-MCM-41		433±8			3.58
20%B-MCM-41		429±5			4.08
30%B-MCM-41		438±4			2.97
0.5 M HNO_3					
Si-MCM-41	455±8	436±5	25	0.50	2.18
5%B-MCM-41		442±5			1.47
10%B-MCM-41		446±4			1.01
20%B-MCM-41		448±7			0.78
30%B-MCM-41		440±7			1.70
Deionised water (pH 5.60)					
Si-MCM-41	462±10	371±5	25	0.50	12.26
5%B-MCM-41		361±3			13.99
10%B-MCM-41		436±7			2.98
20%B-MCM-41		425±8			4.35
30%B-MCM-41		421±8			4.87

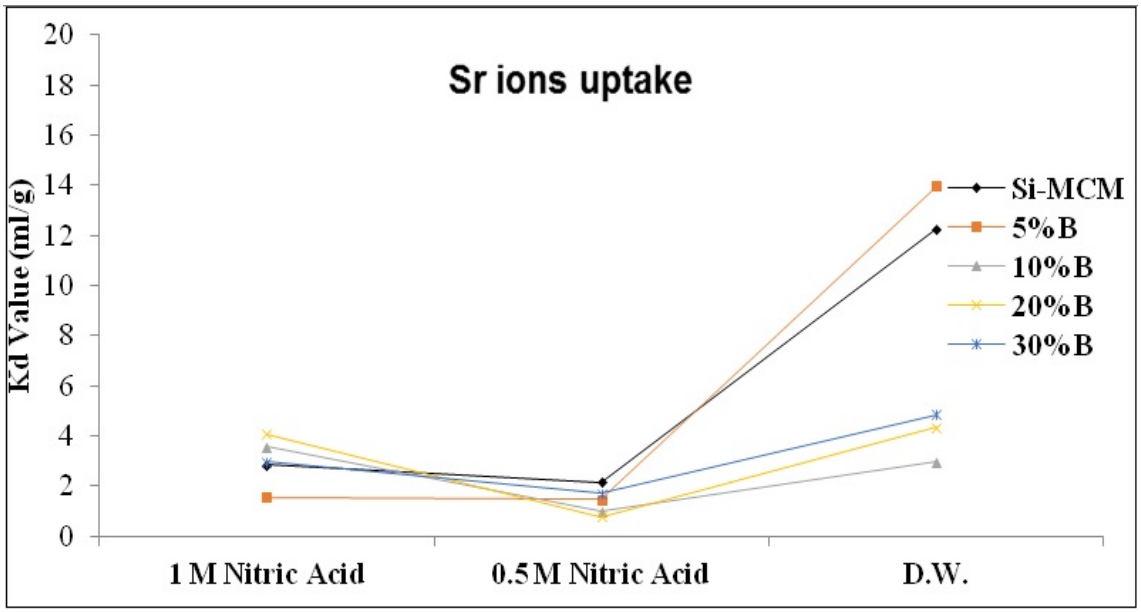

Figure 4.19 Sr ion Kd value for various aqueous systems

Table 4.13 Mixed ions concentrations in various aqueous systems

Samples	Initial (ppm)			Final (ppm)			Volume (ml)	Weight (g)	Kd (ml/g)		
	Sr	Cs	Ce	Sr	Cs	Ce			Sr	Cs	Ce
1 M HNO_3											
Si-MCM-41	444±7	627±11	6829±94	435±5	611±7	6728±158	25	0.50	0.72	1.31	0.75
5%B-MCM-41				450±11	630±14	6457±109			0.00	0.00	2.88
10%B-MCM-41				447±6	628±11	6519±210			0.00	0.00	2.37
20%B-MCM-41				445±6	626±6	6665±92			0.00	0.08	1.23
30%B-MCM-41				441±7	619±13	6446±238			0.24	0.65	2.97
0.5 M HNO_3											
Si-MCM-41	445±7	640±12	7068±212	442±8	632±10	6640±158	25	0.50	0.23	0.63	3.22
5%B-MCM-41				445±4	634±5	6445±172			0.00	0.47	4.83
10%B-MCM-41				448±5	636±7	6553±188			0.00	0.31	3.92
20%B-MCM-41				437±8	623±13	6342±317			0.63	1.36	5.72
30%B-MCM-41				456±8	650±12	6304±104			0.00	0.00	6.05
Deionised water (pH 1.20)											
Si-MCM-41	416±9	591±21	4357±113	427±5	607±15	3993±87	25	0.50	0.00	0.00	4.56
5%B-MCM-41				441±6	625±12	4100±43			0.00	0.00	3.13
10%B-MCM-41				417±4	592±13	4355±100			0.00	0.00	0.02
20%B-MCM-41				411±6	590±16	4260±83			0.00	0.08	1.14
30%B-MCM-41				429±8	608±18	4164±195			0.00	0.00	2.32

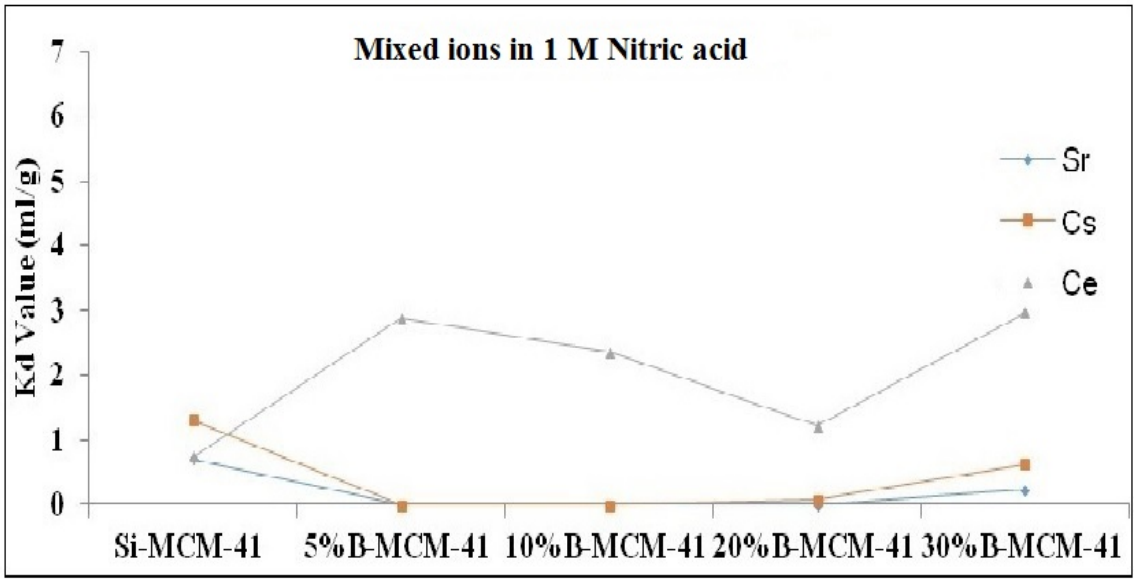

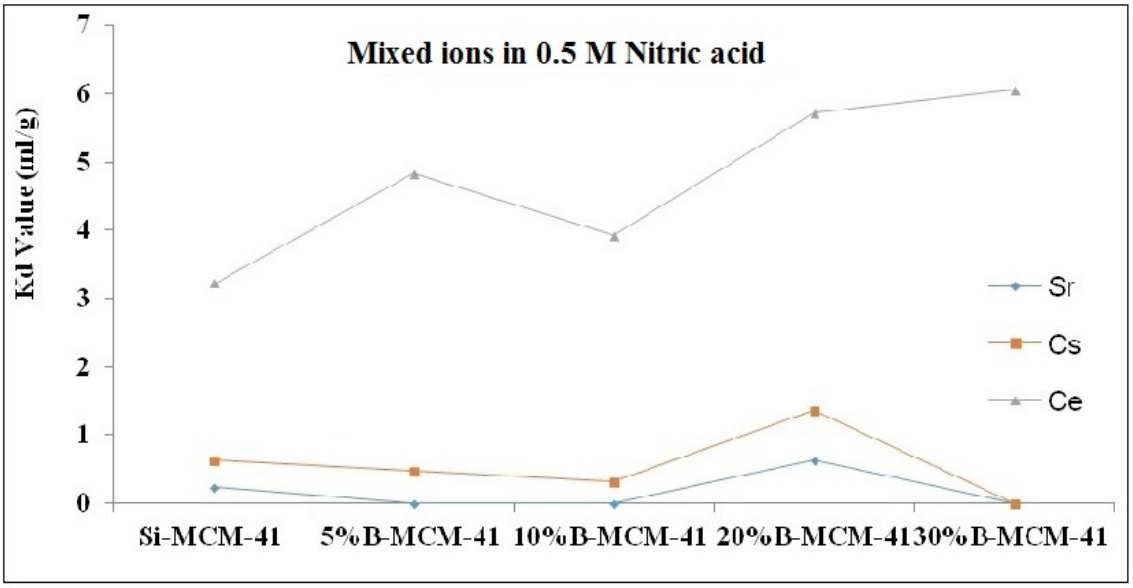

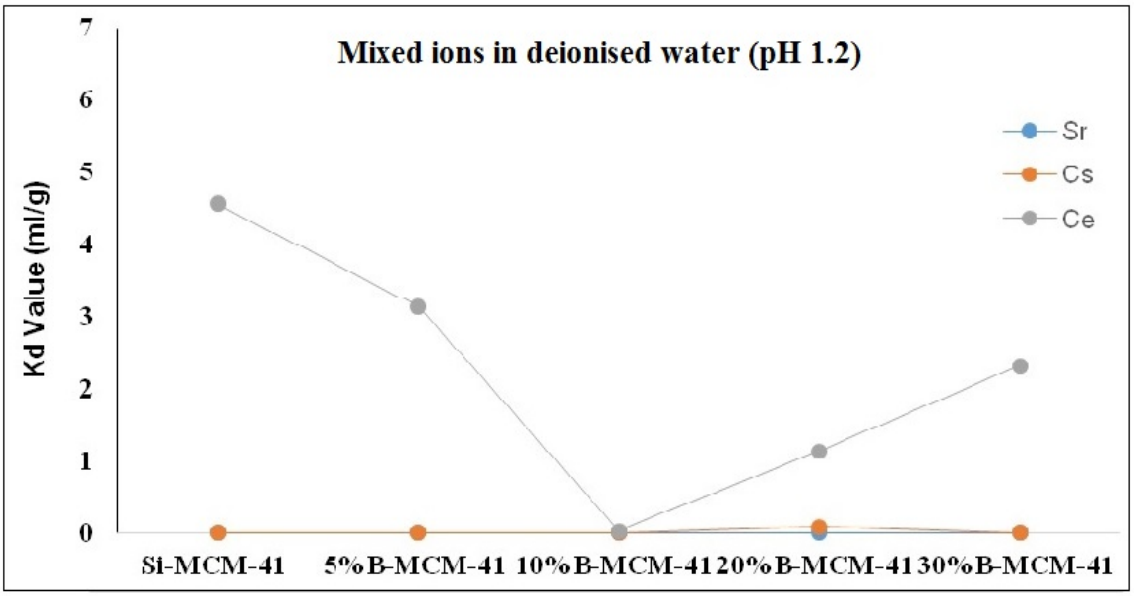

Figure 4.20 Mixed ions Kd values for various aqueous systems

Observation in single ion solutions

The uptake behaviour of all the materials showed similar properties in presence of Cs ions in different media (table 4.11 and figure 4.18). The materials were only capable of adsorbing trace amounts of cations in acidic (0.5 M and 1 M HNO_3) conditions. This is likely to be due to highly competing H^+ ions in the solution. It was expected to behave slightly better in deionised water system, as the hydrogen ion completion would be much lower however, the result was not too encouraging. This was due to the pH value of the deionised water was reduced to 4.60 when $CsNO_3$ dissociates in water. It was again H^+ ions, which were believed to be competing against cations. Similar results have been reported with zeolites uptake in acidic media [20].

A similar study was performed with a different cation, 5 mM Sr ion as the nitrate salt $Sr(NO_3)_2$. The study revealed that the uptake was low which was similar to Cs ions measurement (table 4.12 and figure 4.19). Hence a similar explanation for Sr ions as for Cs ions could be made; a small difference however was measured in weakly acidic system, which was due to the slightly difference in pH values (cf. pH 4.2 with pH 5.60). The rate of uptake studies were not performed since the uptake capacity of the materials were negligible in acidic media.

Observation in mixed ions solutions

Further experiments were carried out with mixed ions solution at different acidic strengths. The media consisted of 10 times the concentration of Ce ions compared to Cs and Sr ions counterparts to mimic actual dissolver liquor composition as mentioned earlier in chapter 1 (table 1.1).

The cation uptake measurements in acidic media were low which were similar to previous measurements. The pH value was 1.20 when different salts dissociated in deionised water hence, similar type of uptake were obtained as reported earlier.

The analysis showed that incorporation of boron into silica structure had no significant advantages for Cs and/or Sr removal and that weakly acidic media (media with moderate pH) were the best for all examples.

4.4 Conclusions

The main objective of the project was to make suitable stationary phases for the column separations for UCLan's continuous chromatography concept explained in chapter 1.3

MCM-41 type materials were used primarily because of their unique structure and easy modification properties, which could mimic zeolites or molecular sieves. The size of the particles were measured approx. ≤ 2 µm, which was an important consideration for packing columns.

The preparative route was easy and a one pot synthesis ideal for preparing large quantities at industry level. The surface area and large pore size of the materials benefitted maximum interaction of metal ions.

Silica affords high stability in acidic media and should provide good radiolytic stability; these two considerations have a major influence on matrix selection. Boron incorporation into the silica matrices was selected as first, it provides a negative charge imbalance thus favouring cation uptake and second it is a good neutron poison [10] in the event of liquors to be treated containing fissile material.

The various characterisation techniques employed have provided extensive knowledge and sound understanding of the synthesised materials; the data are also consistent with previous studies on similar materials.

Cation uptake measurements were somewhat disappointing in acidic media, which was not too surprising as it is a known problem and has been reported on various occasions with zeolites.

4.5 References

1. Alothman Z., A Review: Fundamental Aspects of Silicate Mesoporous Materials. Materials, 2012. 5(12), p. 2874 - 2902.
2. Meynen V., Cool P., and Vansant E.F., Verified syntheses of mesoporous materials. Microporous and Mesoporous Materials, 2009. 125(3), p. 170 - 223.
3. Brinker C.J., Porous inorganic materials. Current Opinion in Solid State and Materials Science, 1996. 1(6), p. 798 - 805.
4. Corma A., From Microporous to Mesoporous Molecular Sieve Materials and Their Use in Catalysis. Chemical Reviews, 1997. 97(6), p. 2373 - 2420.
5. Kresge C.T., Leonowicz M.E., Roth W.J., Vartuli J.C., and Beck J.S., Ordered mesoporous molecular sieves synthesized by a liquid-crystal template mechanism. Nature, 1992. 359(6397), p. 710 - 712.
6. Makowski P., Deschanels X., Grandjean A., Meyer D., Toquer G., and Goettmann F., Mesoporous materials in the field of nuclear industry: Applications and perspectives. New Journal of Chemistry, 2012. 36(3), p. 531 - 541.
7. Oberhagemann U., Kinski I., Dierdorf I., Marler B., Gies H., Synthesis and properties of boron containing MCM-41. Journal of Non-Crystalline Solids, 1996. 197(2–3), p. 145 - 153.
8. Dyer A., Newton J., and Pillinger M., Synthesis and characterisation of mesoporous silica phases containing heteroatoms, and their cation exchange properties. Part 1. Synthesis of Si, Al, B, Zn substituted MCM-41 materials and their characterisation. Microporous and Mesoporous Materials, 2009. 126(1–2), p. 192 - 200.
9. Melo R.A.A., Giotto M.V., Rocha J., Urquieta-González E.A., MCM-41 ordered mesoporous molecular sieves synthesis and characterization. Materials Research, 1999. 2, p. 173 - 179.
10. Martin J.E., Physics for Radiation Protection: A Handbook, 2nd Edition, Completely Revised and Enlarged. Wiley, 2008. ISBN: 978-3-527-61880-4, p. 659.
11. Kresge C.T., Vartuli J.C., Roth W.J., and Leonowicz M.E., The discovery of ExxonMobil's M41S family of mesoporous molecular sieves, in Studies in Surface Science and Catalysis, Elsevier. 2004. 148, p. 53 - 72.

12. Sayari A., Moudrakovski I., Danumah C., Ratcliffe C., Ripmeester J.A., and Preston K.F., Synthesis and Nuclear Magnetic Resonance Study of Boron-Modified MCM-41 Mesoporous Materials. The Journal of Physical Chemistry, 1995. 99(44), p. 16373 - 16379.
13. Dyer A., Newton J., and Pillinger M., Synthesis and characterisation of mesoporous silica phases containing heteroatoms, and their cation exchange properties. Part 2. Cation exchange isotherms for MCM-41 phases. Microporous and Mesoporous Materials, 2009. 126(1–2), p. 201 - 212.
14. Sing K.S.W., Reporting physisorption data for gas solid systems with special reference to the determination of surface area and porosity. Pure and Applied Chemistry, 1982. 54(11), p. 2201 - 2218.
15. Baur W.H., Variation of mean Si-O bond lengths in silicon-oxygen octahedra. Journal of Solid State Chemistry, 1977. 22(4), p. 445 - 446.
16. Coulson C.A. and Dingle T.W., The B-O bond lengths in boron-oxygen compounds. Acta Crystallographica Section B, 1968. 24(1), p. 153 - 155.
17. Jing D.X., Evans D.G., and LI Cheng-yue, Studies on the Surface Properties of MCM-41¸ 2002. 18(3), p. 242 - 245.
18. Zholobenko V.L., Holmes S.M., Cundy C.S., and Dwyer J., Synthesis of MCM-41 materials: an in situ FTIR study. Microporous Materials, 1997. 11(1–2), p. 83 - 86.
19. Dekamin, M.G., Mokhtari Z., and Karimi Z., Nano-ordered B-MCM-41: An efficient and recoverable solid acid catalyst for three-component Strecker reaction of carbonyl compounds, amines and TMSCN. Scientia Iranica, 2011. 18(6), p. 1356 - 1364.
20. Dyer A., Newton J., and Pillinger M., Synthesis and characterisation of mesoporous silica phases containing heteroatoms, and their cation exchange properties. Part 3. Measurement of distribution coefficients for uptake of Cs-137, Sr-89, and Co-57 radioisotopes. Microporous and Mesoporous Materials, 2010. 130(1-3), p. 56 - 62.
21. Bond G., and Eccles H., Continuous Chromatographic Separation of fission Products and Minor Actinides from Irradiated Fuel, UK patent Application No. 1317553.4, Nov 2013.

Chapter 5
Zeolite molecular sieves and mesoporous zeolite molecular sieves

5.1 Introduction

This chapter focusses on the examination of commercially available LTA type zeolite A in their various cationic forms. Zeolite A, often known as molecular sieves are available in three different pore sizes 3 Å, 4 Å, and 5 Å and their and cationic form K^+, Na^+ and Ca^{2+}. The study was conducted to examine the possibilities of Cs and Sr ion separation, as they possess different hydrous ionic radii. The study further explored the creation of a mesoporous coating around the zeolite to confer bimodal (microporous- mesoporous) structure. This structure in this thesis is termed 'mesoporous zeolite'. The idea was to create a protecting layer (coating), which incorporate channels, around the zeolite, that would minimise direct acid attack on the zeolite but would influence ion diffusion during ion exchange. Various characterisation techniques were employed for their structure confirmation and measurement of their ion-exchange properties.

5.1.1 Molecular Sieves

The most common type of zeolite molecular sieves are Type A and X [1]. These molecular sieves are generally synthesised by a sol-gel method, in common with other zeolites. In a typical process, a 1:1 molar ratio of alumina and silica are mixed in basic aqueous solution to give a gel, followed by heat treatment (100 - 300 °C) to give a crystallise form of zeolite [1].

Molecular sieves are very important in various industries such as catalysis, gas sorption and purification, ion exchange etc. because of their distinct crystal structure. Type A zeolite molecular sieves exhibit Linde Type A (LTA) structure [1] which has a 3-dimensional pore structure where pores are situated perpendicular to each other in x, y and z planes. The framework is composed of truncated octahedral (sodalite cages) in a cubical array which forms an internal cavity approx. 11 Å in diameter (alpha cage) [1]. Each alpha cage is entered through six circular apertures formed by a regular ring of 8 oxygen atoms with a free diameter of 4.2 Å [1]. The truncated octahedra enclose a second set of smaller cavities approximately 6.6 Å in internal diameter (beta cages). The

smaller cavities are connected to larger cavities via a ring of six oxygen atoms (figure 5.1) [1].

In general, Type A zeolite molecular sieves are synthesised in the form of Na^+ which can be replaced with other cations to alter the pore size.

The general element composition of Type A molecular sieves is

$Na_{12}[(AlO_2)_{12}(SiO_2)_{12}].27H_2O$

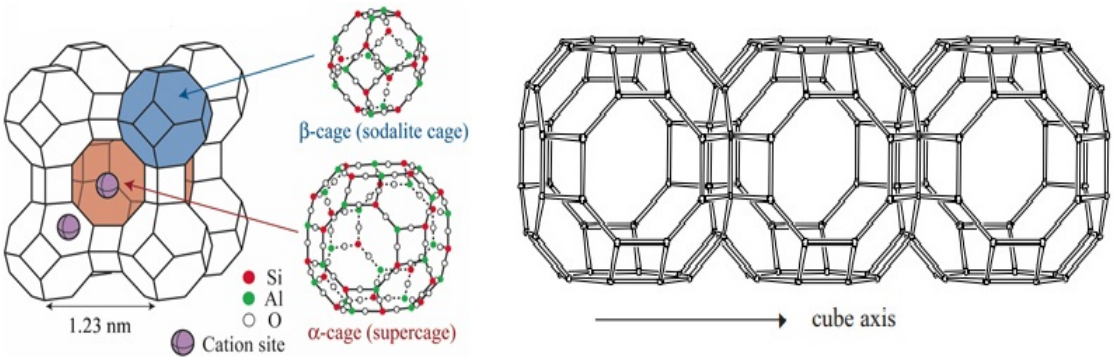

Figure 5.1 Schematic representation of type A zeolite molecular sieve [1]

Type 3A are produced by replacing Na^+ ions by K^+ ions , since potassium ions have a larger ionic radius than sodium ions hence the pore size is reduced to approx. 3Å. Na^+ form of type A molecular sieves exhibits pore size approx. 4 Å diameter and in type 5A molecular sieves, Ca^{2+} replaces Na^+ ions, resulting into pore size approx. 5Å.

Along with size exclusion property, Type A zeolite modified with different cations also behaves as ion exchange molecular sieves. The cations in the zeolites are exchangeable with other cations giving zeolites an ion exchange property. The silica in the framework structure i.e. shared oxygen atoms with the corresponding aluminium atoms, which itself is sharing adjacent oxygens has a valence of +4 making the SiO_4 tetrahedra neutral, while the AlO_4 tetrahedra are negatively charged because aluminium has a valence of +3, creating a Brönsted acid site due to the resulting charge imbalance in the framework structure, which imparts exchangeable sites to the zeolite structure [1]. Therefore, the ion exchange capacity of zeolites depends on its chemical composition [2].

A batch and column comparative study of Cs ions sorption has been previously carried out on various commercially available synthetic zeolites 13X, 4A, AR-1 (mordenite) and ZSM-5, which demonstrated the performance of these zeolites in moderate pH

liquid solution [2]. The study suggest zeolite AR-1 (mordenite), 13X, and 4A had high Cs ion exchange capacity and fast kinetics under moderate pH ionic solutions but not suitable for actual waste clean-up due to instability in higher acidic solutions of pH 2 or less [2].

A separate batch and column study was performed on zeolite A for the removal of Cs and Sr ions from an aqueous chloride solution [3]. The reported data indicates that the performance of zeolite A is largely affected by pH changes [3]. An increase in the acidic pH results in the degradation of the zeolite structure with a significant reduction in cation uptake. [3] The best performance of this zeolite was between pH 6-8 and higher Sr ion capacity than Cs ions [3].

Another study was performed on zeolite A for the removal of Sr ions, as they have preference over Cs ions at various pH values; the study also included zeolite A's performance in presence of Na ions [4]. The experimental data were consistent with other results and an appropriate working pH was reported between 6 and 8, the concentration of Na ions had a negative effect on Sr ions sorption [4].

5.1.2 Mesoporous zeolite molecular sieves

These molecular sieves exhibit two types of porous (microporous and mesoporous) structure in a single structure. The idea is to prepare a porous structure with the benefit of having different size pores.

There are few synthesis options for this type of molecular sieves

5.1.2.1 Post treatment synthesis

This technique involves partial extraction of cations (aluminium, silica) from the zeolite framework by steaming or partial leaching by HCl and/or NaOH [5]. This process removes some of the crystal framework species and creates voids in the mesopore size (figure 5.2) [5]. The steaming process leads to hydrolysis of Al-O-Si in the framework, which subsequently partially removes the hydrolysed products leaving mesopores in the structure. The strong acid and base treatment removes Al ions Si atoms respectively from the framework and creates gaps in the zeolite [5]. It is often reported that synthesised mesoporous zeolite structures possess low crystallinity compared to parent zeolite due to structure deformation and disordered pores by various treatments.

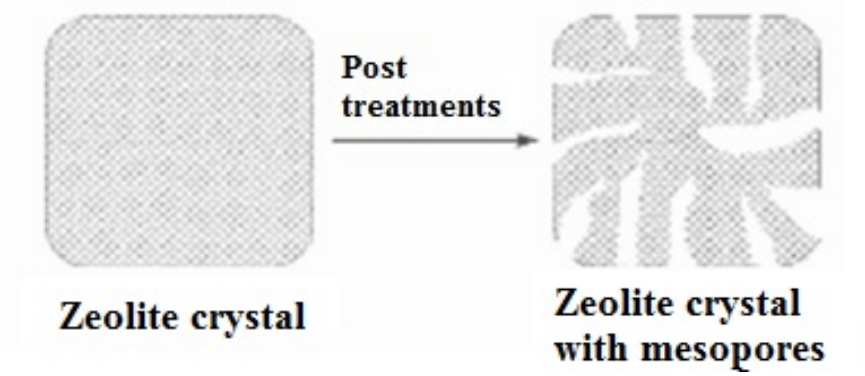

Figure 5.2 Synthesis of mesoporous zeolite by post treatment [5]

5.1.2.2 Template assisted synthesis

There are two approaches for this technique hard and soft templating as mentioned below,

5.1.2.2.1 Hard/ solid templating

As the name suggest, this technique requires the use of a mesoscale inorganic nanostructure as a hard template. During zeolite synthesis, the hard templates are slowly encapsulated in the growing zeolite crystal, which is then removed by combustion. The space left by combustion creates mesopores in zeolites (figure 5.3) [5]. Carbonaceous nanomaterials such as carbon nanopowders, nanotubes, and nanofibers are the most common hard templates in the size range of 5 - 15 nm used in this technique [5]. The synthesised mesoporous zeolites show good crystallinity but possess disordered pore structure and the synthesis procedure are often complex and time-consuming [5].

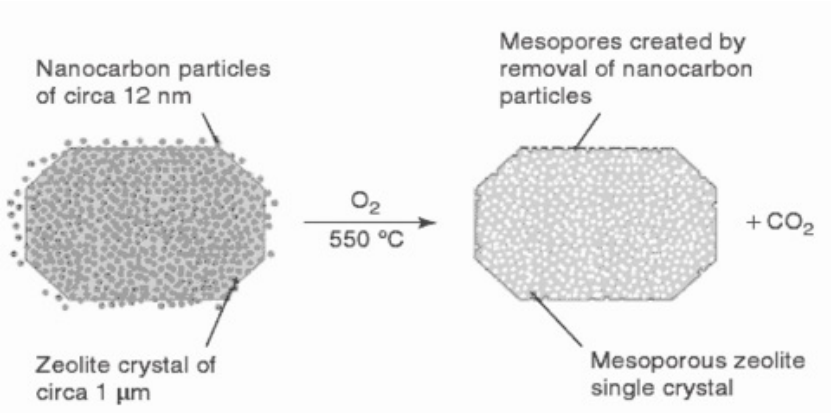

Figure 5.3 Synthesis of mesoporous zeolite by hard/solid templating method [5]

5.1.2.2.2 Soft templating

This technique involves self-assembly of surfactant molecules, which results in regular large patterns such as micelles and appears as templates for mesopore formation in zeolites [5]. A variety of mesoporous zeolite morphologies can be synthesised by fine tuning geometrical packing parameters of the surfactant molecules and the functional groups. This technique relies highly on properties of the selected templates (surfactants) such as interaction, stability, morphology, and cost [5]. The most common type of surfactants used are CTAB and Pluronic P123 due to their strong interactions with silica species, strong stability in alkaline media and high thermal stability (up to 400 °C), ability to form fibre-like morphology (micelles) and low cost. Figure 5.4 represents a soft template method of synthesising mesoporous zeolite Y [6].

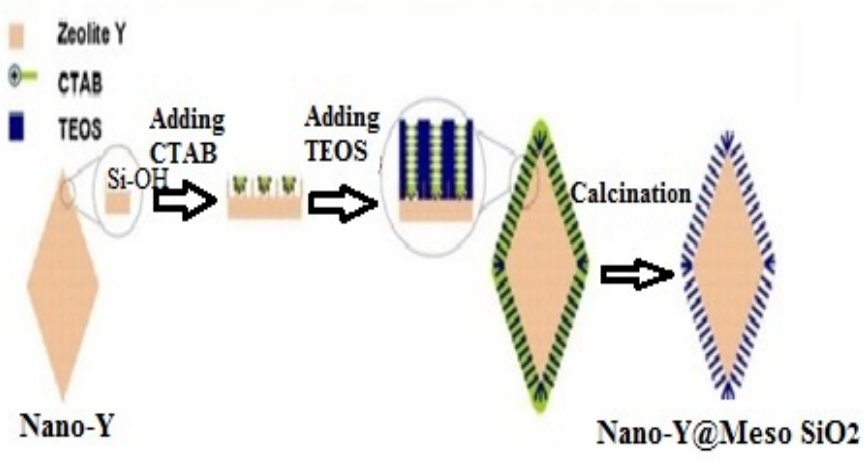

Figure 5.4 Synthesis of mesoporous zeolite Y by soft templating method [6]

A study of the effective removal of Mg^{2+} and Ca^{2+} ions by mesoporous zeolite A (LTA type) to understand the enhancement of cation exchange sites created by additional mesoporous surface area on conventional zeolite A has been undertaken [7]. The study demonstrated the synthesis technique for preparing inter-crystalline mesopores of 3 nm by using organic functionalised fumed silica as source. The reported surface area suggested the increased surface area and pore volume were due to mesopores. The comparative ion exchange study of zeolite A and mesoporous zeolite A for Mg^{2+} and Ca^{2+} ions suggested that mesoporous zeolite A possess higher cation exchange volume due to mesopores and it has two kinds of ion exchange sites suitable for Mg^{2+} and Ca^{2+} ions [7]. The study also reported that mesoporous zeolite A had improved Mg^{2+} ions

kinetics compared to parent zeolite A hence, a promising candidate for water softening application [7].

A similar study was conducted to remove Hg^{2+} ions from an industrial waste stream by a composite of polypyrole/thiol-functionalized beta zeolite/MCM-41[8]; which involved a two-step hydrothermal route. The ion exchange data suggested that a suitable working condition was between pH 6 - 8 and the cation exchange capacity significantly decreased below pH 5 [8]. The synthesised composite had fast kinetics (10 minutes) and high sorption capacity for Hg^{2+} ions due to enhance mesoporous surface area and higher cation exchange sites [8].

5.2 Material and Methods

5.2.1 Materials

Table 5.1 Reagents, their purity and source of purchase

Chemical	Company	Purity
Sodium Silicate	Sigma Aldrich	Reagent grade
Aluminium sulphate octadecahydrate $Al_2(SO_4)_3.\ 18H_2O$	VWR	≥98%+
Hexadecyltrimethylammonium bromide (CTAB)	VWR	≥98%
Tetraethylorthosillicate (TEOS)	Sigma Aldrich	≥99%
Molecular sieves 3A	Sigma Aldrich	Pellets 1.6 mm
Molecular sieves 4A	Sigma Aldrich	Pellets 1.6 mm
Molecular sieves 5A	Sigma Aldrich	Beads 8-12 mesh
Nitric Acid (HNO_3)	Sigma Aldrich	ACS reagent grade ≥69%
Sodium Hydroxide (NaOH)	Sigma Aldrich	≥98% pellets
Deionised Water (H_2O)	Nanopure	≥18.2 MΩ.cm
Caesium nitrate ($CsNO_3$)	Sigma Aldrich	≥99.9%
Strontium nitrate ($Sr(NO_3)_2$)	Sigma Aldrich	≥99.9%
Ammonium cerium nitrate ($Ce(NH_4)_2(NO_3)_6$)	Sigma Aldrich	≥99.9%

The reagents, their purity, and source of purchase used in this chapter are reported in table 5.1

5.2.2 Zeolite Molecular sieves 3A, 4A and 5A

Zeolite Molecular sieves 3A, 4A, and 5A in various granular forms are illustrated in figure 5.5.

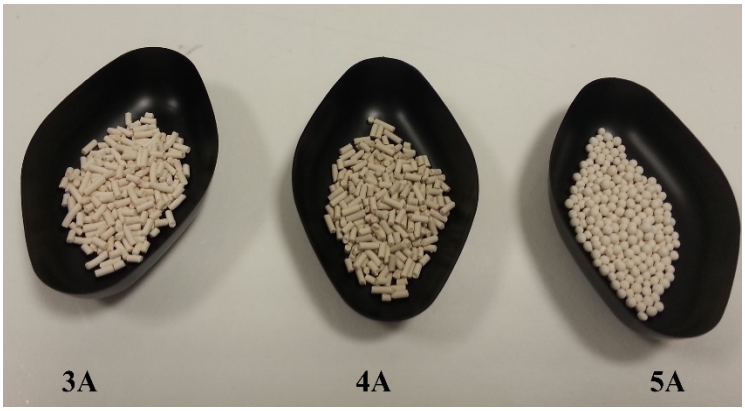

Figure 5.5 Zeolite Molecular sieves 3A, 4A, and 5A

5.2.3 Synthesis of mesoporous zeolite molecular sieve 5A

The synthesis of mesoporous zeolite 5A was carried out by the sol-gel technique, with minor modifications, using CTAB as structure directing agent [6, 10]. Instead of synthesising zeolite nanocrystals, zeolite 5A pellets were purchased ground in a mortar and pestle and screened (stainless steel sieve) to produce 2 µm or smaller particles.

The thickness of the mesoporous coating depends on mass ratio of TEOS: zeolite [10]; mass ratio of 1.12 was considered for this study.

For preparing only silica-coated mesoporous 5A, a mixture of CTAB, ethanol, ammonium hydroxide, and deionised water was prepared by weighing appropriate quantities as reported in table 5.2. The mixture was allowed to stir at room temperature until clear solution was produced. 2 gm of ground zeolite was suspended in the prepared mixture followed by ultrasonication treatment at r.t. for 30 minutes. TEOS was added to the mixture drop wise and the mixture was stirred at r.t. for 4 hours. The synthesised composites were gravity filtered through a Whatman No 6 filter paper and washed several times by deionised water, followed by pure ethanol. The collected samples were air dried at 100 °C for 24 hours. After this, the samples were calcined with a heating rate of 2 °C/min up to 560 °C and held at this temperature for 6 hours in presence of air to remove the templates. The resultant materials were named 5A@Si.

The study was expanded to incorporate Al ions and Si ions to coat zeolite 5A. Two different Al and Si coated zeolites were synthesised by varying the Al:Si mass ratio. Synthesis of these two materials was similar to the process previously explained but up to the ultrasonication treatment. After the addition of the ground zeolite, aluminium sulphate octadecahydrate (dissolved in small quantity of water) was added drop wise, followed by addition of TEOS. The mixture was allowed to stir for 4 hours at room temperature. Further filtration, washing, drying, and template removal procedures employed as describe previously. The synthesised materials were named as 5A@Si-Al 0.31, and 5A@Si-Al 0.72.

Table 5.2 Reagent quantities used to synthesis mesoporous zeolites

Samples	Sample (g)	CTAB (g)	Ethanol (ml)	Ammonium hydroxide (ml)	Water (ml)	TEOS (ml)	Aluminium sulphate (g)
5A@Si	2	1.4	15.20	2.77	400	2.40	NA
5A@Si-Al 0.31						1.20	1.12
5A@Si-Al 0.72						0.94	2

5.2.4 Characterisation

The structural characteristics of mesoporous zeolite 5A was analysed by PXRD and SAXS. The analysis of pore structure and surface area were characterised by nitrogen sorption studies. The particle morphology was imagined by SEM. The ion exchange and ion sieve properties of the various forms of zeolite, and synthesised mesoporous zeolites were examined by contacting them with nitrate salts of caesium, strontium, and cerium in different strength nitric acid solutions. In addition, the rate of uptake of cations by zeolite 5A was also undertaken. The experimental details have already been described in chapter 3.

5.3 Results and Discussion

The purchased zeolite molecular sieves were used without prior treatment. The amount of synthesised mesoporous zeolites obtained were approx. 2.25 g after calcination in powder form with average particle size 2 µm. the sol-gel technique had produced a mesoporous coating around the parent zeolite particle that appeared to have higher surface area and pore volume. Various structural and ion exchange properties are reported later.

5.3.1 PXRD

The PXRD pattern of parent zeolite 5A shows a characteristic diffraction peak assigned to typical LTA structure. The crystal structure of this type of zeolite was reported as cubic with cell parameter 11.9 Å [1, 11].

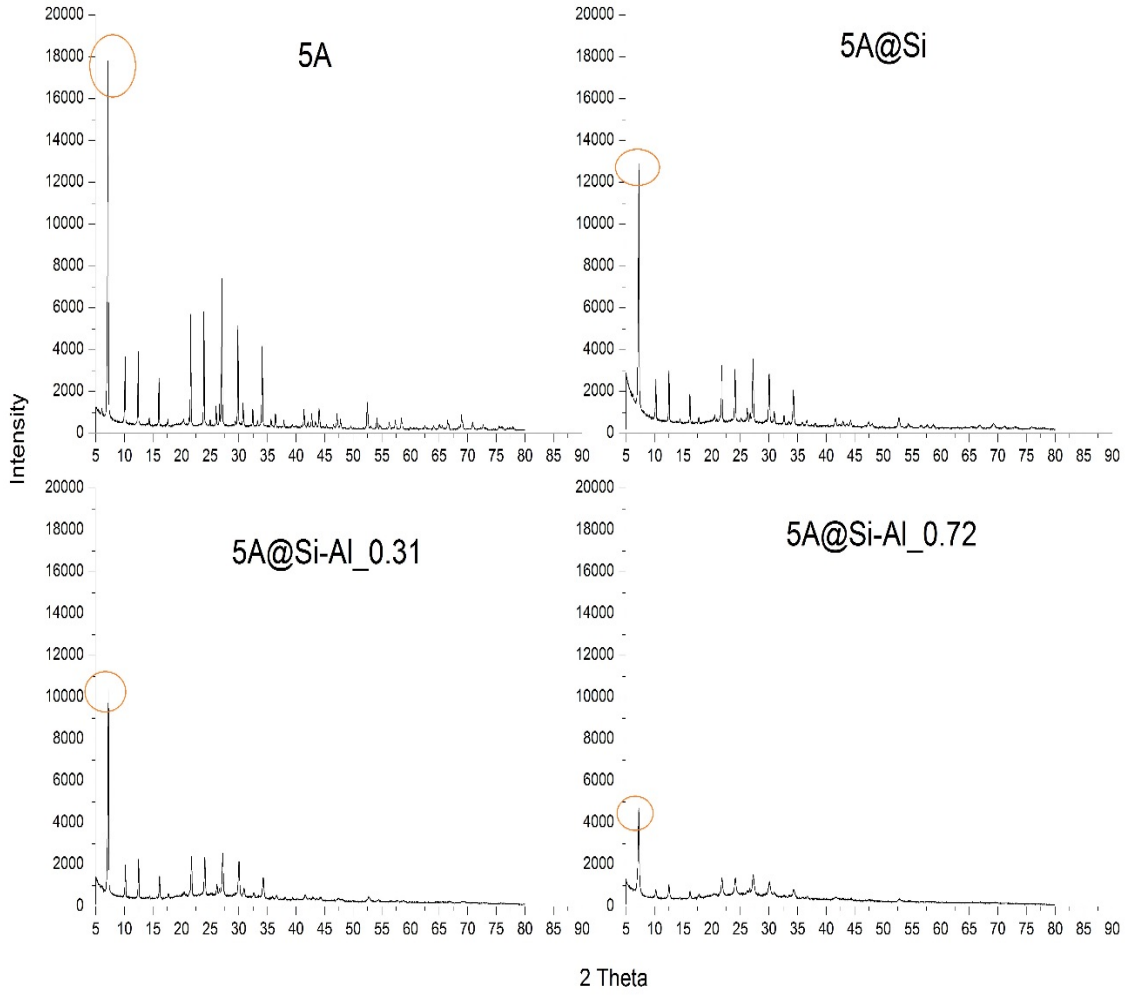

Figure 5.6 PXRD profile comparison of molecular sieves 5A and mesoporous molecular sieves 5A

The synthesised mesoporous zeolite materials had lower intensities when compared to parent zeolite 5A however, the peak position were retained (figure 5.6). This suggests that formation of thin layer of mesopores had occurred, which can be further verified by change in their surface area (gas sorption technique) and negligible effect on their crystalline zeolite structure.

Further, the possibility of mesoporous structure can be identified by performing small angle scattering as characteristics pattern of mesoporous structure are typically observed at low angle (1 - 5° 2θ).

5.3.2 SAXS

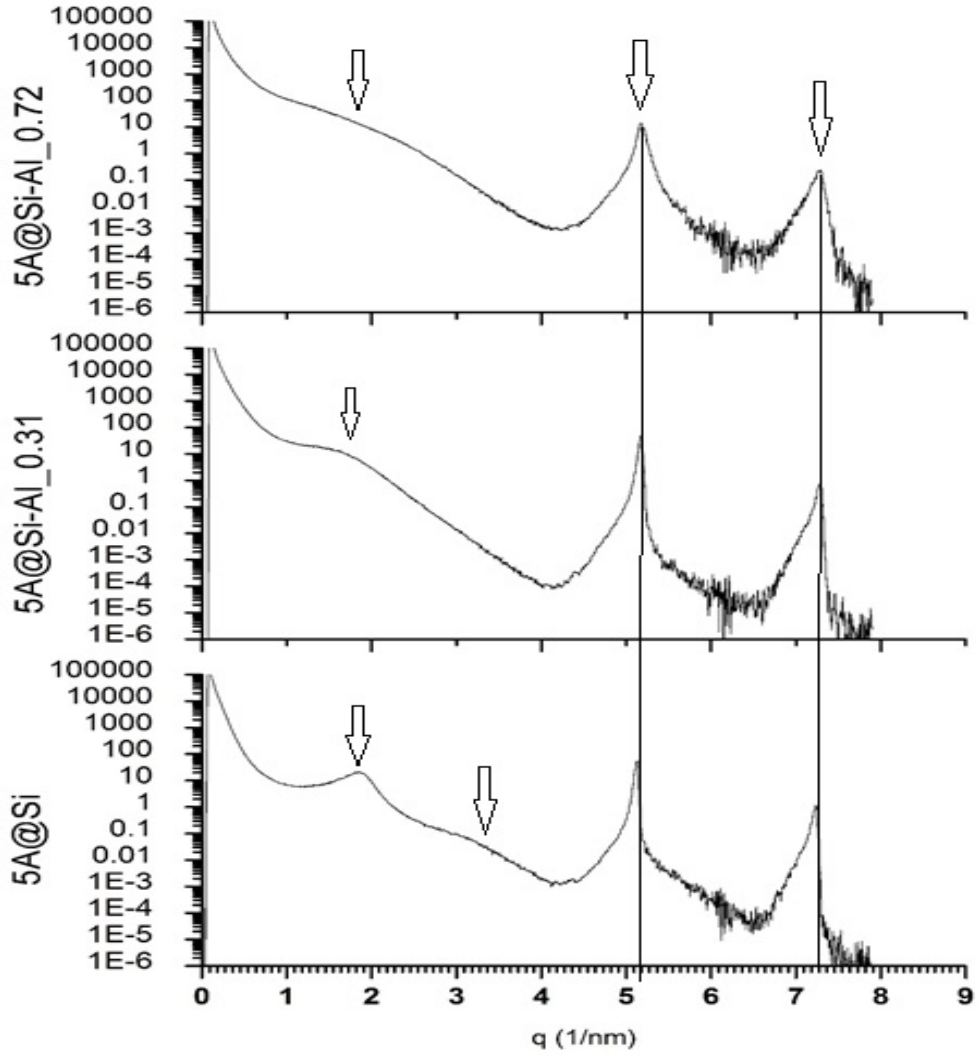

Figure 5.7 SAXS profile comparison of synthesised mesoporous 5A zeolites

The SAXS pattern of synthesised mesoporous zeolite clearly shows the appearance of mesoporous structure at lower scattering vector (q) between 1- 4 nm^{-1}, which is ascribed to mesoporous structure. The appearance of sharp peaks at 5 nm^{-1} and 7 nm^{-1} was believed to be due to microporous structure. In comparison, 5A@Si mesoporous peaks were more pronounced and peaks broader with Si and Al mixture coatings. The comparison suggests, mesoporous structure in 5A@Si were highly ordered compared to 5A@Si-Al 0.31, and 5A@Si-Al 0.72.

5.3.3 Surface area and pore analysis

The textural properties of microporous parent zeolite 5A and synthesised mesoporous zeolite 5A were analysed by gas (nitrogen) sorption technique. This measurement technique provides the specific surface area, microporous and mesoporous surface area, pore volume of micropores and mesopores, and pore size distribution. The method of gas sorption has been explained in chapter 3.2.3

Nature of Isotherm

The nature of the isotherm obtained for parent zeolite 5A was similar to type I isotherm according to IUPAC classification [9]. This type of isotherm exhibits very sharp gas adsorption at very low relative pressure followed by straight line indicating no or negligible gas sorption at higher relative pressure (figure 5.8) [9]. The synthesised mesoporous zeolite 5A@Si isotherm began at high gas sorption profile, similar to parent zeolite A and exhibits mesoporous characteristic loop between 0.3 and 0.5 relative pressure (isotherm type IV). The presence of both type I and IV isotherm indicated a structure consisting both mesopores and micropores in the synthesised material and the study further support the PXRD and SAXS results.

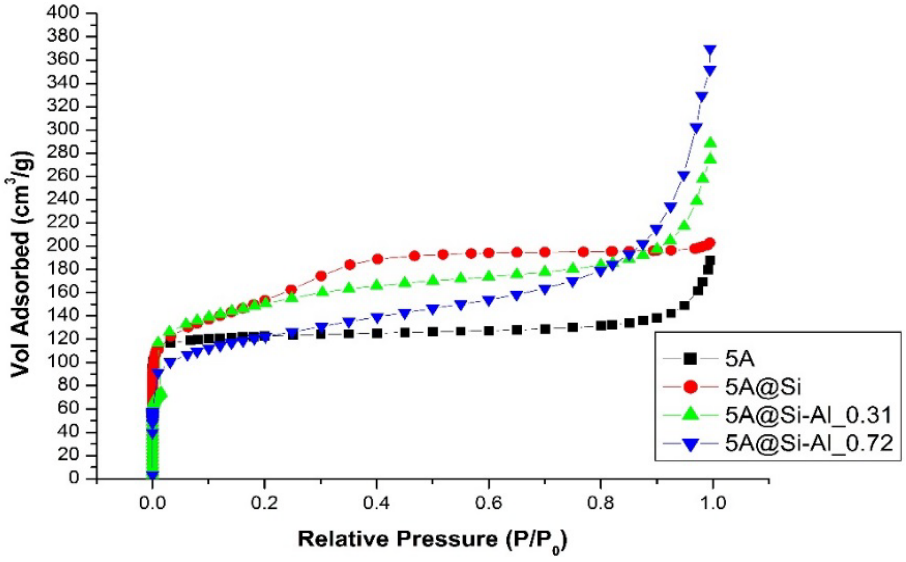

Figure 5.8 Isotherm comparison of 5A and mesoporous 5A

The adsorption and desorption of the gas sorption followed the same path which can be seen in figure 5.8. The materials zeolite 5A@ Si-Al 0.31 and zeolite 5A@ Si-Al 0.71 synthesised by mixture of Al and Si ions lead to similar isotherm profiles to silica zeolite 5A@Si but exhibit lower gas adsorption which indicates the mesoporosities affected by high Al:Si ratio.

Surface area, pore volume and poresize distribution

The surface area of the parent zeolite 5A and synthesised mesoporous zeolite 5A were calculated by BET method. Table 5.3 reports the data related to surface area, pore volume, and pore diameter. The surface area (S_{BET}) of parent zeolite 5A was expected to be lower than the synthesised mesoporous zeolites as zeolites consists of micropores, which exhibit lower surface area than mesopores. The reported data were consistent with this hypothesis. The highest surface area was found for zeolite 5A@Si, which reduced when, Al:Si ratio increased (table 5.3). The surface area of micropores (S_{Micro}) were found highest in parent zeolite and tend to reduce with mesopore coating. A similar trend was found with lowest surface area of mesopores (S_{Meso}) in parent zeolite. Examination of the micropore volume of mesoporous zeolite suggests that the highest value is for parent zeolite and reduces with mesopore coating. The average micropore pore size distribution was calculated by HK method and found to be consistent for all samples. The mesopore pore size distribution was calculated by BJH method and it varied with increasing Al:Si ratio. The absence or negligible amount of mesopores were found in parent zeolite 5A (table 5.3).

Table 5.3 Surface area and pore analysis of various molecular sieves

Sample	S_{BET} (m^2/g)	S_{Micro} (m^2/g)	S_{Meso} (m^2/g)	V_{Total} (cm^3/g)	V_{Micro} (cm^3/g)	V_{Meso} (cm^3/g)	$Dia._{Micro}$ (Å)	$Dia._{Meso}$ (Å)
5A	369	319	49	0.250	0.160	0.089	5.7	-
5A@Si	530	150	380	0.308	0.071	0.229	5.7	23.5
5A@Si-Al_0.31	484	228	256	0.370	0.120	0.242	5.7	38.0
5A@Si-Al_0.72	396	175	220	0.468	0.092	0.375	5.7	47.1

5.3.4 SEM

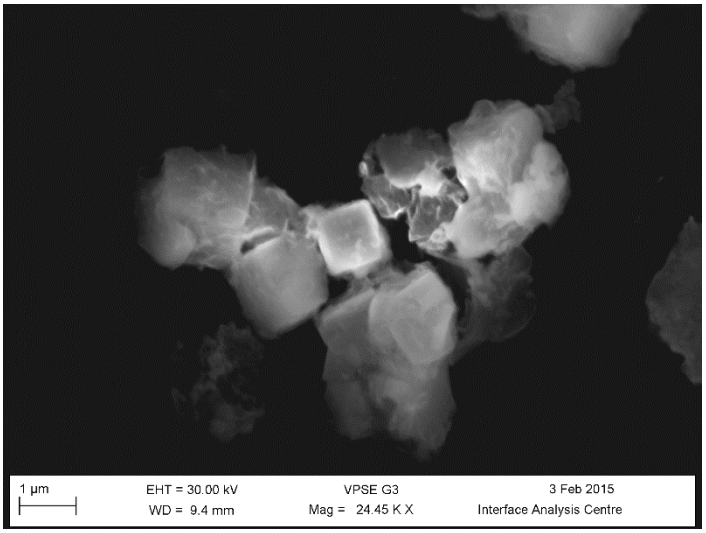

Figure 5.9 SEM image of zeolite 5A

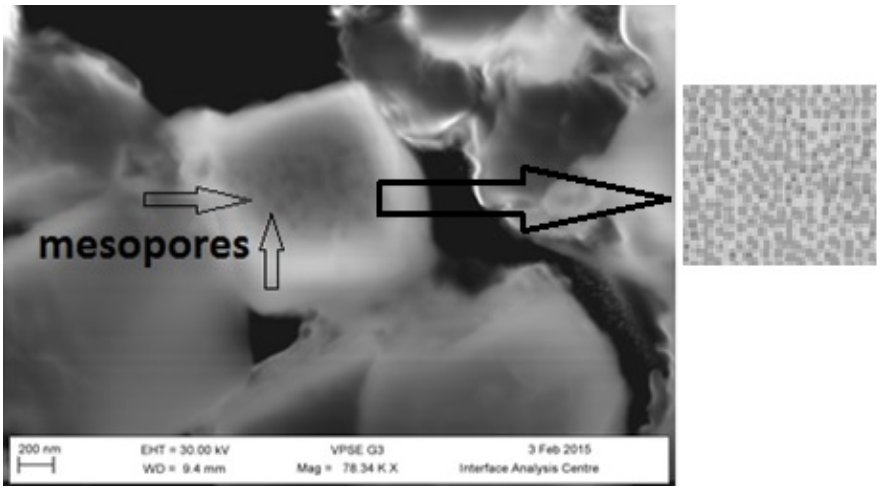

Figure 5.10 SEM image of mesoporous zeolite 5A@Si

The SEM images show that most of the particles were of cubic shape but some were distorted (with rough corners) due to grinding. Figure 5.9 shows the absence of mesopores in the parent zeolite 5A, whereas figure 5.10 clearly shows the appearance of mesopores in silica coated zeolite 5A which further confirms the PXRD, SAXS, and surface area and pore analysis results.

5.3.5 Cation uptake measurements

The objective of using molecular sieve zeolite with different pore sizes was to understand size dependant Cs and Sr ions separation in acidic medium. The study was also extended to weakly acidic media. The molecular sieve zeolites used were in the form of K, Na, and Ca that exhibit 3Å, 4Å, and 5Å pore size respectively. Batch equilibrium experiments were employed to understand the molecular sieves' performance for various cations e.g. Cs, Sr, and Ce ions in acidic media. The study was also expanded to mesoporous zeolites to understand the effect of different pore size on their ion uptake performance.

Table 5.4 Caesium ion concentrations in various aqueous systems

Samples	Initial (ppm)	Final (ppm)	Volume (ml)	Weight (g)	Kd (ml/g)	Capacity (mg/g)
1 M HNO_3						
3A	658±9	620±13	25	0.50	3.06	1.90
4A		600±11			4.83	2.90
5A		572±13			7.51	4.30
0.5 M HNO_3						
3A	652±9	580±3	25	0.50	6.20	3.60
4A		538±2			10.59	5.70
5A		514±2			13.42	6.90
Deionised water (pH 4.60)						
3A	660±11	63±1	25	0.50	473.80	29.85
4A		32±1			981.25	31.40
5A		28±1			1128.57	31.60

Table 5.5 Strontium ion concentrations in various aqueous systems

Samples	Initial (ppm)	Final (ppm)	Volume (ml)	Weight (g)	Kd (ml/g)	Capacity (mg/g)
1 M HNO_3						
3A	436±6	420±4	25	0.50	1.90	0.80
4A		390±6			5.80	2.30
5A		337±4			10.89	3.90
0.5 M HNO_3						
3A	445±11	387±5	25	0.50	7.49	2.90
4A		393±5			6.61	2.60
5A		343±4			14.86	5.10
Deionised water (pH 5.60)						
3A	499±6	23±1	25	0.50	1025.21	23.78
4A		23±1			1039.51	23.80
5A		20±1			1197.50	23.95

Table 5.6 Mixed ions concentrations in various aqueous systems

Samples	Initial (ppm)			Final (ppm)			V (ml)	W (g)	Kd (ml/g)			Capacity (mg/g)		
	Sr	Cs	Ce	Sr	Cs	Ce			Sr	Cs	Ce	Sr	Cs	Ce
1 M HNO_3														
3A	402±5	626±9	6752±75	430±12	647±11	6113±90	25	0.50	0.00	0.00	5.22	0.00	0.00	31.95
4A				428±10	634±7	6057±110			0.00	0.00	5.73	0.00	0.00	34.75
5A				334±6	487±14	4704±101			10.24	14.21	21.76	3.40	6.95	102.4
0.5 M HNO_3														
3A	426±8	676±11	6364±67	424±14	616±9	5189±91	25	0.50	0.23	4.77	11.32	0.10	3.00	58.75
4A				365±10	530±13	5128±130			8.38	13.59	11.97	3.05	7.30	61.80
5A				311±8	448±5	4361±80			18.49	25.35	22.91	5.75	11.40	100.10
Deionised water (pH 1.20)														
3A	425±5	668±13	6587±80	373±9	506±12	4328±75	25	0.50	6.97	16.00	26.09	2.60	8.10	112.95
4A				379±7	490±9	4486±86			6.06	18.16	23.41	2.30	8.90	105.05
5A				189±5	259±5	2710±98			62.43	78.95	71.53	11.8	20.45	193.85

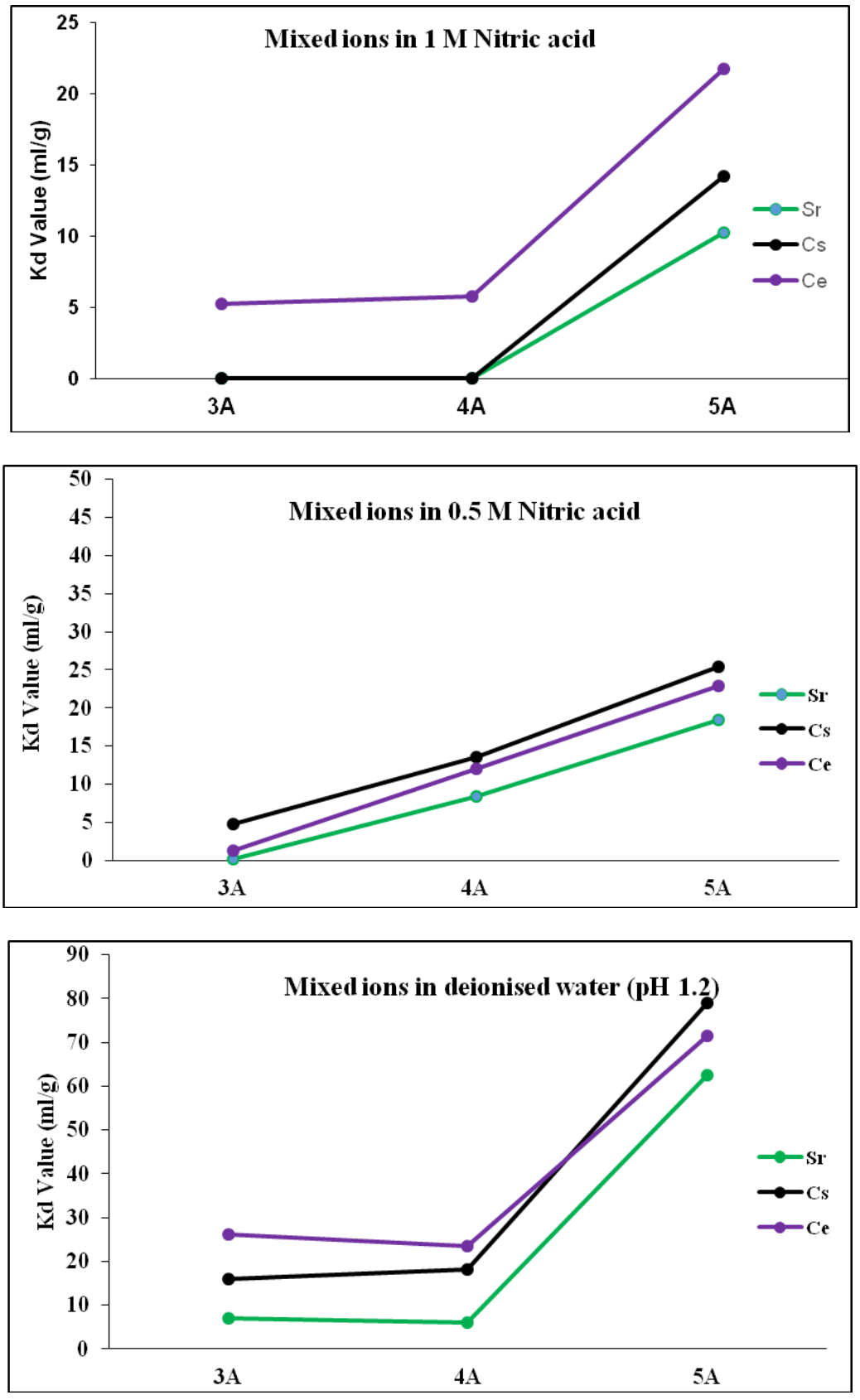

Figure 5.11 Mixed ions Kd values for various aqueous solutions

Observation in single ion solutions

The uptake behaviour of various molecular zeolites has shown similar trends in presence of Cs ions in various aqueous media (table 5.4). The area of interest is the uptake performance of zeolites in presence of acidic media; the materials were only capable of adsorbing trace amount of cations from 0.5 M and 1 M HNO_3 media. This is due to highly competing H^+ ions in these solutions, which is a similar observation to data reported in the previous chapter. In addition it could be due to acid attack of the zeolite framework, destroying the structure as Al-O-Si bonds are weaker than Si-O-Si bonds as reported elsewhere [3]. The materials, however, have performed exceptionally well in weakly- acidic media (pH 4.60) due to less competing hydrogen ions.

The higher uptake was also related with higher pore size, allowing cations with higher hydrated diameter into the pore structure. Table 5.8 reports hydrated ionic diameters for the three cations studied.

Table 5.7 Hydrated ionic diameter [12]

Ions	Hydrated ionic diameter (Å)
Cs^+	~2.5
Sr^{2+}	~5.0
Ce^{4+}	~11

A similar Sr study ion was performed and the results were consistent with zeolite performance for Cs ions (table 5.5). Hence, a similar explanation can be made that competing ions and acid attack were the main reasons for poor performance in 0.5 and 1.0 M nitric acid solutions but at pH 5.6 (weakly acidic system) the Sr uptake has increased to about 24 mg/g.

Observation in mixed ion solutions

Mixed ions solution experiments at different acidic strengths were undertaken. The media consisted of 10 times the concentration of Ce ions compared to Cs and Sr ions to mimic actual dissolver liquor composition as mentioned earlier in chapter 1 (table 1.1).

The cation uptake measurements in acidic media (1 M and 0.5 M nitric acid) were low similar to previous measurements. The increased pore size had a similar effect on ion sorption into the zeolite framework (table 5.6 and figure 5.11). The pH value of the three cation nitrate salts (Cs, Sr and Ce) when dissolved in deionised water was 1.20

resulting in higher uptake values, similar trend to single cation solutions as reported earlier. The Ce ions sorption was higher in all aqueous system, which was likely due to a concentration effect i.e. 10 times more concentrated than Cs and Sr ions. The poor performance of all the zeolites in mixed ions weakly acidic system compared to single ions weakly acidic system (pH 1.20) could explained due to pH value. The lower pH value had influenced the zeolite performance.

5.3.6 Uptake measurements of mesoporous zeolite in 0.5 M HNO_3

A mixed ion sorption study was performed on the prepared mesoporous coated molecular zeolite. The coated zeolite 5A (mesoporous layer) was studied as it had better uptake performance as described earlier. Mesoporous zeolite 5A was coated with Si and two different Al:Si ratios. Table 5.8 reports the competitive ions uptake study of zeolite 5A and mesoporous zeolite 5A in mixed ions 0.5 M HNO_3 system.

Synthesised 5A@Si sample compared with 5A showed only marginal increase in Sr and Ce ion uptake. This uptake increase was likely due to increased surface area formed by Si framework; the silica surface contains Si-OH in hydrated form hence H^+ could have exchanged with available ions. The higher uptake of Sr and Ce ions were observed due to preference towards multivalent ions compare to single valent ions (figure 5.12).

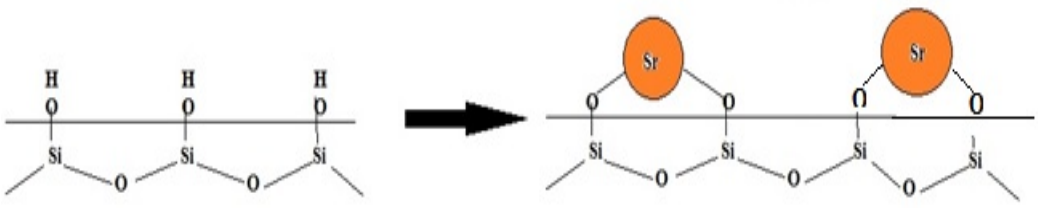

Figure 5.12 Proposed mechanism of multivalent ion sorption on Si surface

Al:Si coated zeolite 5A has shown diminishing uptake compared to only silica coated zeolite. This was due to the nitric acid destroying the mesoporous framework structure resulting from Al-O-Si bonds being weaker than Si-O-Si bonds. As the mesoporous zeolite materials did not show any significant improvement in their ion uptake. Further study of various aqueous system was abandoned.

Table 5.8 Mixed ions concentrations in 0.5 M HNO_3

Samples	Initial (ppm)			Final (ppm)			V (ml)	W (g)	Kd (ml/g)		
	Sr	Cs	Ce	Sr	Cs	Ce			Sr	Cs	Ce
5A@Si	429±7	669±10	6656±145	309±5	474±9	3936±81	25	0.50	19.42	20.57	34.55
5A@Si_Al_0.31	429±7	669±10	6656±145	326±4	497±9	4711±73			15.73	17.23	20.56
5A@Si_Al_0.72	429±7	669±10	6656±145	326±7	500±6	4648±69			15.73	16.83	21.51
5A	426±8	676±11	6364±66.9	311±8	448±5	4361±80			18.49	25.35	22.91

5.3.7 Rate of uptake of molecular sieves 5A

The kinetics of exchange enables the viability of an ion exchange material in separation technology to be understood, helps in identifying the reaction pathway and rate dependence on the limiting reacting systems. These rates and mechanisms are governed by ion exchange conditions, nature of the exchanger and exchanging ionic species. Ion exchange kinetics involves the diffusion of metal ions through the solution to the surface and particle pores of the resin followed generally by the chemical exchange between hydrogen ions and metal ions at the exchanging sites and the diffusion of the displaced hydrogen ions out of the interior and surface of resin into the solution. Both film and particle diffusion mechanisms are prevalent in ion exchange process, although normally the slowest step (rate-limiting step) for a given system controls the speed of ion exchange. Earlier studies noted that film diffusion control prevail in systems with ion exchangers of high concentrations of fixed ionic groups, small particle size, dilute solutions and with inefficient agitation; while high metal ion concentration, relatively large particle size of the ion exchanger and vigorous shaking of the exchanging mixture favour a particle controlled process.

Zeolite 5A was selected, has it had better uptake capacities than other zeolites studied, for kinetic studies. Table 5.9 and figure 5.13 reports the rate of various ions uptake in 0.5 M HNO_3. The investigation indicated that rate of uptake for Cs, Sr ions were quite rapid, and up to 80% equilibrium was achieved within first 60 minutes but uptake of Ce ions was much slower. The difference in rate of uptake for Ce ion in two different concentrations suggest high concentration of Ce ions in mixed ion system (10 times) could have influenced Cs and Sr ion uptake performance.

Table 5.9 Rate of uptake on molecular sieve 5A in 0.5 M HNO_3

Samples (Minutes)	5 mM Cs(I) (%)	5 mM Sr(II) (%)	5 mM Ce(IV) (%)	50 mM Ce(IV) (%)
0	0	0	0	0
60	85	72	23	54
180	100	88.3	68.6	97
720	100	100	100	100
1440	100	100	100	100
2880	100	100	100	100

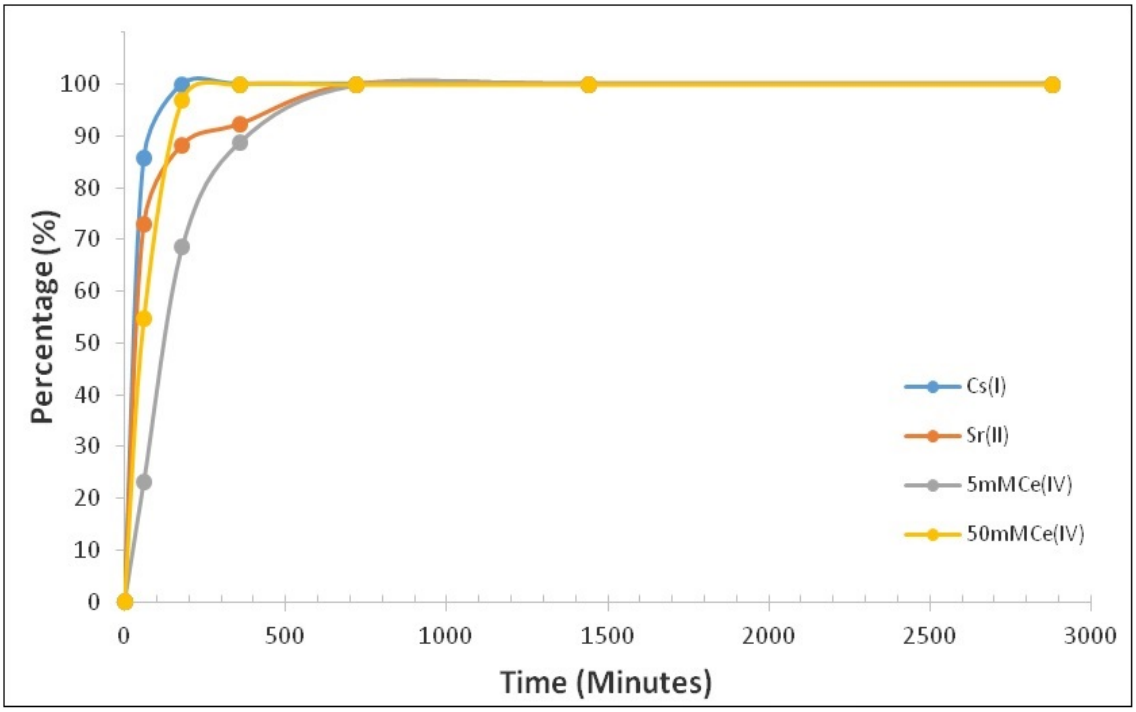

Figure 5.13 Rate of uptake of various ions on molecular sieve 5A in 0.5 M HNO_3

5.4 Conclusions

The objective of the research was to identify potential use of size exclusion property of zeolite A with various pore sizes to selectively remove FPs. The study was expanded to include the synthesis of mesoporous zeolite 5A; a mesoporous layer was coated around zeolite particles and expected to act as a protection layer against its direct contact with the aqueous system.

The synthesised materials were characterised by various analytical techniques. The mesoporous coating on zeolite 5A were successfully accomplished by sol-gel technique and characterised by PXRD, SAXS, surface area, and SEM imaging. The x-ray diffraction comparison of zeolite 5A and three different mesoporous coatings were observed where peak positions remains same however, the intensity of those peaks were reduced with various coatings. The mesoporosity was also confirmed by SAXS and surface area studies. The surface area for 5A@Si was highest 530 m^2/g in comparison to 369 m^2/g for zeolite 5A. The increased surface area suggest mesoporosity with pore size 23.5 Å. The characteristic loop (type IV) in gas sorption isotherm further confirms mesoporosity of synthesised mesoporous 5A particles.

The cation uptake studies in single ions and mixed ions suggest zeolite A was not capable of separating the cations based on hydrated ion size exclusion. Zeolite A had shown uptake of Ce ions although the hydrated diameter was 11 Å, larger than biggest pore size zeolite 5A.

All the zeolite A's have shown marginal uptake of Cs, Sr and Ce ions in 0.5 M and 1 M HNO_3 system for both single and mixed ions system. The uptake was remarkably higher (up to 31 mg/g for single ions) in weakly acidic systems and pH value higher than 4, which was consistent from previous research on zeolites.

The rate of uptake values were encouraging; up to 80% equilibrium for Cs and Sr ions were achieved within 60 minutes in 0.5 M HNO_3 system at room temperature.

Mesoporous coating only has a marginal effect, not more than 10% on cation uptake performance and was therefore further studies were discontinued.

5.5 References

1. Chmielewská E., Environmental Zeolites and Aqueous Media. SAIF Zone, Sharjah, UAE: Bentham Science Publishers. 2014

2. Sinha P.K., Panicker P.K., Amalraj R.V., and Krishnasamy V., Treatment of radioactive liquid waste containing caesium by indigenously available synthetic zeolites: A comparative study. Waste Management, 1995. 15(2), p. 149 - 157.

3. El-Kamash A.M., Evaluation of zeolite A for the sorptive removal of Cs^{+} and Sr^{2+} ions from aqueous solutions using batch and fixed bed column operations. Journal of Hazardous Materials, 2008. 151(2–3), p. 432 - 445.

4. Merceille A., Weinzaepfel E., Barré Y., and Grandjean A., The sorption behaviour of synthetic sodium nanotitanate and zeolite A for removing radioactive strontium from aqueous wastes. Separation and Purification Technology, 2012. 96, p. 81 - 88.

5. Yang X., Hierarchically Structured Porous Materials: From Nanoscience to Catalysis, Separation, Optics, Energy, and Life Science (2nd Edition), Chapter 14 Somerset, USA, John Wiley & Sons, 2011. ISBN: 978-3-527-32788-1, p. 435 - 452

6. Lv Y., Qian X., Tu B., and Zhao D., Generalized synthesis of core–shell structured nano-zeolite@ordered mesoporous silica composites. Catalysis Today, 2013. 204, p. 2 - 7.

7. Xue Z., Li Z., Ma J., Bai X., Kang Y., and Hao W., Effective removal of Mg^{2+} and Ca^{2+} ions by mesoporous LTA zeolite. Desalination, 2014. 341: p. 10 - 18.

8. Javadian H. and Taghavi M., Application of novel Polypyrrole/thiol-functionalized zeolite Beta/MCM-41 type mesoporous silica nanocomposite for adsorption of Hg^{2+} from aqueous solution and industrial wastewater: Kinetic, isotherm and thermodynamic studies. Applied Surface Science, 2014. 289, p. 487 - 494.

9. Sing K.S.W., Reporting physisorption data for gas solid systems with special reference to the determination of surface area and porosity. Pure and Applied Chemistry, 1982. 54(11), p. 2201 - 2218.

10. Qian X.F., Li B., Hu Y.Y., Niu G.X., Zhang D.Y.H, and Che R.C., Exploring Meso-/Microporous Composite Molecular Sieves with Core–Shell Structures. Chemistry – A European Journal, 2012. 18(3), p. 931 - 939.

11. Baerlocher C.H., Meier W., and Olson D., Atlas of Zeolite Framework Types, 5th edition, , Amsterdam: Elsevier, 2001

12. Kielland J., Individual Activity Coefficients of Ions in Aqueous Solutions. Journal of the American Chemical Society, 1937. 59(9), p. 1675 - 1678.

Chapter 6

AMP composites

6.1 Introduction

6.1.1 Ammonium phosphomolybdate (AMP)

Ammonium phosphomolybdate (AMP) is a salt of 12-heteropoly-acids family and their first synthesis mechanism was reported by Berzelius [1]. It was synthesised by heating ammonium molybdate in a mixture of concentrate phosphoric acid and nitric acid, which yields yellow fine precipitate of ammonium phosphomolybdate and ammonium nitrate in solution and water [1- 3].

The detailed x-ray crystal structure of AMP was first reported by Illingworth and Keggin [4].

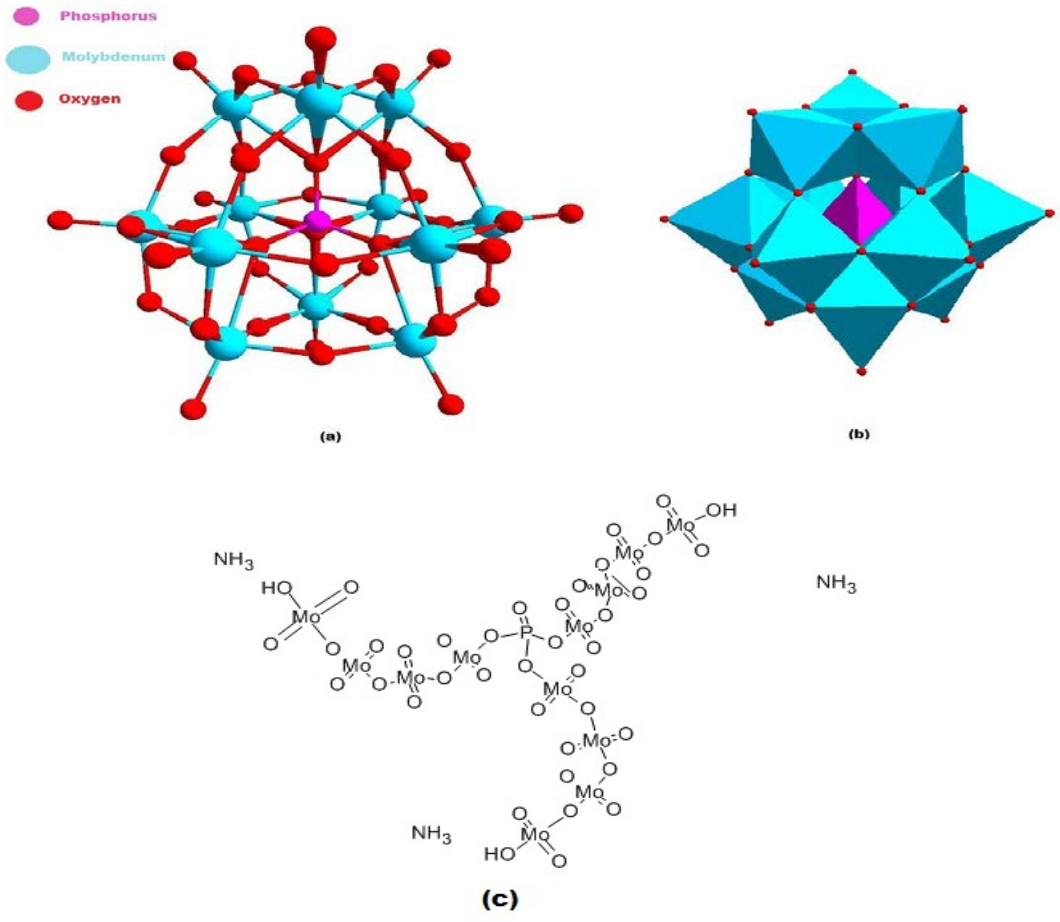

Figure 6.1 Schematic representation of AMP in (a) Ball stick structure, (b) crystal structure, and (c) chemical structure [5]

The reaction can be represent as

$$12(NH_4)_2MoO_4 + H_3PO_4 + 21\ HNO_3 \rightarrow (NH_4)_3PMo_{12}O_{40}\downarrow + 21\ NH_4NO_3 + 12\ H_2O$$

According to their findings, the phosphomolybdate complex ($PMo_{12}O_{40}$) consist of a hollow sphere formed by $12MoO_6^{6-}$ octahedra with PO_4^{3-} group in the centre of the crystal structure of the ammonium salt of this ion. The ammonium ions (NH_4^+) are probably fitted between these spheres thus balancing the crystal charge in the lattice (Figure 6.1) [5].

The first ion exchange properties of AMP were reported by Smit *et al.*, who investigated the exchange of monovalent alkali metal ions by ammonium ions. The study concluded that AMP had an excellent distribution coefficient (Kd) and good selectivity for caesium ions compared to other ions in up to 10 M HNO_3 media [6, 7].

A different study was carried out with K^+, Rb^+, Cs^+, Sr^{2+}, Ag^+, Hg^{2+}, and Tl^{3+} ions uptake on AMP from pH solution of 2 - 5 [8]. The study revealed that metal ions that form insoluble heteropolyacid salts will exchange significantly with the ammonium ions in acidic solutions (pH < 2) [9]. A similar ion exchange capacity study has been reported where monovalent ions (Na^+, K^+, Rb^+, and Cs^+) were exchanged by NH_4^+ [7, 10].

Caesium separation from highly salted nuclear waste was carried out with AMP that demonstrated there was no significant difference in Kd uptake in presence of 10g/l Na ions [12]. Various studies were also performed to measure rate of uptake of caesium on AMP all of them recorded fast kinetics (< 30 min) and equilibrium was established immediately [8, 11, 12].

The caesium uptake of AMP was also studied in acidic conditions (0.2 - 10 M) before and after irradiation at approximately 1 MGy and the study reported no significant change in capacity and minor change in caesium Kd after irradiation [13].

A solubility study was performed by Archer, where they reported its finite solubility in water and acids and it dissolves readily in alkaline solution (pH > 8) [14].

Advantages of AMP are:

- rapid rate of sorption equilibrium
- high distribution coefficient in acidic media
- high loading capacity
- high selectivity for caesium in complex matrices
- soluble in alkaline solutions
- elution is possible with ammonium nitrate solutions.

Disadvantages of AMP are:

- it is a microcrystalline structure which is not suitable for column use,
- the high Cs loadings of AMP result in high radiation doses and hotspots on the column requiring cooling systems,
- heat generation could affect the support (i.e. melt the organic support)

6.1.2 AMP- Al_2O_3 composite

To overcome the particulate size and solubility in acidic media, a granular (microsphere) form of composites were developed based on metal oxides which are practically insoluble in 1 - 5 M HNO_3 and provides support matrix to Cs selective zeolites [16, 17].

Preparation of granular (microsphere) form can provide ideal flow dynamics for column operations. Microspheres can also be tailored by varying physical and chemical parameters to control selectivity and loading capacity of the ion exchanger [16].

First synthesis of metal oxide microspheres by internal gelation method was demonstrated to make spheroidal uranium oxide in the nuclear fuel cycle and later it was extensively researched in the area of inorganic ion exchangers at ORNL [15, 16].

Internal gelation process is a chain of reactions where hydrous metal oxides undergo stepwise hydrolysis and polymerisation [17]. In a typical synthesis of aluminium microspheres mixing of pre-cooled solution of hexamethylenetetramine (HMTA) and urea to pre-cooled aluminium nitrate solution and then dispersing it as droplets into hot oil is involved [17]. The key of internal gelation process is a slow or delayed gelation at low temperature (0 – 5 °C) and quickly transferred into hot organic media (silicon oil) to allow rapid gelation.

Aluminium nitrate internal gelation chemistry

$Al(NO_3)_3 + xH_2O \longrightarrow Al(NO_3)_{3-x}(OH)\,x + xHNO_3$ ……. (1)

$HNO_3 + NH_4OH \longrightarrow NH_4NO_3 + H_2O$…….. (2)

$(CH_2)_6N_4 + HNO_3 \longrightarrow (CH_2)_6N_4.HNO_3$…… (3)

$Al(NO_3)_{3-x}(OH)\,x + (3-x)\,H_2O \longrightarrow Al(OH)_3 + (3-x)\,HNO_3$……... (4)

Reaction (1) describes the partial hydrolysis of aluminium nitrate, which release free acid. In the internal gelation process, free acid (nitrates) have to be neutralised as excess acid to aluminium ratio affect the retention of the spherical shape [17]. The neutralisation of free acid can be achieved by strong base (NaOH) but NH_4OH is usually preferred because of easy volatisation and thermal decomposition of NH_4^+ [18]. Reaction (3) describes the neutralisation of free acids when mixture of hydrolysed metal oxide was added to HMTA solution. HMTA plays a very critical role during gelation; excessive amount of HMTA results in premature gelation and insufficient amount results in softer gel or incomplete gelation [18]. Internal gelation process also requires urea, which forms a complex with metal ions (Al^{3+}) when hydrolysed aluminium nitrate solution was added to the mixture of HMTA, and urea [17, 18]. Urea reacts with free nitrate in acidic solution of aluminium nitrate and yields gaseous nitrogen and CO_2 [18]. Thus, it shields Al^{3+} ions during addition of HMTA and prevents premature precipitation [18].

A detailed study of the preparation of ZrHP-AMP microspheres by internal gelation and their caesium uptake was performed on actual INEEL acidic waste [16]. The evaluation revealed that a spheroidal inorganic composite was successfully produced which possessed good strength, low tendency for surface erosion and high caesium selectivity and loading capacity in acidic high salt INEEL waste [16].

Synthesis of AMP loaded aluminium oxide microspheres were investigated for production of granular form of caesium selective ion exchangers in acidic media [19, 20]. The studies concluded that maximum of 16 wt % of AMP was able to load into Al_2O_3 spheres by internal gelation technique [20]. The study also reported that increased quantity of AMP resulted in a softer gel of AMP-Al_2O_3, which did not retain its shape; increased quantities of HMTA and urea did not further improve the gel structures [20].

The study was also extended to separate Cs^+ ions from Ba^{2+} ions in up to 8 M HNO_3 media the spheres exhibited respectable distribution coefficient and selectivity for Cs^+ in up to 2 M HNO_3 [20].

A different preparative method of producing AMP-Al_2O_3 spheres was investigated by Onodera *et al.* where phosphomolybdic acid was used as the starting chemical, which was converted to ammonium phosphomolybdate after loading into commercially available aluminium microspheres [21]. The study reported that about 50% AMP loading was possible after series of impregnations of Al_2O_3 spheres. The caesium sorption study in mixed ion high-level waste reported that Cs^+ possessed high Kd value in presence of other ions except Na^+ in 1 M HNO_3 media [21].

6.1.3 AMPPAN composite

Polyacrylonitrile (PAN) is a synthetic, semi-crystalline organic polymer with the linear formula $(C_3H_3N)_n$. It is a copolymer made from a mixture of monomers with acrylonitrile as the main chemical species [22]. A typical one-step synthesis process, involves a radical polymerisation of acrylonitrile monomers initiated by peroxides or redox systems at temperature below 100 °C. It is classified as thermoplastic and varies in their molecular weight from 40,000 - 150,000 g/mol.

The most common properties are:

- Fast, simple and cheap synthesis
- Easy modification of physiochemical properties (mechanical strength, porosity, and hydrophilicity)
- Hardness and Stiffness
- High melting point
- Thermoplastic
- Resistant to most solvents and chemicals, UV, heat, microorganisms [23, 24]
- Radiation stability [24]
- Can be moulded into different shapes and size

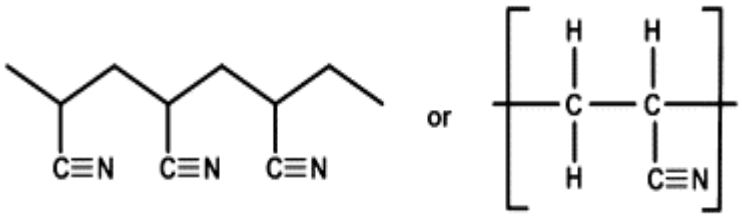

Figure 6.2 Molecular structure of polyacrylonitrile (PAN) [22]

The first discovery of AMPPAN composite was made by Sebesta *et al*. by using PAN as a binding or support material for microcrystalline AMP [23]. The concept was to overcome the particulate structure of AMP to produce a granular form, which would be suitable for column work. The study reported that the rate of uptake of Cs ions in 0.1 M HCl was little slower than particulate pure form of AMP however, the difference was not significant and could be employed for Cs ions separation in acidic nuclear waste [23]. The study also emphasised that binding polymers had no major effect on Cs ions sorption and its properties do not change when reacting in acidic or in the presence of reducing agents [23].

A separate caesium uptake study on AMPPAN composite was performed with a simulated sodium bearing waste, which contained different radionuclides [23]. The study demonstrated excellent caesium selectivity and capacity of the composite in mixed ions acidic solution [23].

Similar research was performed by Todd *et al.*, where AMPPAN composites were evaluated for removal of caesium from Idaho National Engineering and Environment Laboratory (INEEL) concentrated acidic tank waste [25]. The study evaluated different concentrations of sodium, potassium and in different acid strength, the results showed that sorption of caesium was in order $Cs^{+}>>K^{+}>H^{+}\approx Na^{+}$ [25]. The study also extended to columns where the caesium sorption capacity was reported as 22.5, 29.8, and 19.6 mg Cs/g, for 5, 10, and 20-bed volume respectively [25]. The evaluation also confirmed the thermal stability of the composite up to 400 °C [25].

6.2 Material and Methods

6.2.1 Materials

The source and purity of the reagents are presented in table 6.1.

Table 6.1 Reagents, their purity and source of purchase

Reagents	Source	Purity/Grade
Ammonium phosphomolybdate (AMP) $(NH_4)_3PMo_{12}O_{40} \cdot 3H_2O$	Alfa Aesar	Reagent Grade
Aluminium Nitrate $(Al(NO_3)_3 \cdot 9H_2O)$	Sigma Aldrich	≥99%
Urea (NH_2CONH_2)	VWR	≥98%
Hexamethylenetetramine $(C_6H_{12}N_4)$	Sigma Aldrich	≥99%, ACS reagent
Ammonium hydroxide, (NH_4OH)	VWR	Reagent Grade 28%-30% NH_3 basis
Tween 80	Sigma Aldrich	Reagent Grade
Dimethyl Sulfoxide $((CH_3)_2SO)$	Fisher	Reagent Grade
Polyacrylonitrile $(C_3H_3N)_n$	Sigma Aldrich	Reagent Grade
Dichloromethane (CH_2Cl_2)	VWR	≥99.8%
Deionised Water (H_2O)	NA	≥18.2 $M\Omega.cm^{-1}$
Silicon Oil (Polydimethylsiloxane)	Mistral Industrial Chemicals	100%
Caesium nitrate $(CsNO_3)$	Sigma Aldrich	≥99.9%
Strontium nitrate $(Sr(NO_3)_2)$	Sigma Aldrich	≥99.9%
Ammonium cerium nitrate $(Ce(NH_4)_2(NO_3)_6)$	Sigma Aldrich	≥99.9%

6.2.2 Synthesis Method

6.2.2.1 AMP-Al_2O_3 composites

The synthesis of AMP-Al_2O_3 composites was initiated by preparing Al_2O_3 and further encapsulating AMP in the process.

Synthesis of Al_2O_3 granules

The synthesis Al_2O_3 granules were prepared using the same technique reported by Pillai *et.al.* with slight modification [17]. The preparative route was initiated by preparing 100 ml stock solution of 3 M aluminium nitrate and 3 M mixture of HMTA and urea in a volumetric flask by weighing required quantity of each reagents and making up the solution to 100 ml with d.w. (table 6.2). Further, 5.12 ml of ammonium hydroxide was added to the aluminium nitrate stock solution to adjust molarity to 2.85 M.

Table 6.2 Amount of reagents used for preparation of stock solution

Reagents	**Molarity (M)**	**Weight (g)**
Aluminium Nitrate ($Al(NO_3)_3 \cdot 9H_2O$)	3 M	112.5
Urea (NH_2CONH_2)	3 M	18
Hexamethylenetetramine ($C_6H_{12}N_4$)	3 M	42.05
Ammonium hydroxide, (NH_4OH)	NA	4.60

For synthesis of Al_2O_3 granules, 49.2 ml of ammonium treated aluminium nitrate stock solution (2.85 M) was measured into a beaker; to this a further 10.36 ml NH_4OH was added to this solution and cooled in an ice bath at between 0 - 5 °C, solution-A. In a separate beaker, 45 ml of 3 M mixture of HMTA and urea stock solution was dispensed and cooled in an ice bath at between 0 - 5 °C, Solution- B.

Chilled Solution B was added slowly to Solution A with constant stirring by magnetic stirrer in an ice bath. After stirring for about 10 minutes, the chilled viscous mixture (gel) was added dropwise by a pipette into hot (90 °C) silicon oil. The synthesised

granules were separated from oil and degreased by washing twice with dichloromethane (CH_2Cl_2) which was followed by at least 4-washings with 2 M NH_4OH and measuring the solution conductivity. The granules were then dried in an air oven at 80 °C under vacuum overnight followed by calcination in a furnace at 380 °C with 2 °C/min in air.

Synthesis of AMP-Al_2O_3 granules

AMP-Al_2O_3 composites granules were synthesised in a similar technique as Al_2O_3 granules by adding "X" quantity of AMP to Solution-A (table 6.3). The whole process was repeated as mentioned earlier with exception of washing stage where granules were washed with 0.1 M NH_4OH at least 4-times and measuring the solution conductivity.

Table 6.3 Amount of AMP used during AMP-Al composite preparation

Samples	"X" AMP (g)
AMP-Al_2O_3-1	0.8
AMP- Al_2O_3-2	0.7
AMP- Al_2O_3-3	0.5

Al_2O_3 and AMP- Al_2O_3 composite granules were prepared using two different equipment set-ups. As shown in figure 6.3 (a), a temperature controlled pumping system filled with silicon oil was connected to approx. two 60 cm long glass jacked columns by rubber tubing. Inlet and outlet of both columns connected in such a way that hot oil passes through vertical column first and then inclined column and back to the heated pump reservoir. The flow of the pumping system was regulated by a manual valve that maintained the oil level of the vertical column half-full. The end of the inclined column was placed on a sieve supported by funnel on the Erlenmeyer flask with DURAN side outlet.

The Erlenmeyer flask, which contained silicon oil, was placed on a magnetic hot stirrer plate. The temperature was elevated to 150 °C with constant stirring and the oil was directed to pumping system to maintain the required temperature in the vertical column. The vertical column was insulated with aluminium foil.

A quick fit glass connector was placed on top of the vertical column to achieve two inlets. The hot silicon oil passes through side inlet and composite mixture was introduced by 2 ml Pasteur pipette drop wise through the other.

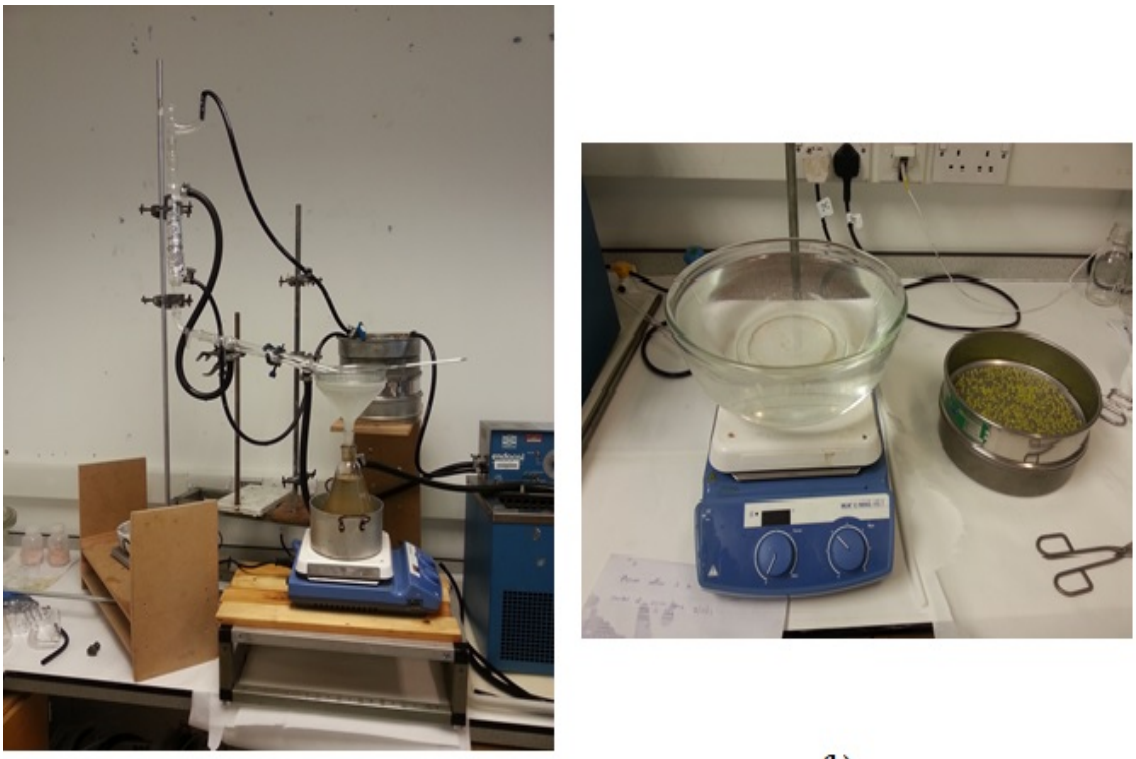

Figure 6.3 Synthesis of Al_2O_3 and AMP-Al_2O_3 (a) Column setup, and (b) Bowl setup

A different system was constructed which is shown in figure 6.3(b). An easier setup, which consisted a 2.5 L Pyrex glass bowl, filled with silicon oil up to 85% capacity. The bowl was placed on a magnetic hot plate and oil was stirred continuously for homogeneous heat transfer. The temperature was constantly recorded by a thermometer. A 45 microns stainless steel sieve was submerged in the heating oil and allowed to achieve a constant temperature of 90 - 95 °C. The composite mixture was injected by 25 ml syringe into the hot silicone oil to produce the required granules. The injected composite mixture was allowed to gel in the oil for 2 - 3 minutes and the sieve containing the granular was lifted out of the oil. The oil was allowed to drain and retained materials were processed further as explained in synthesis method.

6.2.2.2 AMPPAN composites

AMPPAN composites were prepared by same method as previously reported by Park *et al.* [27]. The matrix of required quantities of reagents are reported in table 6.4. The synthesis of AMPPAN composite was initiated by dissolving “z” quantity of Tween 80

in “L” amount of dimethylsulfoxide (DMSO) and mixed by an overhead stirrer at approximately 250 rpm. “Y” quantity of ammonium phosphomolybdate (AMP) was added to the solution and the mixture was kept in a water bath at 50 °C for 1 hour. After one hour, a homogeneous yellowish green colour mixture was obtained, “X” amount of polyacrylonitrile (PAN) powder was added and the solution was maintained at 50 °C with constant stirring (~250 rpm) for 6 hours. The composite mixture was allowed to drop under gravity into ~400 ml of d.w. The spheres were left overnight in d.w and further washed 3 times with fresh d.w. every 30 minutes. The washed beads were separated and dried in an air oven at 60 °C for 24 hours. The synthesised composites were identified as AMPPAN weight percentage (table 6.4).

Table 6.4 Amount of reagents used AMPPAN composite preparation

wt% AMP	Sample	PAN (g) “X”	AMP (g) “Y”	TWEEN 80 (g) “Z”	DMSO (ml) “L”
70	AMPPAN 70	4	10	0.4	100
50	AMPPAN 50	20	20	0.8	200 - 225
25	AMPPAN 25	18.75	6.25	1.6	200 - 250
12.5	AMPPAN 12.5	20	2.5	1.6	200 - 250

In the first experiment the AMPPAN 70 composite mixture was allowed to drop under gravity through a 2 mm ID pipette; in the second series of experiments a Watson Marlow peristaltic pump was used to provide a constant head of composite mixture in the 25 ml pipette (figure 6.4). The in-house nozzle system was developed as commercially available vibrating nozzle systems had long lead times and are expensive. As shown in figure 6.3, one end of the plastic tubing was dipped in the mixture container and other end was passed through peristaltic pump to 25 ml glass pipette. The peristaltic pump was operated between 100 - 200 rpm to maintain an appropriate flow rate and constant head in the pipette. The viscosity of the mixture was adjusted by adding extra amount of DMSO directly into warm mixture. The pipette end was capped with 1 ml pipette tip to make 2 - 3 mm spheres and the mixture was dropped in to a beaker containing d.w. Second pipette was installed to make the synthesis process quicker. The video of the actual working arrangements can be found on youtube [31].

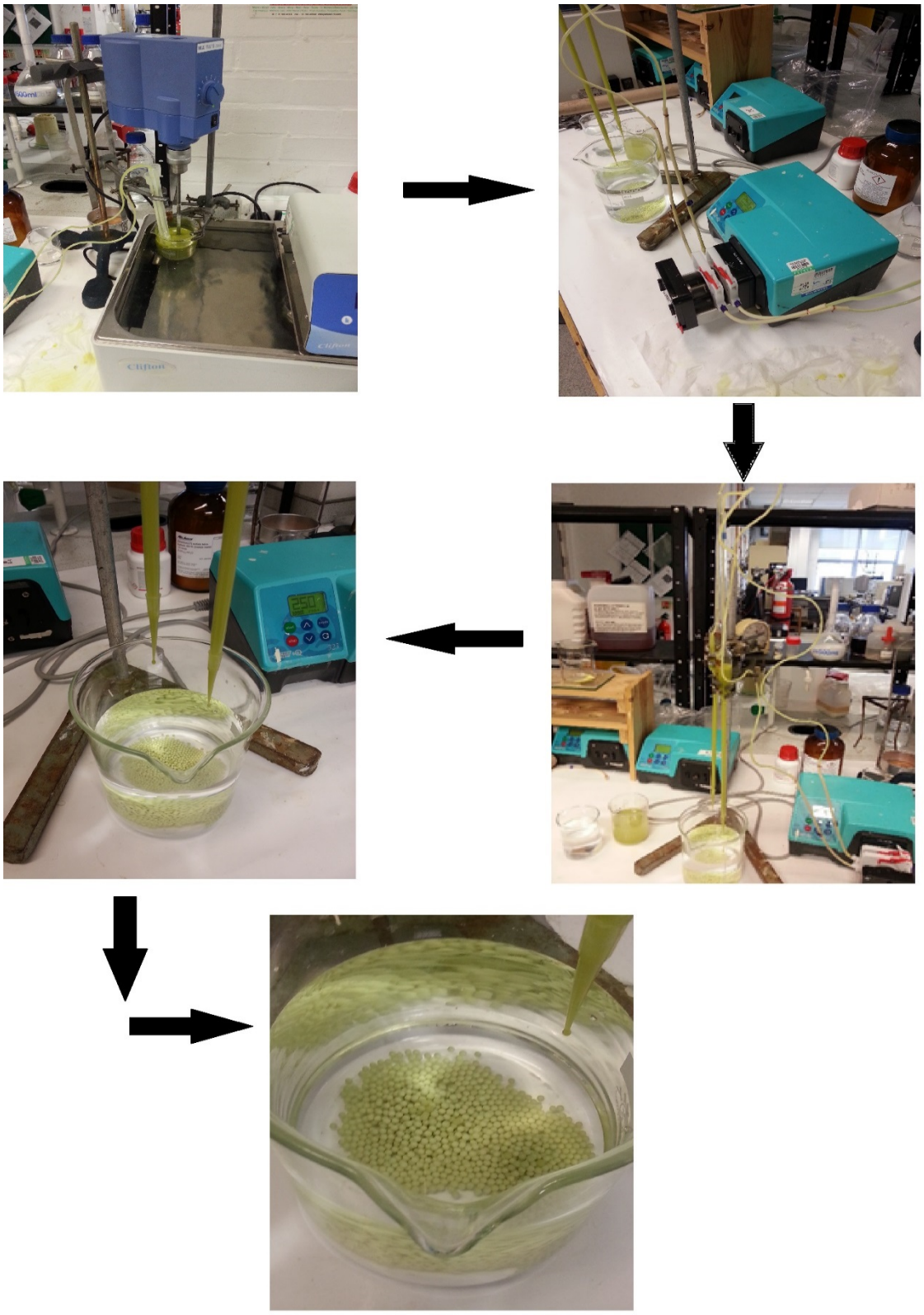

Figure 6.4 Continuous pumping setup for AMPPAN composite production

6.2.3 Characterisation

The structural morphology of all the composites were studies by SEM. The textural characteristics were evaluated by nitrogen sorption. ATR-IR was used to study the changes that have occurred during synthesis. The thermal properties of various composites were evaluated by TGA at 10 °C/min and in air supply of 20 ml/min. The experimental details of the uptake and rate of uptake measurements were performed by ICP-MS and explained in chapter 3.

The chemical stability of the composites was studied using a known quantity of material (0.5 g) with 25 ml of various HNO_3 solutions (0.5 M, 1 M and 3 M) in a 150 ml Duran glass bottle. The bottles were placed in a shaking water bath and composites/solutions were agitated for 24 hours at ~170 rpm at 25 °C. Subsequently, the composites were separated from HNO_3 solutions, and the ions leached from the composite into the acid measured by ICP-MS. Al and Mo ions were measured to evaluate chemical stability of AMP-Al_2O_3 composites and only Mo ions were measured for AMPPAN study. The experimental detail has been explained in chapter 3.2.9

6.3 Results and Discussions

Preparation of Al_2O_3 and AMP- Al_2O_3

The synthesis of composites using the continuous column set up (figure 6.3 (a)) did not produce the required spheres and after several modifications to the apparatus it was abandoned in favour of the much easier arrangement. The bowl set up produced different shape and size of the composites however; the major challenge with this equipment was product yield. The granules were dropped into hot oil that collected on a submerged sieve. The spontaneous gelling property of the composite mixture, coupled with the close proximity of spheres or granules on the sieve produced gelled material that had no specific shape. In an attempt to overcome these challenges, only small quantities of material were prepared thus preventing gelling on the sieve. This process was time consuming.

The internal gelation technique was not without significant challenges starting with the aluminium nitrate crystals not being of the stoichiometric ratio of 1:3 and this required the excess nitrate to be neutralised by the addition of the appropriate quantity of ammonia solution. The correct Al to nitrate ratio was crucial as it influenced the nature of the gel (softer or harder); a ratio of 1:3.25 produced a softer gel. A series of experiments was carried out in which the ratio of Al to nitrate was changed by the addition of ammonia solution to ascertain which conditions produced the better harder gels. The harder gel in this research referred to gel which retains the shape (granules and/or spherical) after washing stage. The different feed composites were evaluated as reported earlier by Pillai *et.al*. [17].

Table 6.5 Stock solution for Al_2O_3 and AMP- Al_2O_3 preparation

Trial	Al/NO_3 mole ratio	Remarks
1	1:3	Softer gel
2	1:3.15	Softer gel
3	1:3.25	Softer gel

Table 6.6 Feed composition for Al_2O_3 and AMP-Al_2O_3 preparation

NO_3/Al mole ratio	Feed composition		Remarks
	Al (M)	HMTA-Urea/Al mole ratio (M)	
2.85	1.40	1	Harder gel

Table 6.7 Conductivity monitoring during washing

Wash number	Conductivity (mS)		Retained shape during calcination (Yes/No)	
	Al_2O_3	AMP-Al_2O_3	Al_2O_3	AMP-Al_2O_3
2	17.81	18.30	No	No
4	3.25	7.15	Yes	No
6	NA	4.35	NA	No
8	NA	2.85	NA	Yes

NA- Not Applicable

Table 6.5 represents series of experiments with different stock solutions for the synthesis of Al_2O_3 and AMP-Al_2O_3 granules. Table 6.6 represents the feed solution composition used for the study and table 6.7 represents the significance of washing stage. Due to AMP solubility in NH_4OH, AMP- Al_2O_3 composite was washed with 0.1 M NH_4OH and Al_2O_3 granules were washed with 2 M NH_4OH. The study was conducted to prevent the powder formation during calcination. This was due to high osmotic pressure inside the granules due to high presence of NH_4NO_3, which resulted into cracking of granules [17]. Repeated washing step would remove excess nitrates in the structure.

The obtained materials were hard granules, which referred to harder gel of approx. 1 mm wide and 3 - 4 mm long (figure 6.6 and 6.7). The colour of Al_2O_3 and AMP- Al_2O_3 granules were white and yellow respectively. The yellow colour was due to AMP entrapment during Al_2O_3 polymerisation.

Figure 6.5 Softer gel formation

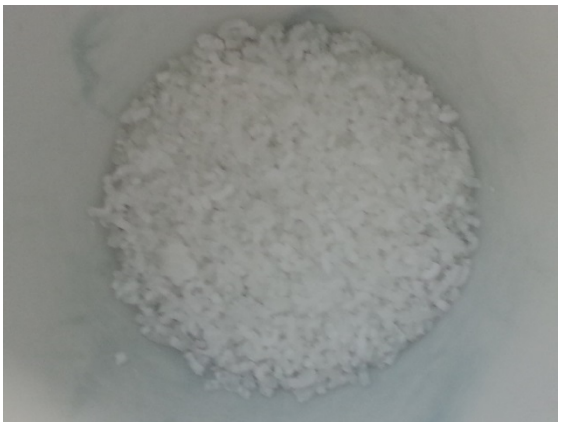

Figure 6.6 Synthesised Al_2O_3 granules

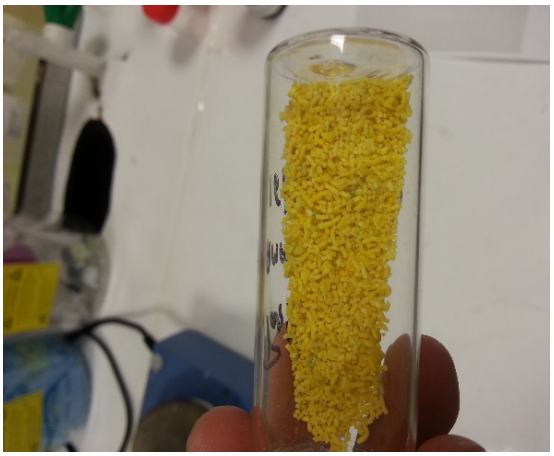

Figure 6.7 Synthesised AMP- Al_2O_3 composite granules

Preparation of AMPPAN composite spheres

The AMPPAN composites were easier to synthesise and for the scale up of the equipment. The AMPPAN 70 spheres produced by manual dropping technique (using a 25 ml syringe) under gravity produced non-uniform spheres (1 - 3 mm) where other composites produced by continuous pumping system were of a more consistent diameter (1.5 - 2 mm). Although the viscosity of the AMPPAN solution was not measured, if necessary, it could be adjusted by additional DMSO, with little change to the morphology of the composites. Figure 6.8 represents AMPPAN composites and colour variation from dark green to pale yellow was considered to be due to amount of AMP entrapped in PAN.

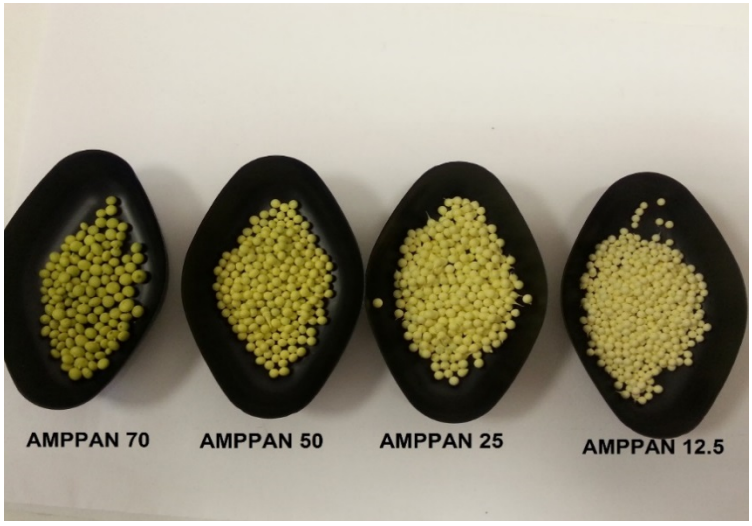

Figure 6.8 Image of synthesised AMPPAN composites

6.3.1 SEM

SEM on various composites was carried out to understand the morphology of the synthesised materials. Figure 6.9 represents SEM granules micrograph of (a) AMP-Al_2O_3 and (b) Al_2O_3 composites respectively. The surfaces of the granules were rough and cracked which could be due to the synthesis technique. There was no channel like structure since no surfactant was used. AMPPAN composites had a distinctive morphology (figure 6.10 – 6.13). The outer surface was smooth however, dissection of spheres revealed a continuous channel-like structure as reported previously [27]. This could be due to pore formation by surfactant, which was removed during the washing step.

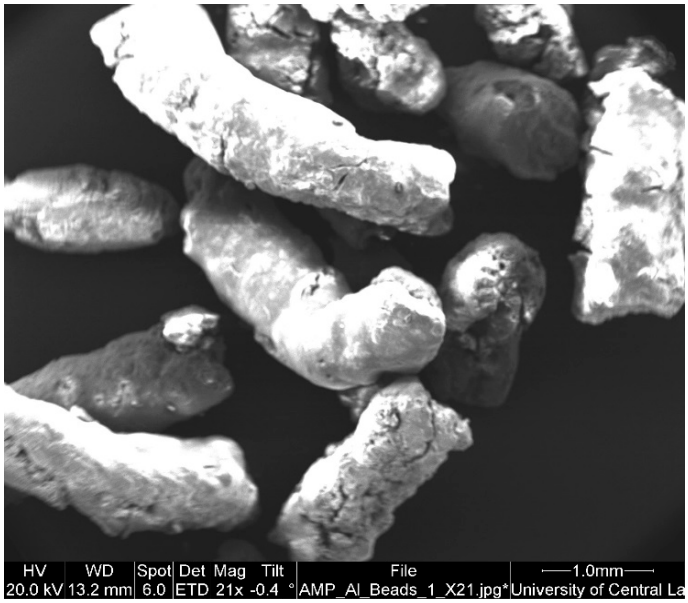

(a)

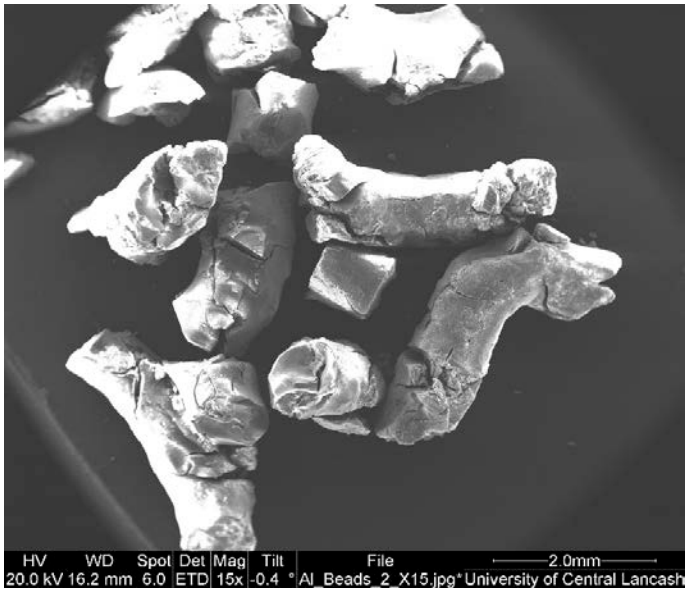

(b)

Figure 6.9 SEM image of (a) AMP- Al_2O_3 granules and (b) Al_2O_3 granules

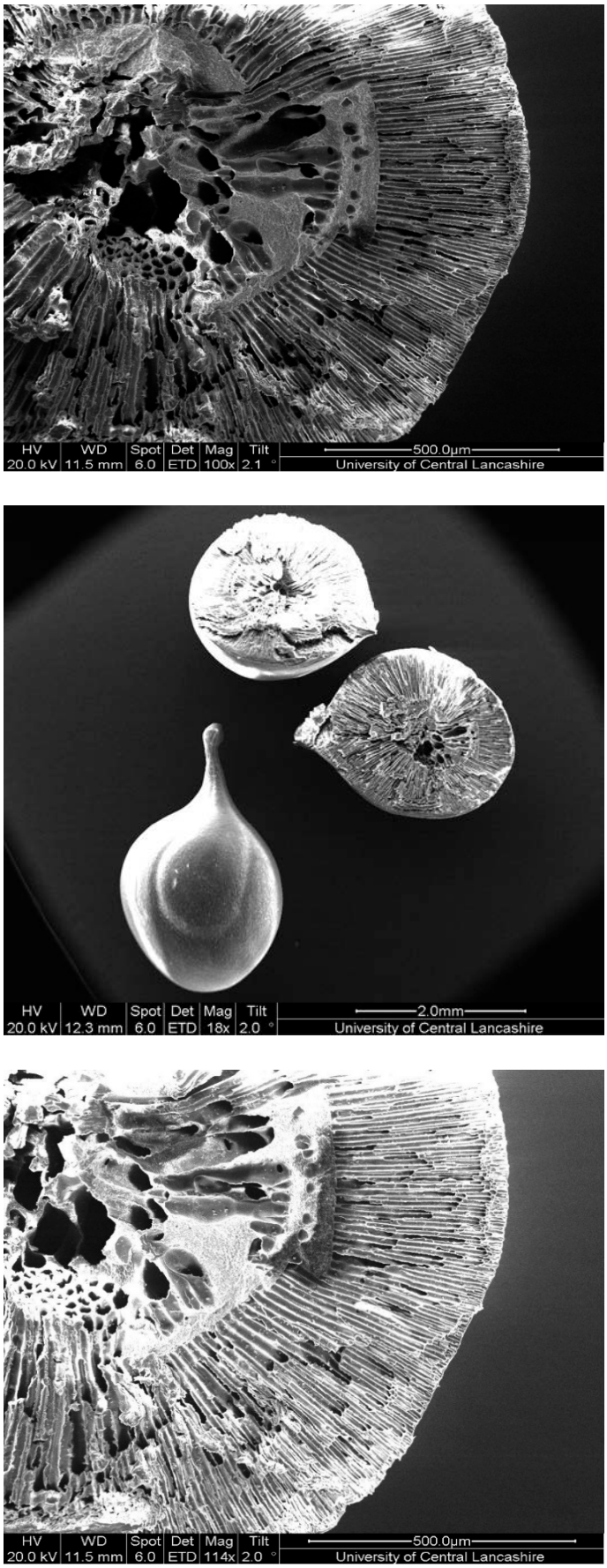

Figure 6.10 SEM images of AMPPAN 12.5 composite

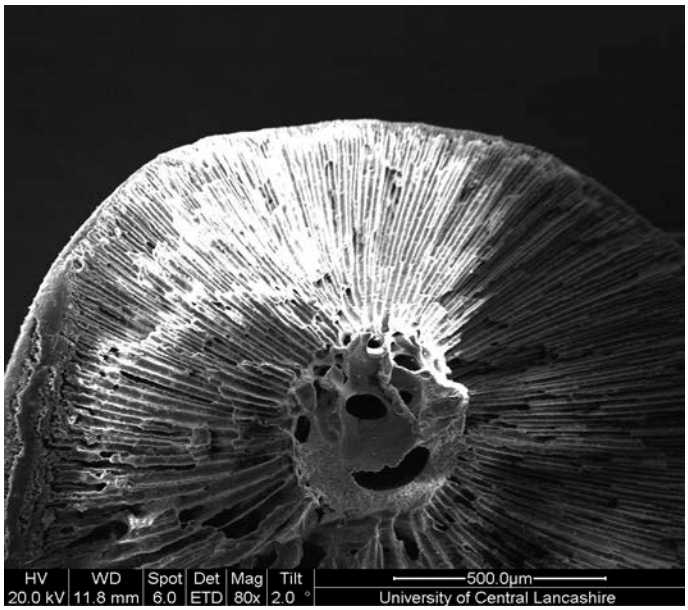

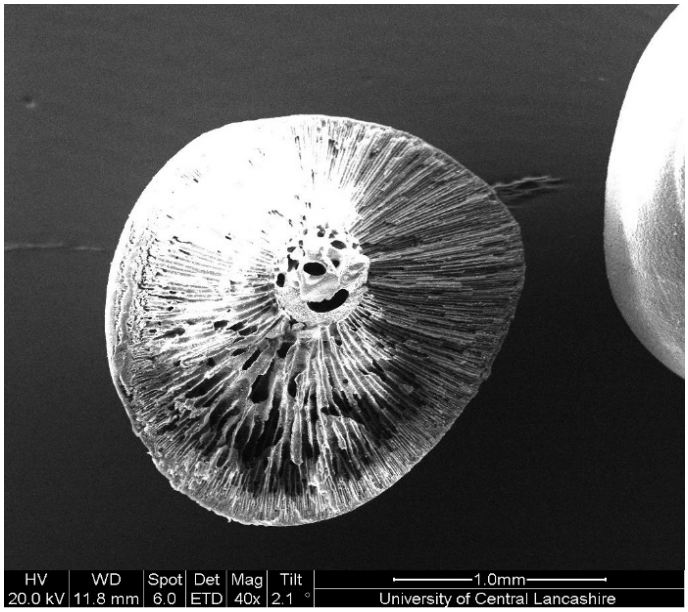

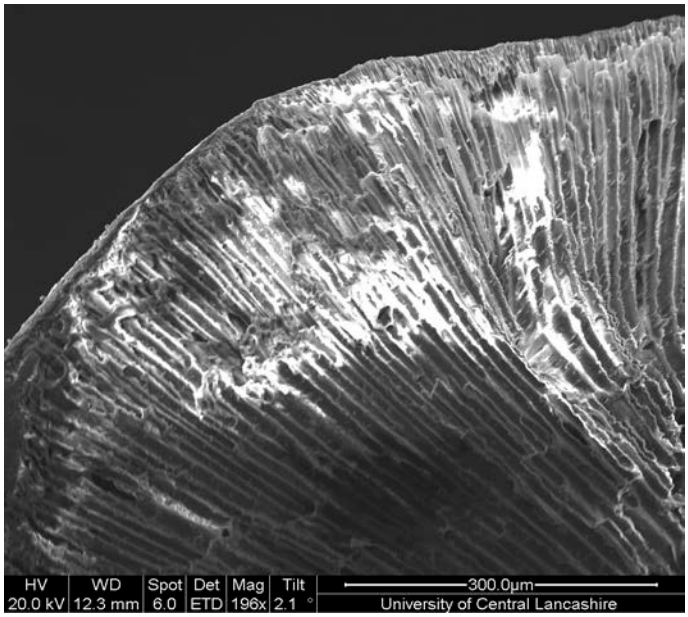

Figure 6.11 SEM images of AMPPAN 25 composite

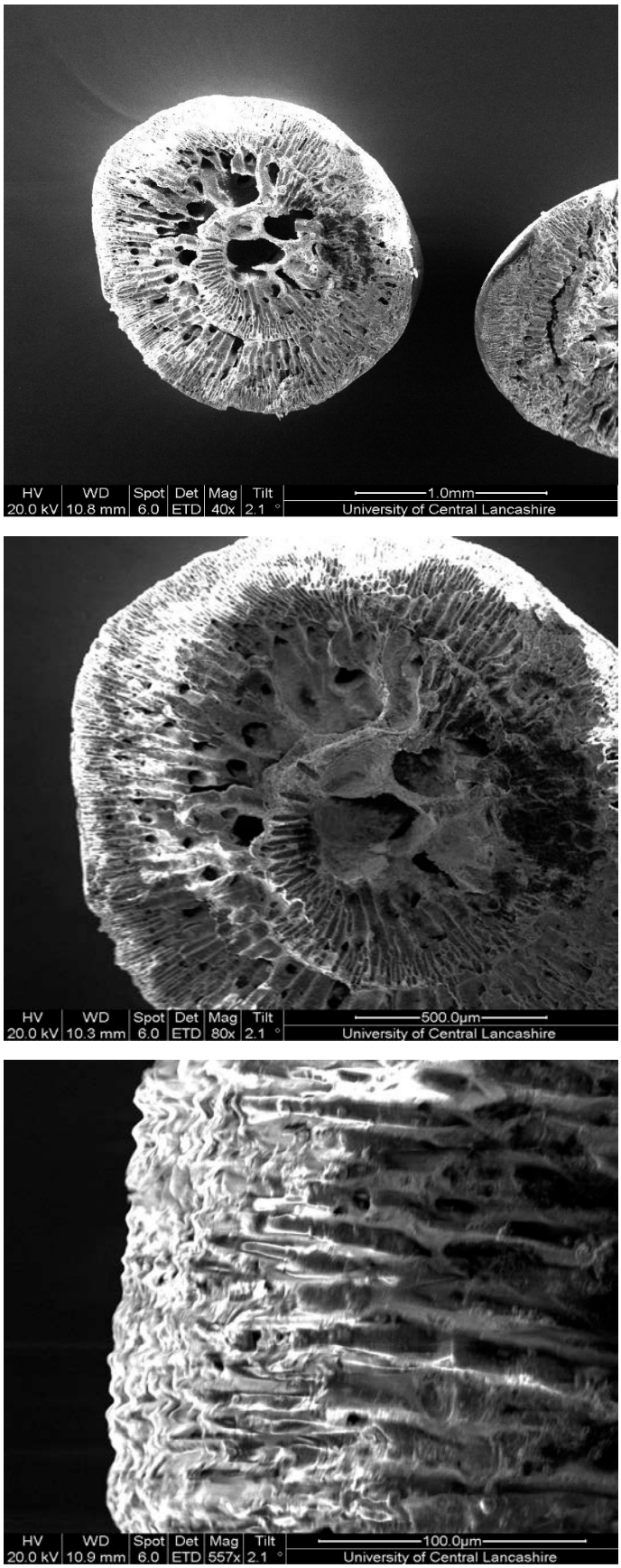

Figure 6.12 SEM images of AMPPAN 50 composite

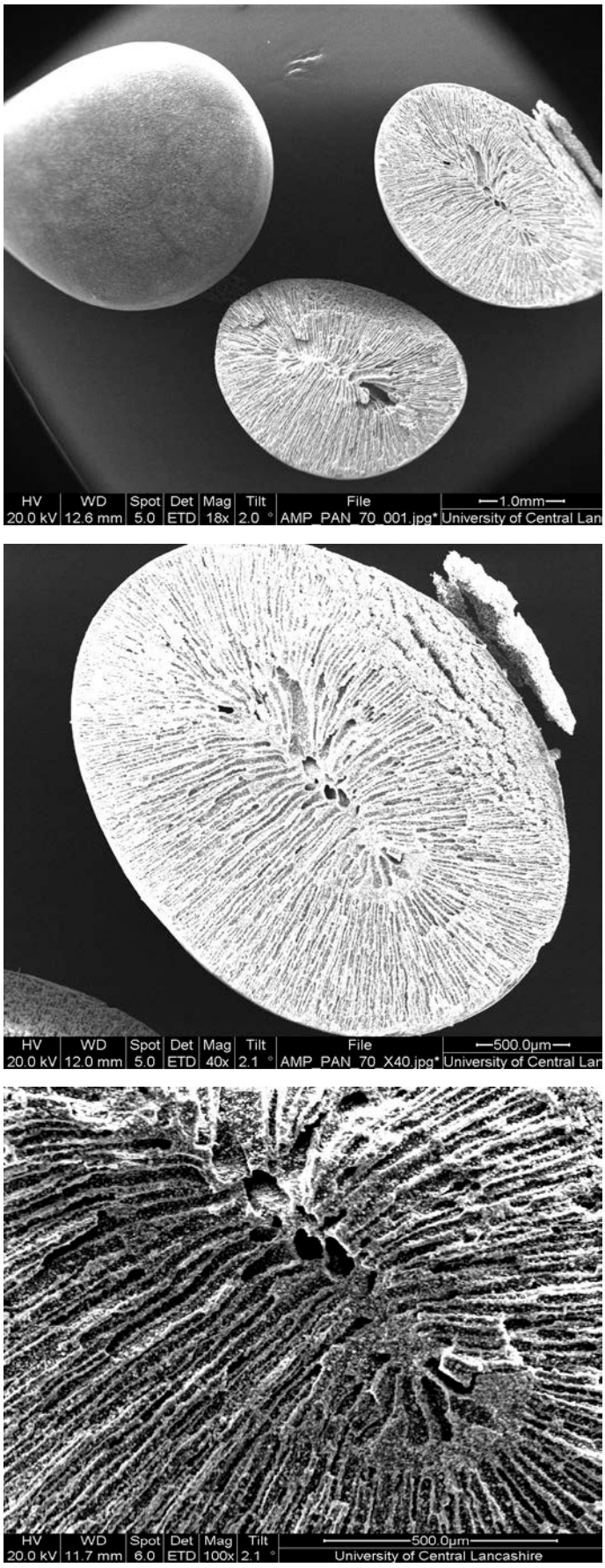

Figure 6.13 SEM images of AMPPAN 70 composite

6.3.2 Surface area and pore analysis

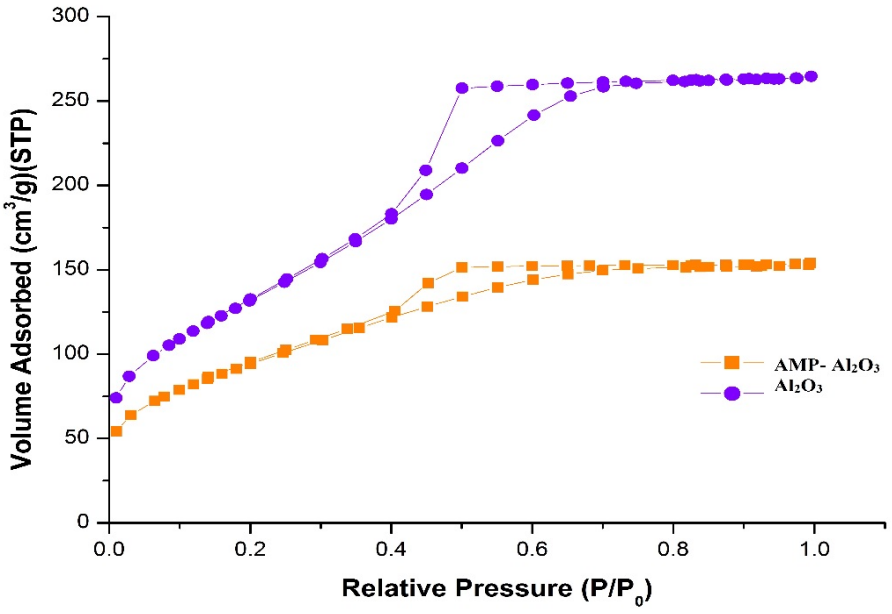

Figure 6.14 Isotherm comparison of AMP- Al_2O_3 and Al_2O_3 materials

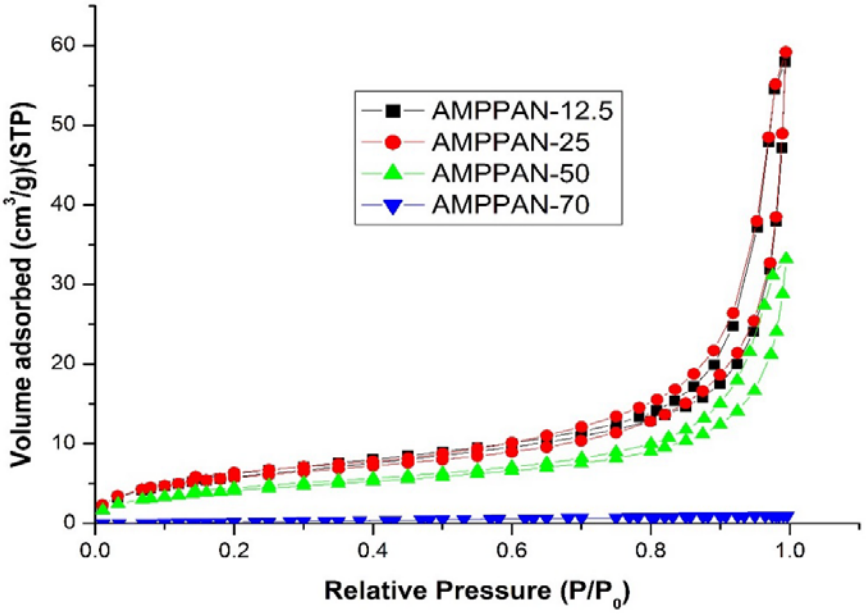

Figure 6.15 Isotherm comparison of AMPPAN composites

Nature of isotherm

The isotherm in figure 6.14 represents a typical mesoporous gas sorption profile similar to type IV isotherm as per IUPAC [27]. Both composites (Al_2O_3 and AMP-Al_2O_3) had shown similar profiles but volumes of gas sorption varied. The decreased sorption data was largely due to AMP encapsulation producing small pores (micropores) of AMP, which resulted in negligible gas adsorption. The characteristic loop in relative pressure (P/P_o) 0.4-0.6 indicates mesoporosity and well uniform pore structure. The BET calculation also supports isotherm data; the Al_2O_3 composite surface area higher than AMP- Al_2O_3 composite (table 6.8).

In figure 6.15, the isotherm comparison indicates higher population of macropores present at relative pressure (P/P_0) close to 1 in AMPPAN 25 and AMPPAN 12.5. This was attributed to the increased amount of surfactant (Tween 80) (table 6.4) employed in the preparation of the composites. The volume adsorbed and the isotherm profile looks identical for these two composites (figure 6.15). The decreased quantity of Tween80 and increased quantity of AMP in AMPPAN 50 had a little effect on sorption volume but the profile was similar to AMPPAN 25 and AMPPAN 12.5, i.e. similar in profile but different volumes of the gas sorption. The most distinct isotherm was observed for AMPPAN 70 composite where very little gas sorption was found which could be attributed to the lowest quantity of surfactant and the highest quantity of used AMP. The surface areas of the composites were also consistent with isotherms where increased quantity of surfactant and decreased quantity of AMP resulted into higher surface area (table 6.8).

Table 6.8 Surface area and Pore analysis of various AMP based composites

Samples	Amount		Specific Surface area(BET) (m^2/g)	Total Pore Volume (cm^3/g)	Av. Desorption pore diameter "d_p" (Å)
	AMP wt%	Tween 80 (g)			
AMPPAN 12.5	12.5	1.6	21.52	0.049	152.99
AMPPAN 25	25	1.6	20.64	0.050	167.91
AMPPAN 50	50	0.8	15.05	0.032	128.82
AMPPAN 70	70	0.4	2.54	0.004	80.52
AMP- Al_2O_3	2	NA	388.94	0.306	32.02
Al_2O_3	NA	NA	486.77	0.407	32.01

NA- Not applicable

Surface area, pore volume and poresize distribution

The pore analysis of these composites was performed by the BJH method. The results indicate that higher pore volume in Al_2O_3 composite compared to AMP- Al_2O_3, which is consistent with surface area data. There was narrow pore size distribution observed and average pore diameter for both composite of the order 32 Å (table 6.8). The pore analysis data indicated that AMP was not affecting formation of pore diameter however; it reduced the pore volume because of micro-porosity.

The effect of surfactant had a key role during formation of porous structure in composites. Higher the quantity, higher the pore volume as reported in table 6.8. The BJH method of pore diameter calculations was performed to observe the uniformity of the porous structure.

The study indicated that all the AMPPAN composites had large pore size distribution in the structure and pore diameter varied from micropores to macropores. The average pore diameters are reported in table 6.8.

The SEM images of AMPPAN 70 (figure 6.13) have shown good porosity; but significantly lower surface area (table 6.8). This was possibly due to the incorporation of the highest amount of AMP, which resulted in most prominent microporosity in AMPPAN 70; thus preventing gas molecules entering into the structure

6.3.3 ATR-IR

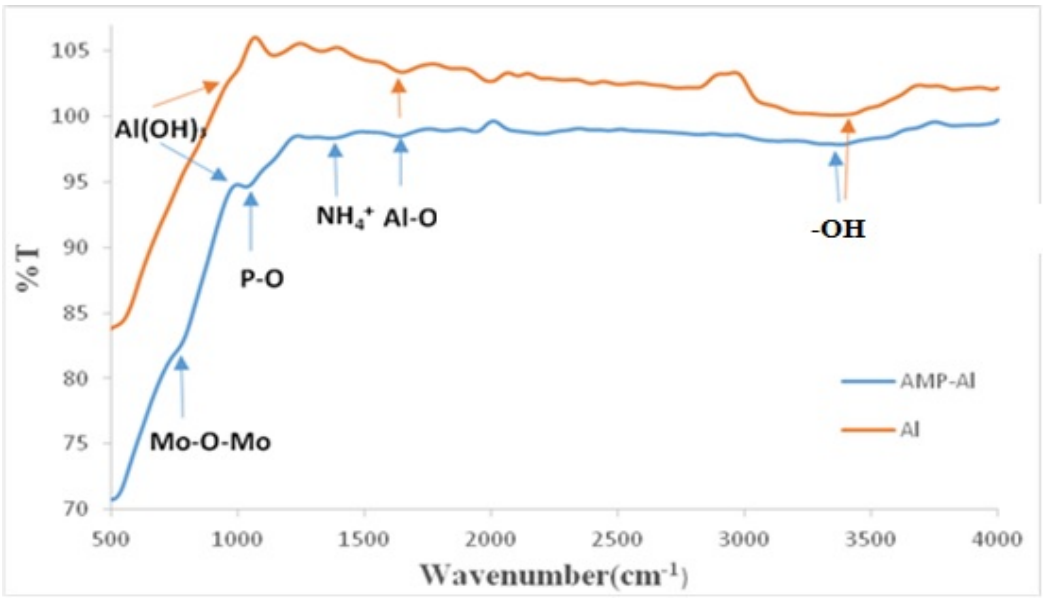

Figure 6.16 IR spectra comparison for Al_2O_3 and AMP- Al_2O_3 composite

Table 6.9 Observed IR band position in Al_2O_3 and AMP- Al_2O_3 composites

Sample	Mo-O-Mo (cm^{-1})	Mo=O (cm^{-1})	P-O (cm^{-1})	NH_4^+ (cm^{-1})	$Al(OH_3)$ (cm^{-1})	Al-OH (cm^{-1})	-OH (cm^{-1})
Al_2O_3	NA	NA	NA	NA	985-1040	1640	3000-3700
AMP-Al_2O_3	752	NA	1041	1380-1400	1033	1639	3000-3700

NA- Not applicable

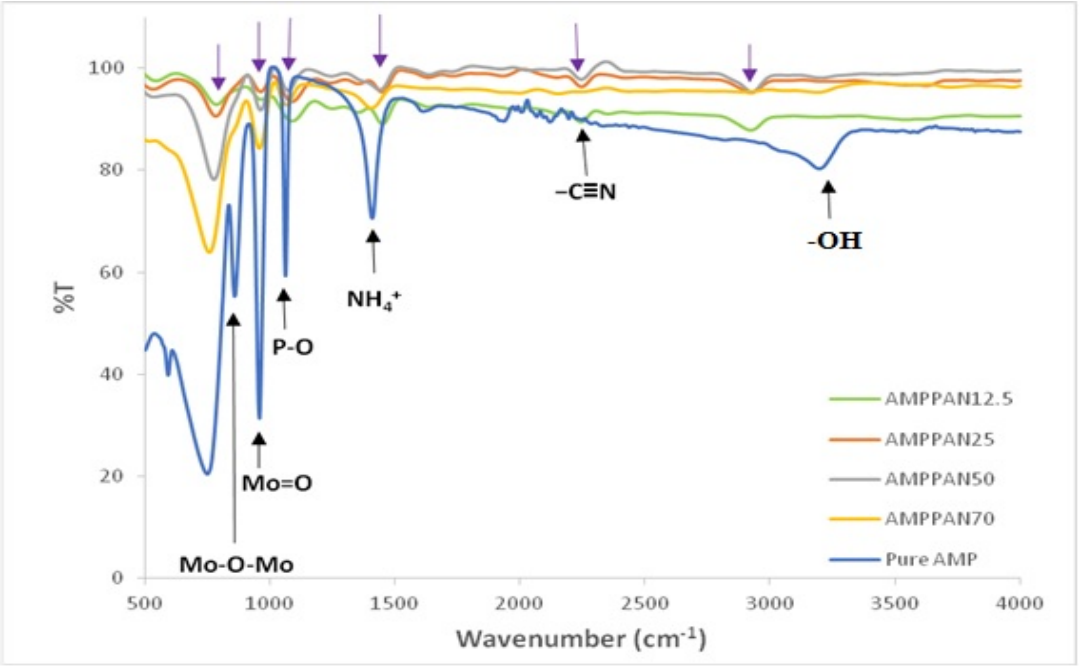

Figure 6.17 ATR-IR Study of various AMPPAN composites

Table 6.10 Observed IR band position in pure AMP and AMPPAN composites

Sample	Mo-O-Mo (cm^{-1})	Mo=O (cm^{-1})	P-O (cm^{-1})	NH_4^+ (cm^{-1})	−C≡N (cm^{-1})	-OH (cm^{-1})
AMPPAN 12.5	770-812	953	1076	1450	2252	2800 - 3000
AMPPAN 25	770-810	955	1075	1446	2248	2800 - 3000
AMPPAN 50	770-805	954	1075	1446	2245	2800 - 3000
AMPPAN 70	770-760	955	1074	1403	2243	2800 - 3000
Pure AMP	770 & 860	956	1060	1400	NA	3000 - 3500

NA – Not Applicable

Figure 6.16, a comparison of ATR-IR spectra for Al_2O_3 and AMP- Al_2O_3 composites. A broad peak starting from 2800 - 3500 cm^{-1} represents adsorbed moisture and can be attributed to -OH stretching which are attached to Al ions [17]. The broad peaks could be due to varied amount and orientation of adsorbed moisture molecules. Another characteristics peak of -OH bending modes from adsorbed water was found at 1640 cm^{-1}. A very weak shoulder found from 985 - 1040 cm^{-1} that can be attributed to

$Al(OH)_3$ as previously reported [17]. The characteristic peaks found in AMP- Al_2O_3 composite were absent in Al_2O_3 composite, such as Mo-O-Mo, vibration between corner MoO_6^{6-} octahedron; P-O symmetric stretching vibration of central PO_4^{3-} tetrahedron and characteristic vibration of NH_4^+ in the region of 752 cm^{-1}, 1041 cm^{-1} and 1400 cm^{-1} respectively (table 6.9) [28].

A weak intensity peak at 1041 cm^{-1} from AMP-Al composite was believed to be a combination of vibration frequencies of $Al(OH)_3$ and P-O species. Few weak signals are also found at 1380 cm^{-1} in the aluminium composite, which can be attributed to impurities present in the structure as reported earlier [17].

Similarly, figure 6.17 illustrates IR vibration spectra and peak attributions are reported in table 6.10. A comparison study of pure AMP showed their characteristic peaks as mentioned earlier P-O, Mo-O-Mo, M=O and NH_4^+ which are shown in figure 6.17 [27]. AMPPAN composites exhibited all of the above peaks including the peak at 2245 cm^{-1}, which corresponds to −C≡N vibration frequencies; these observations are similar to previous study [27].

6.3.4 TGA and DTA analysis

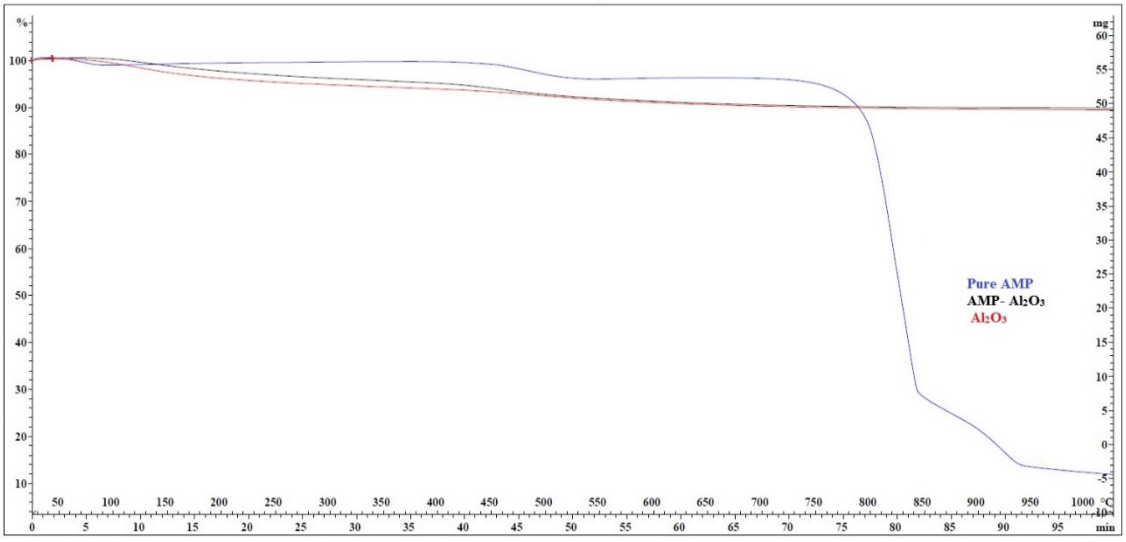

Figure 6.18 TGA comparison profile of AMP- Al_2O_3 composite

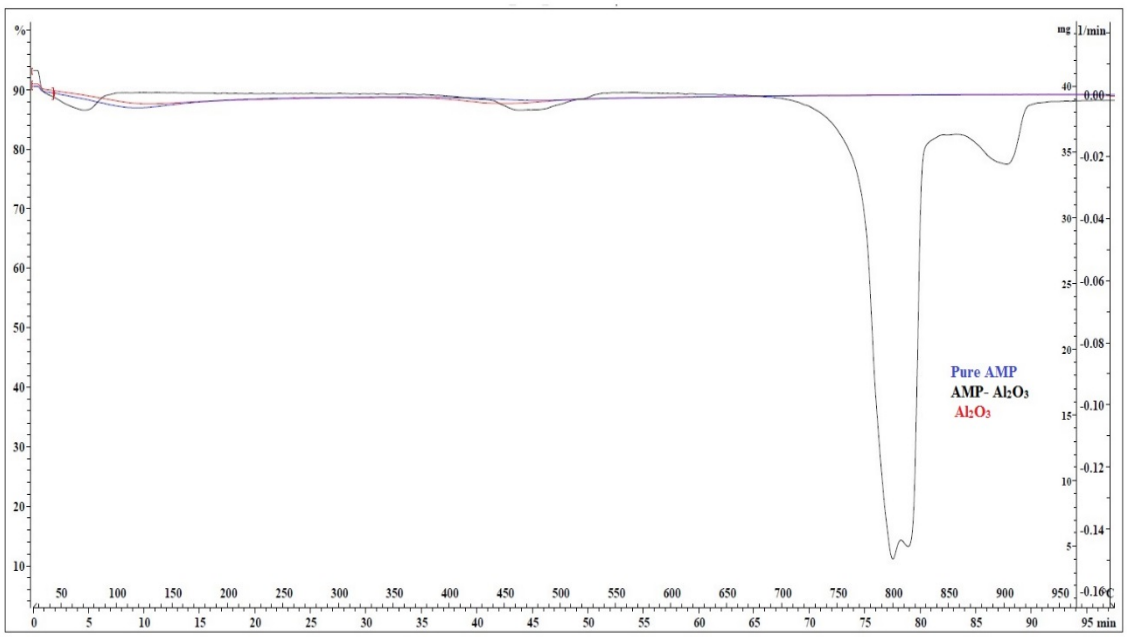

Figure 6.19 DTA comparison profile of AMP- Al_2O_3 composite

Table 6.11 Weight loss comparison in AMP- Al_2O_3 composites

Sample	100 – 300 °C	300 – 550 °C	550 - 950 °C	Weight (mg)
	% / mg	% / mg	% / mg	
Pure AMP	NA / NA	3.19 / 0.29	65.84 / 6.01	9.13
AMP- Al_2O_3	3.9 / 1.21	4.30 / 1.74	1.8 / 0.73	40.61
Al_2O_3	3.5 / 1.50	2.79 / 1.20	1.79 / 0.76	42.97

To determine the thermal stability of the synthesised composites, thermogravimetric analysis (TGA) and differential thermal analysis (DTA) were performed with the following temperature ramp and gas flow respectively; 10 °C/min and 20 ml/min air. Figures 6.18 and 6.19 are the TGA and DTA comparison profiles of AMP- Al_2O_3, Al_2O_3 composites and pure AMP respectively. Both results show similar profile of weight loss in AMP- Al_2O_3 composite and Al_2O_3. The initial weight loss of approx. 4% below 150 °C can be attributed to loss of moisture content in both structures. The previous study reports a weight loss at 280 °C, which belongs to chemically bound

water molecules [17]; no such weight loss was observed in this study. This lack of moisture could be attributed to the use of a vacuum oven for drying the synthesised materials. Loss of weight at higher temperatures are reported in table 6.11; marginal losses of weight are due to removal of hydroxyl groups, which form oxy bridges, which is consistent with a previous study [17]. The thermal study found that a broad weight loss peak between 450 – 550 °C was confirmed by DTA profile (figure 6.19). A similar weight loss was also observed in AMP- Al_2O_3 composites; difference in weight could be due to amount of AMP in the structure. A sharp endothermic peak was observed between 750 – 950 °C that was due to complete decomposition of AMP. There was no such peak observed in AMP- Al_2O_3 composite due the AMP to Al_2O_3 ratio was very low hence it followed Al composite trend.

A similar study was performed that compared AMPPAN composites and are shown in figures 6.20 and 6.21, which represents TGA and DTA comparison respectively. The weight loss data has also reported in table 6.12.

There was marginal weight loss observed below 150 °C in all the composites, which can be due to adsorbed moisture. A very sharp weight loss observed at 280 °C in all the samples except pure AMP, which could be due to chemically bonded water as previously reported [17]. Subsequent weight loss between 450 – 550 °C was due to decomposition of both AMP and PAN. The lowest weight loss was observed for AMP only with AMP to PAN ratio influencing weight loss from the composites; greater weight loss was recorded for the 12.5, 25, and 50% AMP that is confirmed from DTA profile (Figure 6.21, table 6.12. AMPPAN composites are intended to be used for reprocessing of nuclear fuels; the dissolver liquor from the dissolution of ceramic fuel pellets is unlikely to exceed 60 $^{\circ}$C due to radioactive decay of fission products. The synthesised composites would be thermally stable at these temperatures.

Table 6.12 Weight loss in AMPPAN composites

Samples	280 – 300 °C	450 – 550 °C	750 – 950 °C	Weight mg
	% / mg	% / mg	% / mg	
AMPPAN 70	3.82 / 0.80	26.98 / 5.70	52.86 / 11.18	21.15
AMPPAN 50	4.10 / 0.50	37.78 / 4.62	35.02 / 4.29	12.25
AMPPAN 25	6.04 / 0.45	60.61 / 4.59	14.72 / 0.11	7.58
AMPPAN 12.5	7.81 / 0.66	70.68 / 5.99	7.41 / 0.62	8.43
Pure AMP	NA / NA	3.19 / 0.29	65.84 / 6.01	9.13
Pure PAN	8.27 / 0.69	77.17 / 6.46	NA / NA	8.38

NA- Not Applicable

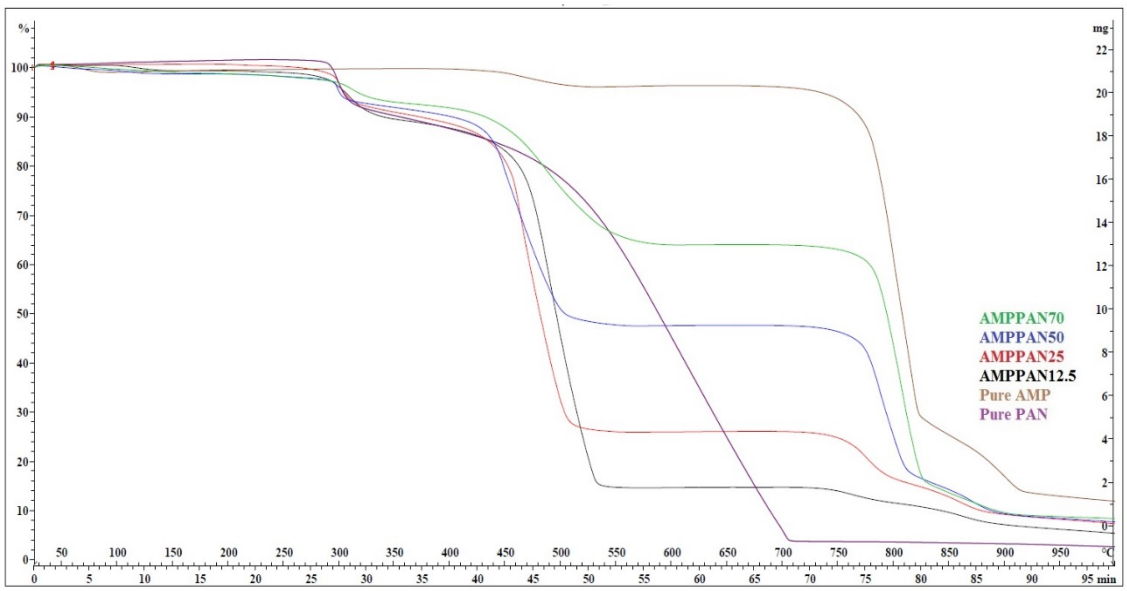

Figure 6.20 TGA comparison profile of AMPPAN composite

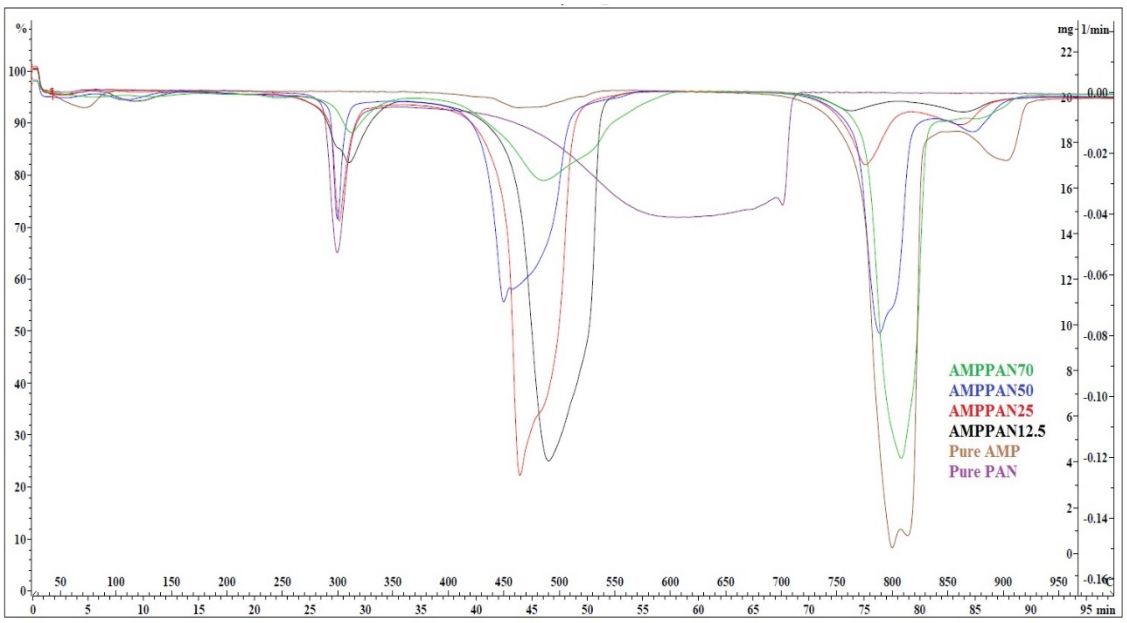

Figure 6.21 DTA comparison profile of AMPPAN composite

6.3.5 Acid Stability

The potential use of these composites for separation of fission products will be dependent on several factors such as their stability in 3 M nitric acid will be one. The composites were tested in different HNO_3 solutions for at least 24 hours and leaching of Al and Mo ions from AMP-Al_2O_3 and Mo ions in AMPPAN composites were measured by ICP-MS. Table 6.13 represents leached ions in different HNO_3 solutions after 24 hours of acid treatment at room temperature.

The results shows that both composites were reasonably stable as maximum of 5 ppm and 0.02 ppm of Al and Mo ions respectively from AMP-Al_2O_3 leached out in higher acid solution (3 M).

Similar results were observed for Mo ions from AMPPAN composites. Leaching of Mo ions increased with higher acidity with a maximum of 12 ppm Mo ions were measured in 3 M HNO_3 solution. Maximum leaching was AMPPAN 70 composites as it contains the highest wt% of AMP.

Table 6.13 Acid Stability of various composites in HNO_3

Samples	Al (ppm)			Mo (ppm)		
	0.5 M	**1 M**	**3 M**	**0.5 M**	**1 M**	**3 M**
AMP- Al_2O_3	2.14±0.02	4.5±0.03	5.2±0.05	$0.01\pm1 \times 10^{-4}$	$0.01\pm1 \times 10^{-4}$	$0.02\pm2 \times 10^{-4}$
AMPPAN 70	NA	NA	NA	8.72±0.08	9.84±0.10	12.04±0.18
AMPPAN 50	NA	NA	NA	2.64±0.02	3.02±0.03	6.73±0.06
AMPPAN 25	NA	NA	NA	1.49±0.01	1.49±0.01	4.84±0.04
AMPPAN 12.5	NA	NA	NA	$0.72\pm7 \times 10^{-3}$	$0.72\pm1 \times 10^{-3}$	3.26±0.03

NA-Not Applicable

6.3.6 Cation Uptake measurements

Table 6.14 Uptake measurements of AMP- Al_2O_3 composites in various conditions

HNO_3 (M)	Initial (ppm)			Final (ppm)			V (ml)	W (g)	Kd (ml/g)			Capacity (mg/g)		
	Sr	Cs	Ce	Sr	Cs	Ce			Sr	Cs	Ce	Sr	Cs	Ce
	Caesium Nitrate													
0.5	NA	806±14	NA	NA	790±11	NA	12.5	0.25	NA	1.0	NA	NA	0.7	NA
1	NA	778±10	NA	NA	672±9	NA			NA	7.7	NA	NA	5.2	NA
3	NA	796±12	NA	NA	710±8	NA			NA	6.0	NA	NA	4.2	NA
	Strontium Nitrate													
0.5	530±6	NA	NA	533±7	NA	NA	12.5	0.25	0.0	NA	NA	0.0	NA	NA
1	526±7	NA	NA	527±6	NA	NA			0.0	NA	NA	0.0	NA	NA
	Ammonium cerium nitrate													
0.5	NA	NA	730±9	NA	NA	330±5	12.5	0.25	NA	NA	59.6	NA	NA	19.7
1	NA	NA	720±7	NA	NA	192±3			NA	NA	136.2	NA	NA	26.2
	Mixed ions													
0.5	524±7	806±14	8146±179	528±7	803±11	6357±146	12.5	0.25	0.0	0.1	14.0	0.0	0.1	89.4
1	522±7	813±15	8143±150	525±8	770±9	7813±123			0	2.7	2.08	0.0	2.1	16.2

In order to understand the uptake behaviour of caesium, strontium, and cerium ions on AMP- Al_2O_3 composite, the distribution ratio (Kd) was measured in different nitric acid solutions containing single ions and mixed ions equilibrated for 24 hours at 25 °C (table 6.14).

Observation in single ion solutions

The calculated data clearly shows that AMP-Al_2O_3 composites have little or no affinity for strontium ions but a respectable distribution ratio for caesium ions in the single (caesium) ions solution. The maximum Cs Kd value was observed in 1 M HNO_3 consistent with previously published data [20]. The distribution ratio value decreased from 1 - 3 M HNO_3, which was a similar trend, reported earlier [20]. Cerium ions had shown maximum uptake, in comparison to other single ion solutions, and the value increased with increasing acidity (up to 1 M) (table 6.14).

Observation in mixed ions solutions

The potential use of AMP-alumina composite as a stationary phase will depend on various factors such as its selective removal of fission products (Cs and/or Sr) from a solution contain several other radionuclides. This selectivity for Cs ions has been demonstrated in these studies as this fission product could be selectively removed from acid solution when ten times the concentration of cerium (IV) ions, as surrogate for U and/or Pu, were present. Hence, for the remit of this project, i.e. separation of fission products from ions in dissolver liquor these composites would not be appropriate.

Similar uptake studies were performed to assess the suitability of AMPPAN composite as a potential stationary phase in acidic solutions. The study has shown AMPPAN's clear affinity for Cs ions in various acidic single ion and mixed ions solutions (tables 6.15 – 6.18). The results indicate that lower the amount of AMP, lower the caesium uptake with the exception of AMPPAN 70. This is most likely due to amount of AMP is directly proportional to amount of NH_4 ions hence less NH_4 ions will exchange with Cs ions . The trend was consistent in the single ion (Cs) acid solutions with the exception of AMPPAN 70. The reason for which are described later in Cs ions rate of uptake results.

The uptake measurements in mixed ions in various acid solutions had lower distribution values than from single ion solutions. This is believed to be due to use of ammonium based cerium nitrate salt (ammonium cerium nitrate). Previous studies reported that Cs

ions were exchanged with NH_4 ions in AMP hence, presence of additional NH_4 and H ions in higher acidity could most likely compete with Cs ions.

Table 6.15 Cs ions uptake measurements in AMPPAN composites

Samples	Initial (ppm)	Final (ppm)	Volume (ml)	Weight (g)	Kd (ml/g)	Capacity (mg/g)
0.5 M HNO_3						
AMPPAN 70	705±10	241±3	25	0.50	95.90	23.10
AMPPAN 50		190±3			135.30	25.70
AMPPAN 25		417±7			34.40	14.30
AMPPAN 12.5		569±6			11.80	6.70
1 M HNO_3						
AMPPAN 70	691±14	232±4	25	0.50	98.50	22.90
AMPPAN 50		190±3			131.70	25.00
AMPPAN 25		433±6			29.80	12.90
AMPPAN 12.5		569±6			10.70	6.10
3 M HNO_3						
AMPPAN 70	808±15	371±5	25	0.50	59.60	21.70
AMPPAN 50		267±4			100.50	26.80
AMPPAN 25		556±6			22.60	12.50
AMPPAN 12.5		723±10			5.80	4.23

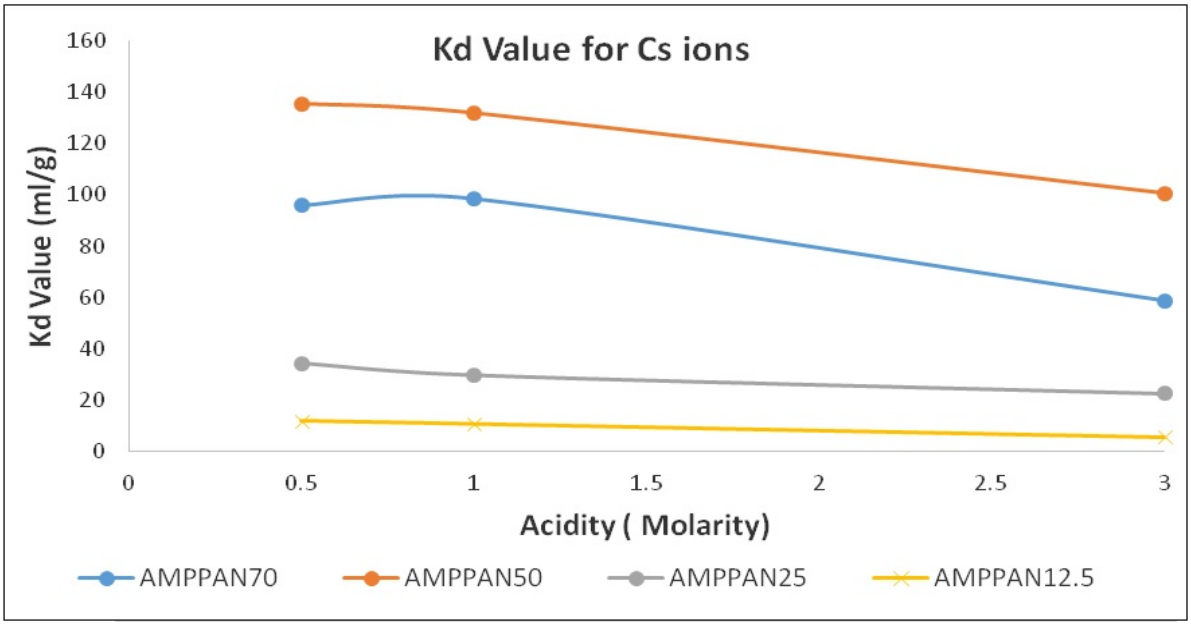

Figure 6.22 Cs ions uptake in AMPPAN composites in different HNO_3 system

Table 6.16 Sr ions uptake measurements in AMPPAN composites

Samples	Initial (ppm)	Final (ppm)	Volume (ml)	Weight (g)	Kd (ml/g)	Capacity (mg/g)
0.5 M HNO_3						
AMPPAN 70	438±6	439±5	25	0.50	0.00	0.00
AMPPAN 50		440±6			0.00	0.00
AMPPAN 25		438±5			0.00	0.00
AMPPAN 12.5		439±5			0.00	0.00
1 M HNO_3						
AMPPAN 70	447±5	449±6	25	0.50	0.00	0.00
AMPPAN 50		447±5			0.00	0.00
AMPPAN 25		448±5			0.00	0.00
AMPPAN 12.5		448±8			0.00	0.00

Table 6.17 Ce ions uptake measurements in AMPPAN composites

Samples	Initial (ppm)	Final (ppm)	Volume (ml)	Weight (g)	Kd (ml/g)	Capacity (mg/g)
0.5 M HNO_3						
AMPPAN 70	730±10	731±8	25	0.50	0.00	0.00
AMPPAN 50		732±9			0.00	0.00
AMPPAN 25		730±8			0.00	0.00
AMPPAN 12.5		731±9			0.00	0.00
1 M HNO_3						
AMPPAN 70	720±7	721±10	25	0.50	0.00	0.00
AMPPAN 50		723±8			0.00	0.00
AMPPAN 25		720±8			0.00	0.00
AMPPAN 12.5		721±7			0.00	0.00

Table 6.18 Mixed ions uptake measurements in AMPPAN composites

Samples	Initial (ppm)			Final (ppm)			V (ml)	W (g)	Kd (ml/g)			Capacity (mg/g)		
	Sr	Cs	Ce	Sr	Cs	Ce			Sr	Cs	Ce	Sr	Cs	Ce
0.5 M HNO_3														
AMPPAN 70	540±11	828±16	8312±154	542±9	270±4	8315±123	25	0.5	0	102	0	0	27	0
AMPPAN 50				540±9	318±6	8311±140			0	80	0	0	25	0
AMPPAN 25				543±10	557±10	8312±160			0	24	0	0	13	0
AMPPAN 12.5				541±15	708±10	8310±139			0	8	0	0	0	0
1 M HNO_3														
AMPPAN 70	537±9	835±17	8398±165	537±8.5	286±5	8396±149	25	0.5	0	95	0	0	27	0
AMPPAN 50				539±10	332±6	8397±175			0	75	0	0.1	25	0
AMPPAN 25				538±13	586±9	8399±140			0	21	0	0.1	12	0
AMPPAN 12.5				536±16	726±9	8400±139			0	7	0	0.1	5	0

Table 6.19 Capacity comparison of Cs ions in AMP- Al_2O_3 composite

Samples	Experimental Capacity (mg/g)	Theoretical Capacity (mg/g)	% Used
AMP	-	213	100
AMP- Al_2O_3 composite			
0.5 M HNO_3	0.7	6.99	0.10
1 M HNO_3	5.2	6.99	74
3 M HNO_3	4.2	6.99	60

Table 6.20 Capacity comparison of Cs ions in AMPPAN composites

Samples	Experimental Capacity (mg/g)	Theoretical Capacity (mg/g)	% Used
0.5 M HNO_3			
AMPPAN 70	23.15	149.10	15.53
AMPPAN 50	25.75	106.50	24.18
AMPPAN 25	14.38	53.25	27.02
AMPPAN 12.5	6.76	26.63	25.41
1 M HNO_3			
AMPPAN 70	22.89	149.10	15.36
AMPPAN 50	25.05	106.50	23.53
AMPPAN 25	12.91	53.25	24.25
AMPPAN 12.5	6.10	26.63	22.93
3 M HNO_3			
AMPPAN 70	21.76	149.10	20.44
AMPPAN 50	26.87	106.50	25.24
AMPPAN 25	12.57	53.25	23.61
AMPPAN 12.5	4.23	26.63	15.89

Tables 6.19 and 6.20 summarise the capacity uptake of Cs ions in various acid media. The theoretical capacity of pure AMP was calculated by assuming all NH_4 ions were exchanged with Cs ions and previously reported as 213 mg of Cs /g of AMP [12].

The reported experimental values for AMPPAN composites were significant lower than the theoretical values which was similar to previous data [24]. The optimum capacity (highlighted in table 6.20) was obtained in 3 M HNO_3 solution and the capacity was reduced with decreasing amount of AMP in the composite. AMPPAN 50 had the highest Cs loading capacity 26.87 mg/g of composite in 3 M HNO_3 solution, which was marginally less than previously reported 32 mg/g but with column studies [24]. The decreased value is most likely due to size and uniformity of beads and amount of AMP in the composite however this comparison was not possible since the reference did not state the composition and bead size. It is inevitable to note that 3 M HNO_3 was the most suitable acidic condition for Cs ions removal from the data, which was also previously reported and this study [24].

6.3.7 Rate of uptake of AMPPAN composites

Table 6.21 Rate of uptake at different temperature in 1 M HNO_3

Time (Minutes)	AMPPAN 70 (%)		AMPPAN 50 (%)	
	50 °C	25 °C	50 °C	25 ˚C
0	0	0	0	0
10	12	9	34	19
30	12	11	50	29
60	16	14	68	35
180	29	23	84	59
360	42	33	87	79
1440	78	75	98	88
2880	100	100	100	100

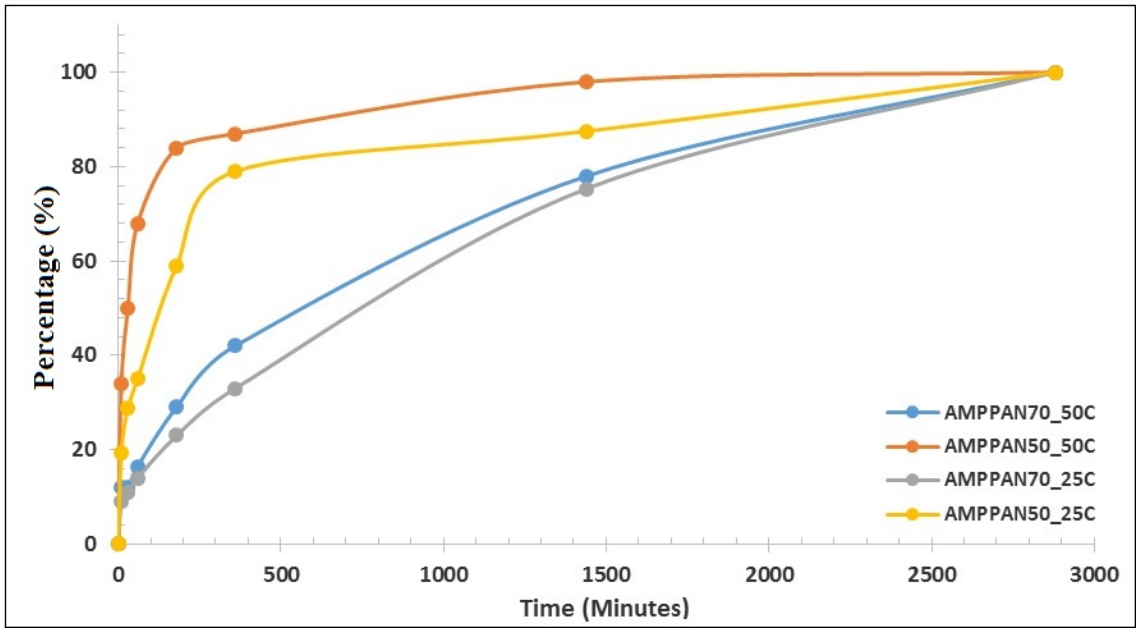

Figure 6.23 Cs ions rate of uptake at different temperature in 1 M HNO_3

Table 6.22 Cs ions rate of uptake at 25 °C in different acidity

Time (Minutes)	AMPPAN 70		AMPPAN 50	
	3 M HNO_3	1 M HNO_3	3 M HNO_3	1 M HNO_3
0	0	0	0	0
10	7	9	10	19
30	9	11	19	29
60	16	14	30	35
180	27	23	63	59
360	39	33	81	79
1440	79	75	91	88
2880	100	100	100	100

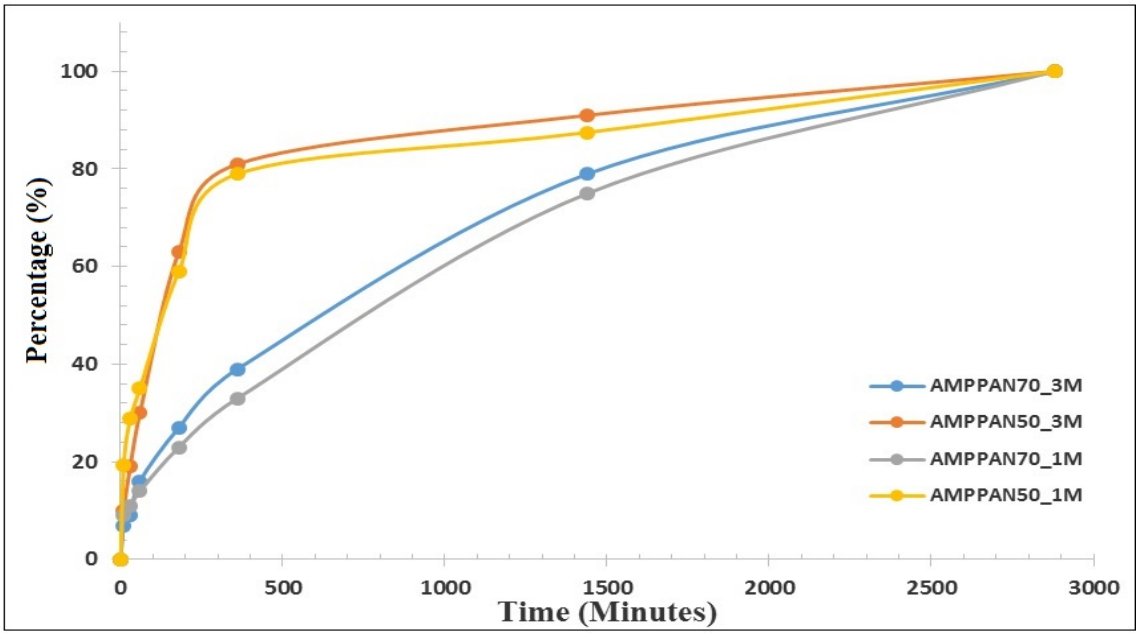

Figure 6.24 Cs ions rate of uptake at 25 °C in different acidity

Rate of uptake or kinetics is the speed with which equilibrium (ion exchange) takes place. Kinetics of Cs ions were studies on two AMPPAN composites (AMPPAN 70 and AMPPAN 50) since both possess good caesium Kd values. The study was carried out as a function of (1) temperature (25 and 50 °C), and (2) acidity of HNO_3 (1 and 3 M).

A general hypothesis was assumed that increased temperature tends to increase the diffusion rate of ions, which alters the ion exchange rate. Hence, rate of uptake at 50 °C was assumed to exhibit faster kinetics. Figure 6.23 and table 6.21 represent the rate of Cs sorption in AMPPAN 70 and AMPPAN 50 at different temperatures. As seen from figure 6.23, both composites have shown faster kinetics with increased temperature. In comparison, AMPPAN 50 had faster kinetics compared to AMPPAN 70 at both temperatures.

A rate of uptake of Cs ions in various acid solutions is represented in figure 6.24 and table 6.22. Kinetics of both composites were similar at different acid conditions. AMPPAN 50 had faster kinetics than AMPPAN 70, which was similar to kinetics study at different temperature. Both composites had faster kinetics in 1 M HNO_3 up to 180 minutes, but for longer time period the kinetics were better in 3 M HNO_3.

Overall comparison of AMPPAN composites with AMP indicate that composites are slower than AMP, which has much faster rate of uptake (within 1 - 15 minutes) as previously reported [12].

The rate of uptake of cations involves the diffusion through the film of solution on the periphery of the spheres and then into the spheres (beads) via the pore solution [29]. This mechanism was not evaluated in this study as the spheres/beads produced were somewhat of irregular shape and pore structure. Producing more beads of greater regularity should be considered for future work.

The equation of ion exchange in AMP can be represent as,

$$(NH_4)_3PMo_{12}O_{40} + {}_xCs^+ (aq) \longrightarrow Cs_x (NH_4)_{3-x} PMo_{12}O_{40} + x (NH_4)^+ (aq)$$

Simple explanation can be derived from hydrated ionic radii that the ion exchange of NH_4 with Cs ions takes place since the hydrated ionic radii of both ions are in close proximity [30]. The hydrated ionic radii of NH_4 and Cs ions were reported as 1.48 Å and 1.69 Å respectively with Sr ions radii 1.13 Å [30]. Therefore, Cs ions most likely to exchange and be retained in the voids created by NH_4 ions in the ion exchange process.

The slower kinetics in AMPPAN 70 could be due to their poor porous structure as reported earlier in pore analysis. The pore volume of AMPPAN 70 was 0.004 cm^3/g compared to 0.032 cm^3/g for AMPPAN 50 (table 6.11). Therefore, the diffusion of ions through the pores were slower hence slower kinetics.

6.4 Conclusion

The aim of the project was to synthesis selective stationary phases for removal of fission products (Cs, Sr) from irradiated fuel dissolver liquor. Ammonium phosphomolybdate (AMP) was chosen as the sorbent due to its Cs ion selectivity and stability in acid media.

The ways of entrapping AMP within different matrices were evaluated by internal gelation technique with Al_2O_3 and polymer encapsulation with PAN. The study was primarily focused on synthesis of suitable shape and size of the composites and further evaluating their suitability for Cs removal from acid media.

There were immense challenges to synthesis AMP-Al_2O_3 composites since the technique required specialised equipment to form beads, their complexity in synthesis and fast gelating property, and limitation with tiny quantity of AMP entrapment. The yield of this technique was also a major flaw for their suitability as a stationary phase.

Polymeric entrapment of AMP was significantly less challenging and an easy to upscale technique. The technique offers easy one pot synthesis, which is a key parameter for industrial use of a stationary phase. The technique offered considerable amount of yield and easy to handle.

Both techniques had offered porous structures, which was important to achieve maximum access for ion exchange. The findings of chemical stability suggests both techniques had lost negligible quantity of Al and Mo ions for AMP-Al_2O_3 and Mo ions for AMPPAN composites. The TGA studies indicate that the composites made by both techniques were stable at temperatures up to 280 °C, which is more than sufficient if these composites were employed to treat spent fuel dissolver liquor. Even allowing for the heat generated from the radioactive decay of isotopes dissolver liquors prior to the solvent extraction circuit would not exceed 60 °C.

The pore volume is an important criterion when considering cation kinetics (rate of uptake); an open pore structure that allows ready access to exchange sites will confer fast kinetics. In this study, AMPPAN 50 had a greater pore volume, which was reflected in its superior rate of uptake of Cs compared with AMPPAN 70.

The uptake measurements on AMPPAN composites have shown significant distribution (Kd) values (up to 135 ml/g) and capacity for Cs ions (up to 26 mg/g) in acid media and remarkable selectivity which was a deciding factor for their potential use as a stationary phase for removal of fission product (Cs) from reprocessing liquors.

6.5 References

1. Berzelius J.J., Beitrag zur näheren Kenntniss des Molybdäns. Annalen der Physik, 1826. 82(4), p. 369 - 392.
2. Gouzerh P., and Che M., From Scheele and Berzelius to Müller: polyoxometalates (POMs) revisited and the "missing link" between the bottom up and top down approaches; L'Actualité Chimique, 2006. 9, p. 298 - 406.
3. Davies W.C., The formation of ammonium phosphomolybdate in the presence of certain organic acids. Analyst, 1942. 67(790), p. 1 - 4.
4. Illingworth J.W., and Keggin J.F., 127. Identification of the 12-heteropoly-acids and their salts by means of X-ray powder photographs. Journal of the Chemical Society, 1935. 0, p. 575 - 580.
5. Thistlethwaite W.P., The determination of the composition and constitution of ammonium phosphomolybdate and the conditions affecting its precipitation. Analyst, 1947. 72 (861), p. 531 - 540.
6. Smit J., Van R., and Robb W., Cation exchange properties of the ammonium heteropolyacid salts. Journal of Inorganic and Nuclear Chemistry, 1959. 12(1–2). p. 95 - 103.
7. Smit J., Van R., Robb W., and Jacobs J.J., Cation Exchange on Ammonium Molybdophosphate-I: The Alkali Metals, Journal of Inorganic and Nuclear Chemistry, 1959. 12, p. 104 - 112.
8. Suess M. and Pfrepper G., Investigations of the sorption of caesium from acid solutions by various inorganic sorbents. Radiochimica Acta, 1981. 29(1), p. 33 - 40.
9. Buchanan J.D., Sorensen B.H., and Armstrong J.C., Separation of Carrier-Free Cs- 131 from Neutron-Irradiated Barium Using AMP And AMP-Asbestos, ORNL-1lC-lOVL, p. 298 - 314.
10. Cunha I.I.L., and Sakai L., Determination of caesium-137 in water by ion exchange. Journal of Radioanalytical and Nuclear Chemistry, 1989. 131(1), p. 105 - 109.
11. Krtil J., Exchange properties of ammonium salts of 12-heteropolyacids—IV: Cs exchange on ammonium phosphotungstate and phosphomolybdate. Journal of Inorganic and Nuclear Chemistry, 1962. 24(9), p. 1139 - 1144.

12. Wilding M.W., Caesium removal from acidic radioactive waste solutions, INEEL, USA, IDO-14544. 1961.
13. Murthy T.S., Balasubramanian K.R., and Narasimha R.K.L, Radiation stability of inorganic exchangers used for fission product separation, India: Department of Atomic Energy, 1981.
14. Archer D.W., and Helslop R.B., The solubility of ammonium 12-molybdophosphate in dilute acids. Analytica Chimica Acta, 1964. 30, p. 582 - 589
15. Van der Brugghen F.W., Kanij J.B.W., Noothout A.J., Hermans M.E.A, and Votocek O., A U (VI) - Process for microsphere production, Symposium on Sol-Gel Processes and Fuel Cycles. UNCL. 1970.
16. Collins J.L., Development of Spheroidal Inorganic Sorbents for Treatment of Acidic Salt-Bearing Liquid Waste, ORNL/TM-2000/367, 2001.
17. Pillai K.T., Kamat R.V., and Vaidya V.N., Preparation of Porous Alumina Microspheres by Internal Gelation Method. Transactions of the Indian Ceramic Society, 2001. 60(3), p. 150 - 154.
18. Haas P.A., Pitt W.W., Robinson S.M., and Ryon A.D., Preparation of metal oxide gel spheres with hexamethylenetetramine as an ammonia donor. Industrial & Engineering Chemistry Product Research and Development, 1983. 22(3), p. 461 - 466.
19. Pillai K.T., Kamat R.V, and Vaidya V.N., Preparation of AMP trapped Alumina Spherical Particles Using Gel Entrapment Technique, National Seminar on Sol-gel Science and Technology, Calcutta, 2000.
20. Chakravarty R., Ram R., Pillai K.T., Pamale Y., Kamat R., and Dash A., Ammonium molybdophosphate impregnated alumina microspheres as a new generation sorbent for chromatographic 137Cs/137mBa generator. Journal of Chromatography A, 2012. 1220, p. 82 - 91.
21. Onodera Y., Mimura H., Iwasaki T., Hayashi H., Ebina T., and Chatterjee M., A New Granular Composite with High Selectivity for Caesium Ion Prepared from Phosphomolybdic Acid Hydrate and Inorganic Porous Material. Separation Science and Technology, 1999. 34 (12), p. 2347 - 2354.
22. Rahaman M.S.A., Ismail A.F., and Mustafa A., A review of heat treatment on polyacrylonitrile fiber, Polymer Degradation and Stability, 2007. 92(8), p. 1421 - 1432.

23. Šebesta F., and Štefula V., Composite ion exchanger with ammonium molybdophosphate and its properties. Journal of Radioanalytical and Nuclear Chemistry, 1990. 140(1), p. 15 - 21.
24. Tranter T.J., Herbst R.S., Todd T.A., Olson A.L, and Eldredge H.B., Evaluation of ammonium molybdophosphate-polyacrylonitrile (AMPPAN) as a caesium selective sorbent for the removal of Cs-137 from acidic nuclear waste solutions. Advances in Environmental Research, 2002. 6(2), p. 107 - 121.
25. Todd T.A., Mann N.R., Tranter T.J., Šebesta F., John J., and Motl A, Caesium sorption from concentrated acidic tank wastes using ammonium molybdophosphate-polyacrylonitrile composite sorbents. Journal of Radioanalytical and Nuclear Chemistry, 2002. 254(1), p. 47 - 52.
26. Brewer K.N., Todd T.A., Wood D.J., Tullock P.A., Sebesta F., and John J., AMPPAN column tests for the removal of 137Cs from actual and simulated INEEL high-activity wastes. Czechoslovak Journal of Physics, 1999. 49(1), p. 959 - 964.
27. Park Y, Lee Y.C., Shin W.S., Choi S.J., Removal of cobalt, strontium, and caesium from radioactive laundry wastewater by ammonium molybdophosphate–polyacrylonitrile (AMP–PAN). Chemical Engineering Journal, 2010. 162(2), p. 685 - 695.
28. El-Naggar M.R., Aglan R.F., and Sayed M.S., Direct incorporation method for the synthesis of molybdophosphate/MCM-41 silica composite: Adsorption study of heavy metals from aqueous solutions. Journal of Environmental Chemical Engineering, 2013. 1(3), p. 516 - 525.
29. Harland C.E., RSC Paperbacks, Volume 6: Ion Exchange: Theory and Practice (2nd Edition). Royal Society of Chemistry. 1994, ISBN: 9780851864846.
30. Nightingale E.R., Phenomenological Theory of Ion Solvation. Effective Radii of Hydrated Ions. The Journal of Physical Chemistry, 1959. 63(9), p. 1381 - 1387.
31. https://www.youtube.com/watch?v=tUNVDOn-QhA

Chapter 7

Summary and future work

7.1 Summary

The current separation process of spent nuclear fuel has been carried out by universally accepted and well-understood solvent extraction technique - PUREX. The major challenge of this technique is its lack of specificity for U and Pu isotopes requiring a multi-stage process, strict process control, solvent and diluent degradation, and other process challenges.

The technique under development at UCLan offers an alternative approach, targeting minor components such as fission products (FPs) and minor actinides (MAs) compared with U and Pu isotopes, the latter represents about 95% of spent nuclear fuel. UCLan's process should provide better waste management and a more flexible separation flow sheet. The proposal offers removal of the major heat generating β/γ emitting components e.g. Cs and Sr first which significantly reduces the heat and radiation dosage to down-stream operations, waste management, and disposal.

Three key approaches to achieve selective stationary phases that were acid stable were evaluated:

(1) Creating charge imbalance into ordered Mesoporous MCM-41 structure (chapter 4),
(2) examination of molecular sieves based on their size exclusion property (chapter 5), and
(3) preparation of ammonium phosphomolybdate encapsulated composites (chapter 6).

A sol-gel process was chosen to prepare all the materials described in this thesis, as the yields from this technique were few gram quantities at a time, achieving some of the initial project criteria, i.e. simple, low cost, and one pot synthesis technique.

The hydrothermal sol-gel process to synthesise ordered MCM-41 and boron modified MCM-41s produced approximately 10 g/batch of final product. Zeolites 3A, 4A, and 5A were purchased in beads/pellets form and modified to mesoporous zeolite 5A which could be produced in approximately 2.25 g/batch. The yield for AMP-Al_2O_3 and AMPPAN composites were approximate 2 g and 10 g/batch respectively.

The synthesised MCM-41s and mesoporous zeolite 5A were fine powders, which were not ideal for column work however; AMPPAN and AMP-Al_2O_3 were spherical beads and granular form respectively.

The synthesis route to produce spheres of AMP-Al_2O_3 composite was unsuccessful due to very fast gelling nature of the components. It was difficult therefore, to transform the gel into uniform spheres/beads shape in comparison to AMPPAN composite route. An alternative approach to use phosphomolybdic acid as starting reagent and later convert that into AMP may be a promising route, proposed by Onodera *et al.* requires further investigations The surfactant assisted AMPPAN synthesis was the most easiest and quickest technique in comparison to all other synthesis techniques and could potentially be scaled-up to kilogram quantities with little modifications.

Various physical and chemical properties of the materials were characterised by several analytical techniques. The surface area and porosity of the MCM-41s were highest (up to 690 m^2/g) in comparison to other materials. They have shown ordered porous structure also confirmed by XRD. The microporosity and the mesoporosity of the mesoporous zeolites suggest the coating of mesoporous surrounding zeolite 5A was achieved which was confirmed by surface area, SEM, SAXS, and XRD analysis. The AMP-Al_2O_3 composite had a rough surface, analysed by SEM, which was due to poor synthesis technique. SEM images of bisected AMPPAN composite beads indicated a channel like porous network; the images also indicated the opening of pores due to increased surfactant amount in AMPPAN composites. The TGA studies showed only 6% loss in up to 1000 °C for MCM-41 materials, with AMP-Al_2O_3 and AMPPAN composites had losses of up to 10% and 100% loss respectively due to their different compositions. AMPPAN composites were stable up to 280 °C which is should be more than sufficient for cation separation since the spent fuel dissolver liquor is unlikely to exceed 70 °C due to radionuclide decay.

The cation uptake performance of the prepared stationary phases were analysed in approx. 5 mM $CsNO_3$, 5 mM $Sr(NO_3)_2$ as single ion and in mixed ions solutions, the latter also contained 50 mM $Ce(NH_4)_2(NO_3)_6$ in various concentrations of nitric acid and deionised water. Ce ions were selected as surrogate for U/Pu ions due to their similar separation chemistry with TBP.

The distribution coefficient value (Kd) and capacity for all the MCM-41s and zeolite A were significantly low in 0.5 M, and 1 M nitric acid system due to highly competing H^+ ions where AMPPAN and AMP-Al_2O_3 composites have shown good uptake in acidic systems. MCM-41 has shown marginal increase in Cs, Sr, and Ce ions uptake in weakly acidic solution (pH ~5) but non-specificity was found for any individual ion.

Boron was chosen to create charge imbalance in the Si-MCM-41 structure and its neutron absorbance property. Boron modified MCM-41 did not show any significant improvement in cation uptake performance.

Zeolite 5A showed significant increase in cation uptake performance at lower acidity however, these were again non-selective for any individual ion. The coating of mesoporous zeolite also has not shown any significant improvement in ion uptake performance for mixed ions studies.

AMPPAN composites had highest Kd value of 135 ml/g and capacity of 26 mg/g in up to 3 M HNO_3 solutions in comparison to all the other materials and has shown remarkable discrimination for Cs to Sr ions, which suggest its suitability for selective Cs ions removal from the acidic liquor. The composite has shown high selectivity for Cs ions and performed exceptionally well even in presence of 10 times Ce ions concentration. AMP-Al_2O_3 composites have shown marginal Cs ions uptake due to the amount of AMP loading which was the biggest limiting factor.

Acid stability studies on best performing AMPPAN composite have shown marginal loss of Mo ions in 3 M HNO_3 which subsequently reduced with lower acidic conditions. The reported data indicates further justification of AMPPAN as the most suitable material for a stationary phase.

The rate of uptake data from 1 M HNO_3 at 25 °C indicates much faster kinetics in AMPPAN 50 compared to AMPPAN 70; this was consistent for the 50 °C results. These faster uptake results for AMPPAN 50 can be explained due to its more open channel/pore structure. This could be due to AMPPAN 50 having more accessible ion exchangeable sites compared to AMPPAN 70. Further studies therefore to optimise the amount of surfactant for preparation of these composites are necessary.

7.2 Future Work

This research was significantly focused on the identification of suitable materials based on:

- various parameters such as Cs and Sr ions selectivity, uptake and rate of uptake performance in acidic media,
- acid, radiation and temperature resistance,
- one pot synthesis, to be potentially scaled-up etc.

The research has shown AMPPAN composites have satisfied all of the above parameters and potential to improve their rate of uptake by modifying structural changes, which could be achieved by:

1) Use of greater quantities of surfactant in the synthesis of AMPPAN composites,
2) Use of surfactants with longer chain length that could possibly improve pore structure.
3) Modified version of droplet technique to improve uniform bead formation and reduced size that could improve overall surface area.

In addition, future studies should address:

(1) Modified AMP compositions to improve the exchangeable sites to increase composite Cs cation capacity;
(2) Identifying Sr ion selective materials which could be encapsulated in PAN with composites similar to AMPPAN;
(3) Column work to simulate continuous chromatography and their breakthrough and elution data;
(4) Selection of other cations such as Na, Zr, Mo, Tc etc.
(5) To expand simulate spent fuel composition which should be used to evaluate further stationary phases;
(6) The potential of zeolites/modified zeolites for Cs and/or Sr removal from slightly acidic and alkaline solutions for other waste management challenges.